Studies of the growth and size distribution of aerorosol particles

R.K. Elleson

STUDIES OF THE GROWTH AND SIZE DISTRIBUTION OF AEROSOL PARTICLES

by

R. K. ELLESON B.A.

Submitted in candidature for the degree of M.Sc. in the University of Durham

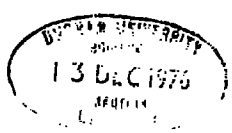

August 1976

ABSTRACT

A study is made of the theoretical growth of soluble aerosol particles with increasing humidity. The growth equation is applied to sodium chloride and ammonium sulphate particles, chosen because of their special significance as atmospheric nuclei. The effect of particle growth on visibility is also considered. An experimental investigation of the effect of humidity on particle size is carried out using artificially generated aerosols of sodium chloride and ammonium sulphate. Inaddition a study is made of the variation in the particle size distribution of the atmospheric aerosol measured continuously over a 49 day period at Durham Observatory.

A theoretical growth relation, based on Mason's equation (1971) relating the size of a solution droplet to the relative humidity of its environment, is derived. Novel approximations are incorporated in the application of the growth equation to particles of sodium chloride and ammonium sulphate and the results for sodium chloride agree with Mason's equation to within 0.5% over the dry particle mass range from 3×10^{-17}g to 3×10^{-11}g. The predicted growth of ammonium sulphate particles with relative humidity indicates agreement with previous work by Garland (1969).

Experimental measurements were made of the growth of sodium chloride ammonium sulphate nuclei with humidity. The particles, with initial radius between 2×10^{-6}cm and 3×10^{-6}cm, were generated by a Collison atomizer and allowed to grow in a storage vessel as the humidity was increased from about 60% to 92%. The experimental measurements agree well with the theoretical growth curves, chosen to correspond as closely as possible to the experimental particle size at the lowest humidity. Average percentage increases in the particle radius of 60% and 95% for ammonium sulphate and sodium chloride particles of initial average radii of 3.0×10^{-6}cm and 2.6×10^{-6}cm respectively were obtained as the humidity was increased from about 60% to 92%.

Approximations to Mie's theory of light scattering were used to calculate the extinction coefficient, σ, for monodisperse aerosols of sodium chloride and ammonium sulphate as a function of solute mass per particle in the range between 3×10^{-17}g and 3×10^{-11}g at humidities of 80%, 95% and 99%. The results indicate that the sodium chloride particles are more efficient in reducing visibility than ammonium sulphate particles by factors varying from about 1.3 to 5.5

over the whole range of humidity and dry particle mass. Calculations show that, for both salts, a Junge particle size distribution is about twice as effective at reducing visibility as a monodisperse aerosol of the same salt with particle radius equal to the mass median of the Junge distribution. /e

A study of the variation in the particle size distribution of the atmospheric aerosol in the radius range 0.25 - 5.0 micrometres, measured at Durham Observatory over a period of 49 days from 21 July to 8 September 1975, indicates that the distribution closely follows the shape of a Junge log-radius distribution with a slope, β, equal to 3.04, The average diurnal variation over the period shows maximum and minimum number concentration occurring between 0200 and 0800 hours B.S.T. and 1400 and 2000 hours B.S.T. respectively. The general increase in the particle number concentration, particularly in the lower size ranges, during the period 0000 to 0600 hours can be partly attributed to an increase in humidity. This is reflected in the positive correlation coefficient between particle number concentration and relative humidity.

CONTENTS

		Page
Abstract		i
Contents		iii
List of Figures		v
List of Tables		viii
Chapter 1	The Growth and Size Distribution of Aerosol Particles	1
1.1	General Introduction	1
1.2	Condensation on Soluble Particles	2
1.3	The Growth of Salt Nuclei with Humidity	3
1.4	The Effect of Atmospheric Particles on Visibility	4
1.5	Aerosol Particle Size Distributions	5
Chapter 2	The Theoretical Growth of Hygroscopic Particles with Humidity and the Effect on Visibility	8
2.1	Introduction	8
2.2	Derivation of an Equation relating Particle Radius to Humidity	9
2.3	Use of the Growth Equation	11
	(a) Molality of the Solution	11
	(b) The density of salt solution as a function of the percentage concentration	12
	(c) The surface tension as a function of molality	13
	(d) The van't Hoff factor	13
2.4	The Effect of Particle Growth on Visibility	15
2.5	Use of the Visibility Equations	18
2.6	Discussion of the Results	21
Chapter 3	The Experimental Apparatus	27
3.1	Introduction	27

3.2 The Aerosol Generator 27
3.3 The Storage Vessel 27
3.4 The Psychrometer 28
3.5 The Photoelectric Nucleus Counter 28
3.6 The Diffusion Battery 30
3.7 The Large Ion Tube 31

Chapter 4 The Experimental Procedure and Results 34

4.1 The Experimental Procedure 34
4.2 The Generated Aerosol 35
4.3 Coagulation Effects 35
4.4 The Experimental Results and Discussion 35

Chapter 5 An Analysis of the Atmospheric Aerosol sampled at Durham University 38

5.1 Introduction 38
5.2 The Instrumentation and Measurement Procedures 38
5.3 The Experimental Results 39
5.4 Discussion and Conclusions 44

References 47
Acknowledgments 51

LIST OF FIGURES

Figure		Following page:
2.1	Density as a function of solution concentration - (NaCl)	12
2.2	Density as a function of solution concentration - $(NH_4)_2SO_4$	12
2.3	Percentage concentration versus $(r/r_o)^3$ (NaCl)	12
2.4	The van't Hoff factor for sodium chloride as a function of molality	14
2.5	The van't Hoff factor for ammonium sulphate as a function of molality	14
2.6) 2.7)	Selected theoretical growth curves of sodium chloride	15
2.8) 2.9)	Selected theoretical growth curves of ammonium sulphate	15
2.10	Refractive index as a function of solution concentration (NaCl)	18
2.11	Refractive index as a function of solution concentration $(NH_4)_2SO_4$	18
2.12	The extinction coefficient of an atmosphere containing 1 $\mu g/m^3$ of ammonium sulphate	18
2.13	Simplified Size Distribution, after Junge	18
2.14	The extinction coefficient as a function of dry particle mass - $(NH_4)_2SO_4$	19
2.15	The extinction coefficient of an atmosphere containing 1 $\mu g/m^3$ of sodium chloride	19
2.16	The extinction coefficient as a function of dry particle mass - NaCl	19
2.17	Sea Spray Size Distribution used by Hanel	20
2.18	The ratio $\sigma(H)/\sigma(K)$ as a function of relative humidity	20

2.19	$\sigma(H)/\sigma(K)$ as a function of relative humidity	20
3.1	Schematic diagram of the apparatus	27
3.2	Schematic diagram of the Nebulizer	27
3.3	The Collison Nebulizer	27
3.4	The Aerosol Generator Unit	27
3.5	The Storage Vessel	28
3.6	Schematic diagram of the Psychrometer	28
3.7	Schematic Diagram of the Photoelectric Nucleus Counter	28
3.8	The Photoelectric Nucleus Counter	29
3.9	The Inverting Amplifier Circuit	30
3.10	Test of the linearity of the amplifier circuit	30
3.11	The Diffusion Battery	30
3.12	Penetration curves of polydisperse aerosols through a parallel-walled channel	31
3.13	Interpolation graph for use with Fuchs's curves	31
3.14	Schematic Diagram of the Large Ion Tube	31
4.1	Typical variation in particle concentration during experiment	34
4.2	Experimental measurements of the size distribution of the generated sodium chloride aerosol	35
4.3	Experimental measurements of the size distribution of the generated ammonium sulphate aerosol	35
4.4	Experimental growth of ammonium sulphate	35
4.5	Experimental growth of sodium chloride	35
4.6	Comparison of theory with experiment (NaCl)	36
4.7	Comparison of theory with experiment $(NH_4)_2SO_4$	36
5.1	Diurnal Variation of particle concentration	39

5.2	Hourly variation in particle concentration over 49 days	39
5.3	Cumulative frequency distribution	41
5.4	Particle Size Distribution	41
5.5	Cumulative percentage plot (July 15-21)	42
5.6	Cumulative percentage plot over 49 days	42
5.7	Particle Number Concentration versus windspeed	44
5.8	Particle Number Concentration versus Relative Humidity	44
5.9	Diurnal variation of the natural aerosol	45

LIST OF TABLES

Table		Page
2.1	The difference between the partial molar volume of water, V_w', and the ratio $\frac{Mw}{\rho'}$ of the molecular weight of water to the solution density as a function of the vapour pressure ratio $\frac{P_\infty'}{P_\infty}$ for aqueous NaCl at 18°C.	10
2.2	Comparison of the growth curves computed using Equation 2.13 with those due to Mason.	15
2.3	The size distribution of ammonium sulphate particles in the atmosphere on 23.8.67 reported by Heard and Wiffen.	19
2.4	Maximum values of the extinction coefficient for monodisperse aerosols with number concentration corresponding to 1 microgram per cubic metre.	22
2.5(a)	Selected values of the extinction coefficient as a function of particle size and relative humidity.	23
2.5(b)	The ratios of extinction coefficients for sodium chloride to the corresponding values for ammonium sulphate.	23
2.6	The extinction coefficient of an ammonium sulphate aerosol as a function of relative humidity.	25
2.7	The extinction coefficient of a sodium chloride aerosol as a function of relative humidity.	25
3.1	Details of the two minute operating cycle of the photoelectric counter.	29
3.2	Dimensions of the Diffusion Battery	31
3.3	Dimensions of the Ion Tube	32
4.1	Typical Experimental Growth of Ammonium Sulphate and Sodium Chloride particles	36
5.1	Summary of statistics of particle concentration	40

5.2 A comparison of the statistics obtained from the cumulative curves with the actual values obtained directly from the data. 42

5.3 The Pearson product-moment correlation coefficient between the variables. 43

5.4 Wind direction during period of counting. 45

CHAPTER 1

THE GROWTH AND SIZE DISTRIBUTION OF AEROSOL PARTICLES

1.1 General Introduction

The natural atmospheric aerosol consists of solid insoluble particles, of soluble particles giving rise to pure solution droplets and of mixed nuclei that have both soluble and insoluble components. Since the last two groups of nuclei are hygroscopic they may be preferred as centres of condensation, their efficiency being determined by their size and chemical nature. It is unlikely that non-hygroscopic particles play a significant role in cloud formation. A considerable proportion of natural aerosol particles consist of hygroscopic salts which grow with increasing relative humidity. Observations using an electron microscope suggest that a large proportion of particles collected overland are of mixed composition and, at relative humidities above 70%, the majority of these mixed particles disappear. In maritime air, the sea-salt nuclei contain practically no insoluble component.

Since the number concentration of aerosol particles is much greater than that of cloud droplets only a small fraction of the potential nuclei is used in the cloud condensation process. If a droplet is formed on a wholly or partially soluble nucleus, the equilibrium vapour pressure is reduced by an amount depending on the nature and solution concentration of the droplet. This means that condensation onto the nucleus will be able to set in at a lower supersaturation than would be the case if the original particle was insoluble. Condensation first occurs in a cooling air mass on the largest hygroscopic nucleus present. The concentration of the more efficient nuclei and the rate at which water vapour is made available for condensation by cooling of the air determines whether or not a nucleus of a particular size is activated to become a cloud droplet.

Condensational growth is the initial growth mechanism for cloud droplets and hence a knowledge of the increase of aerosol particle size with increasing humidity is important in cloud growth studies. The hygroscopicity of atmospheric nuclei can also promote both fog and cloud formation. These topics together with the effect of particle growth on visibility are discussed more fully in the following sections.

1.2 Condensation on Soluble Particles

If a droplet is formed on a wholly or partially soluble nucleus, the equilibrium vapour pressure at the surface of the drop is reduced by an amount which depends on the chemical nature and concentration of the solution. Condensation will occur at a lower supersaturation than on an insoluble nucleus of the same size.

For a pure droplet the critical radius r_c that an aggregate of molecules must attain in order to be in equilibrium with the surrounding vapour was first deduced by Kelvin (1870) and is given by the relation

$$r_c = 2M\sigma / \rho RT \ln(P/P_\infty) \qquad (1.1)$$

where P is the pressure of the supersaturated vapour, P_∞ is the equilibrium vapour pressure at temperature T over a plane surface of the liquid, σ is the surface tension of the droplet, ρ is the density of the liquid, R is the universal gas constant and M is the molecular weight of the liquid. Equation 1.1 was modified, first by Köhler (1921) and later by Wright (1936), to yield an expression for the equilibrium vapour pressure at the surface of a solution droplet. Wright's expression for the vapour pressure $P_{r'}$ of a solution droplet of radius r' is given by the equation

$$\frac{P_{r'}}{P_\infty} = \exp\left(\frac{2\sigma M}{\rho' R T r'}\right) - \frac{3 i m_o M}{4\pi r'^3 \rho' W} \qquad (1.2)$$

where P_∞ is the equilibrium vapour pressure over a plane water surface, m_o is the mass of the solute in grammes, M is the molecular weight of water, ρ' is the density of the solution droplet, W is the molecular weight of the solute and i is the van't Hoff factor which allows for the modification of Raoult's Law to include electrolytic solutions. The van't Hoff factor varies with the chemical nature and concentration of the solution. Wright assumed i to be constant for all concentrations.

Mason (1971) derives a new form for the equilibrium vapour pressure over a solution droplet. This is discussed in more detail in Section 2.2. Using experimentally derived values of the van't Hoff factor, i, from McDonald (1953), Mason found that the numerical difference between his expression and that of Wright was never more than a few per cent except for small highly concentrated droplets. Values of i for eight electrolytes over a range of molality from 0.0001 have been tabulated by Low (1969) and these values are used in the calculations described in Chapter 2.

1.3 The Growth of Salt Nuclei with Humidity

Dessens (1949) was one of the first workers to study the growth of salt nuclei. He used large particles of sodium chloride and zinc chloride suspended from very fine spiders' webs in an unsaturated environment of controlled humidity. Similar results were obtained by Junge (1952a) who measured the equilibrium radii of artificial nuclei of calcium chloride and sodium chloride. He demonstrated (1952b) that the growth of atmospheric aerosol particles in continental air masses showed deviations from the theoretical predictions. The growth curves of individual particles showed considerable variation but the average values were rather uniform with little growth below about 70% relative humidity and a smaller growth above 70% than theory predicted for pure salts. This behaviour was explained at the time by a mixture of soluble and insoluble matter in each particle thus introducing the now generally accepted concept of "mixed nuclei".

Using mobility measurements to determine particle size Orr, Hurd and Corbett (1956) obtained reasonable agreement with the then available growth equations for particles of sodium chloride and calcium chloride and other salts with initial radius between 2×10^{-6}cm and 3×10^{-6}cm. More recently, Winkler and Junge (1972) have described a gravimetric method for determining the growth of atmospheric aerosol particles as a function of relative humidity. They found that the continental aerosol has a growth curve which indicates considerably less water absorption than for pure salts. In addition they found that the presence of insoluble matter in the particles has the effect of reducing total growth and of smoothing the growth curve.

Since sodium chloride in the form of sea-salt constitutes the largest single component of particulate matter in the atmosphere it was decided to study the growth of sodium chloride in the laboratory with increasing relative humidity. The recent work of Eggleton (1969) and Heard and Wiffen (1969) has shown ammonium sulphate to be another important constituent particularly in continental atmospheric aerosols. Heard and Wiffen have shown that on many occasions most of the particles in haze conditions are nearly pure ammonium sulphate. Twomey (1971) is of the opinion that most of the cloud nuclei over the sea are composed of ammonium sulphate, formed by gaseous reactions in the atmosphere over the continents. However, in spite of the importance of ammonium sulphate nuclei in the atmospheric aerosol few calcu-

lations of particle growth have been published. Both theoretical and experimental work on the growth of sodium chloride and ammonium sulphate particles with relative humidity are described in Chapters 2 and 4.

1.4 The Effect of Atmospheric Particles on Visibility

Solid and liquid aerosol particles in the atmosphere reduce the visibility. An important contribution to the lowering of visibility is made by the condensation of water vapour on particles at the higher values of relative humidity. In the most general case both scattering and absorption of light contribute to the extinction of light between object and observer. The general expression for light extinction is

$$I = I_o \exp(-\sigma l) \tag{1.3}$$

where I_o is the initial light intensity, I is the intensity after its passage along a distance l and σ is the extinction coefficient and is the sum of two terms,

$$\sigma = \sigma_{abs} + \sigma_{scatt} \tag{1.4}$$

Here σ_{abs} is due to absorption by gases and particles but is considered small compared with σ_{SCATT}. (Middleton, 1963). The scattering coefficient, σ_{SCATT} , is the dominant factor causing changes in visibility in the atmosphere. The extinction coefficient, σ, is related to the visibility by the Koschmieder relationship,

$$\text{Visual range} = \frac{3.91}{\sigma} \tag{1.5}$$

as derived by Middleton (1963, p. 105). Middleton also shows that the extinction coefficient for a monodisperse aerosol of particle radius a and concentration N is given by

$$\sigma = NK\pi a^2 \tag{1.6}$$

where K is the scattering area ratio or the ratio of the area of the wavefront affected by the particle to the cross-sectional area of the particle itself. K is a function of the particle radius to the wavelength, λ , of the incident radiation and of the refractive index of the particle. It is usually tabulated against the parameter $\alpha = 2\pi a/\lambda$ for specific values of the refractive index.

Interest in the relationship between relative humidity and visual range dates back at least to the studies of Wright (1939) in the atmospheric opacity at Valentia. His results showed that,

in maritime air, the atmospheric opacity varied with relative humidity in much the same way as theory would suggest for a sodium chloride aerosol. More recently, Garland (1969) has made a study of the effect of ammonium sulphate particles on visibility. This work will be discussed in more detail in Chapter 4. Hänel (1972) has computed extinction coefficients of atmospheric aerosol particles with relative humidity. His calculations are based on measurements of the density, refractive index and coefficient of mass increase with humidity of atmospheric aerosol. His results agree to within a few per cent with those obtained by Mie theory, which is the complete rigorous theory for the scattering of light by isotropic, spherical particles developed by Mie (1908).

Covert, Charlson and Ahlquist (1972) have measured the light scattering coefficient of artificially produced nuclei in the laboratory over a wide range of humidity, with an integrating nephelometer. However, Their results have not been compared with predicted values of the extinction coefficient.

The effect of particle mass on the extinction coefficient for monodisperse aerosols of sodium chloride and ammonium sulphate is studied in Chapter 2. In addition, the influence of a range of particle size distributions on the extinction coefficient as the relative humidity is varied is examined.

1.5 Aerosol Particle Size Distributions

The size and concentration of atmospheric aerosol particles influences the rate of growth of cloud droplets and also affects visibility. A considerable amount of experimental work has been carried out in an attempt to understand the natural variations in particle concentration and size distribution, particularly for the large and giant nuclei. Junge (1953) used a two stage konimeter to determine the size distribution of the aerosol at Frankfurt, in the Zugspitze and on Mount Taurus. He found that particles of radius $r > 0.1$ micrometres obeyed a size distribution law of the form

$$n(r) = \frac{dN}{d(\log r)} \tag{1.7}$$

where dN is the number of particles in the radius interval d(log r). Equation 1.7 means that the particles in each logarithmic interval of radius contribute equally to the mass concentration of the aerosol.

Cartwright et al. (1956) used an electron microscope to size

particles, collected by a thermal precipitator, in the radius range 0.03 to 0.9 micrometres. Twomey and Severynse (1964) determined the size distribution of the natural aerosol by means of a diffusion battery in conjunction with a photoelectric nucleus counter at various stages of diffusional decay. Friedlander and Pasceri (1967) measured the size distribution in the radius range 0.4 to 20 micrometres using a four stage Casella impactor. They found good agreement with the Junge form of the size distribution curve.

At the International Workshop on Condensation and Ice Nuclei (1971), Whitby and Husar found that the natural aerosol measured at Fort Collins, Colorado was similar to that obtained by Junge in the South Atlantic. Whitby and Husar used the Minnesota Aerosol Analysing System (MAAS) to make their measurements. This system consists of an optical particle counter operating in the radius range from 0.6 to 12 micrometres, an electrical aerosol analyser operating over the range 0.0075 to 0.6 micrometres and a condensation nucleus counter for the Aitken nuclei range.

Junge and Jaenicke (1971) have presented background aerosol particle size distribution data collected during the Atlantic Expedition of the R. V. Meteor over 24 days from April 13th., 1969. The following apparatus wasused to cover the whole size range of natural aerosols: The rotating impactor covering the size range from 20 to 100 micrometres radius; asingle stage nozzle impactor covering the size range from 3 to 30 micrometres radius; a set of double impactors for the range from 0.1 to 0.7 micrometres; a Royco 220 optical particle counter for the size range from 0.3 to 3 micrometres; a photographic condensation nucleus counter constructed to cover small concentrations in the range from 0.01 to 0.2 micrometres and a diffusion battery to cover the smallest size range from about 0.01 down to about 0.001 micrometres radius. As stated by the authors, further details in addition to the total concentration measured by each instrument would have overcrowded their diagram (Figure 4). They found two maxima in the particle size distribution curve, one above 0.1 micrometre and the other at the small particle end. The distribution above 0.3 micrometres radius shows a steady decrease uninterrupted by secondary maxima.

Whitby et al. (1975) presented particle size distribution data for a 24 hour period on 19th. and 20th. September 1972 of aerosol sampled along the Harbor Freeway in Los Angeles, California.

Four aerosol particle counting instruments were used and consisted of a condensation nucleus counter, a Whitby Aerosol Analyser System and a pair of Royco 220 and 245 optical particle counters. The last three instruments had operating particle radius ranges of 0.005-0.211, 0.211-2.81 and 2.81-19.0 micrometres. They found that the fresh freeway aerosol is mostly below 0.075 micrometres in radius.

In Chapter 5 measurements are presented of the natural aerosol size distribution in the radius range 0.25 to 5.0 micrometres using a calibrated Royco model 225 particle counter. Continuous measurements were made at Durham Observatory over a 49 day period from July 21st. to September 8th. 1975. A correlation analysis of these measurements with the more common meteorological variables is carried out.

CHAPTER 2

THE THEORETICAL GROWTH OF HYGROSCOPIC PARTICLES WITH HUMIDITY AND THE EFFECT ON VISIBILITY

2.1 Introduction

The theory of the growth of water soluble aerosol particles has been considered by many workers, for example by Orr et al. (1958), Low (1969), Hänel (1970) and Mason (1971). There have been three different approaches in the theoretical treatment of the growth of soluble particles with humidity.

Firstly, a growth equation was developed by Mason (1971) which used experimental values of the van't Hoff factor determined by McDonald (1953). Low (1969) derives an analytical expression for the growth equation, using the mean ionic activity coefficient γ as the fundamental parameter upon which the solution effect on particle growth depends. Abundant experimental data on γ is available and possesses the advantage that important properties such as the lowering of vapour pressure in electrolytic solutions can be readily computed.

The third approach, used by Hänel (1970), is based on the measured values of the volume and mass increase of atmospheric aerosol particles and appears to be valid over the entire humidity range. Hänel's growth equations can only be applied to bulk atmospheric aerosol for which the variation of mass with humidity is known.

The theoretical growth of aerosol particles of sodium chloride and ammonium sulphate with humidity is outlined in the following sections. The fundamental growth equation is broadly based on the treatment by Mason (1971). Some new procedures and approximations are used in the application of the growth equation to the prediction of aerosol particle size with varying humidity. A comparison is made between the growth curves and those plotted by Mason.

The effect of particle growth on visibility is also examined using approximations to Mie's theory due to Diermendjian (1960) and Penndorf (1962). Extrapolation procedures similar to those described above are used to predict the variation of particle refractive index with solution concentration. The results are compared with work carried out by Garland (1969) and Hänel (1971). A study is also made of the effect of particle mass and particle size dis-

tribution for sodium chloride and ammonium sulphate on the extinction coefficient σ.

2.2 Derivation of an equation relating Particle Radius to Humidity

The vapour pressure P_r over a droplet of pure water of radius r exceeds that over a plane water surface P_∞ at the same temperature in accordance with the expression

$$\frac{P_r}{P_\infty} = \exp\left(\frac{2\sigma M}{RTr}\right) \tag{2.1}$$

where σ is the surface tension of the droplet, M is the molecular weight of water, R is the universal gas constant and T is the absolute temperature.

Thus the minimum supersaturation at which the droplet can exist is given by

$$S = \left[\exp\left(\frac{2\sigma M}{RTr}\right) - 1\right] \times 100 \tag{2.2}$$

At this supersaturation particles smaller than r will evaporate while larger particles will grow indefinitely as water condenses onto their surface.

The effect of a dissolved salt in the droplet is to reduce the vapour pressure over its surface. For a solution of constant concentration this can be described by the relation

$$\frac{P_{r'}}{P'_\infty} = \exp\left(\frac{2\sigma' V'_w}{RTr'}\right) = \delta \tag{2.3}$$

where the dashed quantities are defined as above but refer to the solution droplet. V_w' is the partial molar volume of water in the solution and δ is known as the curvature correction.

Since the solution concentration is a function of the droplet radius r' the vapour pressure over the plane solution also depends on r'. The vapour pressure $P_{r'}$ over the surface of solution droplet exceeds that over a plane surface of the solution according to the expression

$$\frac{P_{r'}}{P_\infty} = \frac{P'_\infty(r')}{P_\infty} \exp\left(\frac{2\sigma' V'_w}{RTr'}\right) \tag{2.4}$$

The following approximation is used in the calculations:

$$V'_w \simeq V_w \simeq \frac{M}{\rho} \tag{2.5}$$

where ρ is the density of pure water and V_w is the molar volume of pure water. Use of this approximation, as shown by a close examination of the measured densities of aqueous solutions, has been

made by Hänel (1970). On the other hand numerous authors including Orr (1958), Mason (1971), Low (1969) use M/ρ' in place of the partial molar volume of water in the solution, V_w', which leads to substantial error, particularly for small droplets, as indicated in Table 2.1 from Hänel (1970).

$\frac{P_{\infty}'}{P_{\infty}}$	V_w' (cm^3/Mol)	$\frac{M_w}{\rho'}$ (cm^3/Mol)
0.76	17.80	15.04
0.80	17.84	15.36
0.85	17.89	15.79
0.90	17.95	16.35
0.95	18.01	17.05
1.00	18.05	18.05

Table 2.1 The difference between the partial molar volume of water, V_w', and the ratio $\frac{M_w}{\rho'}$ of the molecular weight of water to the solution density as a function of the vapour pressure ratio $\frac{P_{\infty}'}{P_{\infty}}$ for aqueous NaCl at 18°C.

It can be seen from the table that V_w' differs from V_w the molar volume of pure water by less than 3% as the humidity is varied from 76 to 100 per cent.

Equation 2.4 can now be written as

$$\frac{P_r'}{P_{\infty}} = \frac{P_{\infty}'(r')}{P_{\infty}} \exp\left(\frac{2\sigma' M}{\rho R T r'}\right) \tag{2.6}$$

Mason (1971) has derived an expression for $\frac{P_{r'}}{P_{\infty}}$ which is of the form

$$\frac{P_r}{P_{\infty}} = \left[1 + \frac{i m_o M}{W\left(\frac{4}{3}\pi r^3 \rho' - m_o\right)}\right]^{-(\rho/\rho')} \exp\left(\frac{2\sigma' M}{\rho' R T r'}\right) \tag{2.7}$$

where m_o is the mass of the dry solute, W is the molecular weight of the solute and i is the van't Hoff factor.

Direct comparison of Equations 2.6 and 2.7 can be made, noting that a different approximation for V_w' has been made in each case. This yields the result

$$\frac{P_{\infty}'(r')}{P_{\infty}} = \left[1 + \frac{i m_o M}{W\left(\frac{4}{3}\pi r'^3 \rho' - m_o\right)}\right]^{-(\rho/\rho')} \tag{2.8}$$

so Equation 2.6 now becomes

$$\frac{P_{r'}}{P_{\infty}} = \left[1 + \frac{i m_o M}{W\left(\frac{4}{3}\pi r'^3 \rho' - m_o\right)}\right]^{-(\rho/\rho')} \exp\left(\frac{2\sigma' M}{\rho R T r'}\right) \tag{2.9}$$

When the droplet is in equilibrium with the surrounding

atmosphere the vapour pressure over its surface, $P_{r'}$, must equal the partial pressure of water in the air.

Hence
$$\frac{P_{r'}}{P_\infty} = \frac{H}{100}$$
where H is the relative humidity of the air.

Equation 2.9 now becomes
$$\frac{H_{r'}}{100} = \left[1 + \frac{im_0M}{W\left(\frac{4}{3}\pi r'^3\rho' - m_0\right)}\right]^{-(\rho/\rho')} \exp\left(\frac{2\sigma'M}{\rho RTr'}\right) \qquad (2.10)$$

This equation can be used to calculate the radius of the solution droplet in equilibrium with the atmosphere at a specified relative humidity.

Using r_o as the equivalent radius of the dry particle we may write
$$m_0 = \frac{4}{3}\pi r_0^3 \rho_0 \qquad (2.11)$$
where ρ_0 is the density of the dry particle.

From this we obtain the result
$$H_{r'} = \left\{1 + \frac{iM}{W}\left[\frac{1}{\frac{\rho'}{\rho_0}\left(\frac{r'}{r_0}\right)^3 - 1}\right]\right\}^{-(\rho/\rho')} \exp\left(\frac{2\sigma'M}{\rho RTr'}\right) \times 100\% \qquad (2.12)$$

At a temperature T of 25°C (T = 298K), the parameters ρ, M and R possess the values 0.997g cm^{-3}, 18.02g and 8.317×10^7 erg $mole^{-1}K^{-1}$ respectively.

Therefore we can write Equation 2.12
$$H_{r'}(25°C) = \left\{1 + \frac{18{,}02i}{W}\left[\frac{1}{\frac{\rho'}{\rho_0}\left(\frac{r'}{r_0}\right)^3 - 1}\right]\right\}^{-(\rho/\rho')} \exp\left(1{,}459\times10^{-9}\,\frac{\sigma'}{r'}\right) \times 100\% \qquad (2.13)$$

2.3 Use of the Growth Equation

Equation 2.13 is the fundamental equation relating humidity to particle radius. The following procedures are used when the equation is applied since the surface tension, density and van't Hoff factor are all functions of solution concentration (and therefore droplet size). Moreover the van't Hoff factor cannot be expressed in an analytical form.

Approximate relations based on known experimental values were used and extrapolated where necessary.

(a) Molality of the solution

The molality (η) of a solution is defined by the equation
$$\eta = \frac{1000}{M}\,\frac{n_s}{n} \qquad (2.14)$$

where n_s is the number of moles of solute and n the number of moles of solvent. M is the molecular weight of pure water.

For a droplet containing dissolved salt the dry mass of which is m_o,

$$n_s = \frac{m_o}{W} \tag{2.15}$$

where W is the molecular weight of the salt and,

$$n = \frac{m' - m_o}{M} \tag{2.16}$$

where m' is the mass of the solution droplet.

Therefore

$$m_l = \frac{1000}{M}\left(\frac{M}{W}\right)\frac{m_o}{m' - m_o}$$

$$= \frac{1000}{W}\frac{1}{\left(\frac{m'}{m_o} - 1\right)} \tag{2.17}$$

Using equation 2.11 and the relation

$$m' = \frac{4}{3}\pi\rho'(r')^3 \tag{2.18}$$

we obtain the result

$$m_l = \left(\frac{1000}{W}\right)\frac{1}{\left[\frac{\rho}{\rho_o}\left(\frac{r'}{r_o}\right) - 1\right]} \tag{2.19}$$

The percentage concentration of the solution can be expressed as

$$p = 100\left(\frac{\rho_o}{\rho'}\right)\left(\frac{r_o}{r'}\right)^3 \tag{2.20}$$

(b) The density of salt solution as a function of the percentage concentration

The density of various salt solutions is tabulated as a function of the percentage concentration (Handbook of Chemistry and Physics, 43rd. ed., published by Chemical Rubber Co., 1961). The relationship is approximately linear with increasing concentration for sodium chloride and ammonium sulphate until the saturated solution level is reached. Values in the supersaturated region are not known but the density of the dry particle (p = 100%) does not lie on the extrapolated straight line but rather above it. In order to extrapolate the curve into the supersaturated region a quadratic function has been fitted to the data as shown in Figures 2.1 and 2.2. The functions used are given by Equations 2.21 and 2.22 for sodium chloride and ammonium sulphate respectively.

Figure 2,1 Density as a Function of Solution Concentration (NaCl)

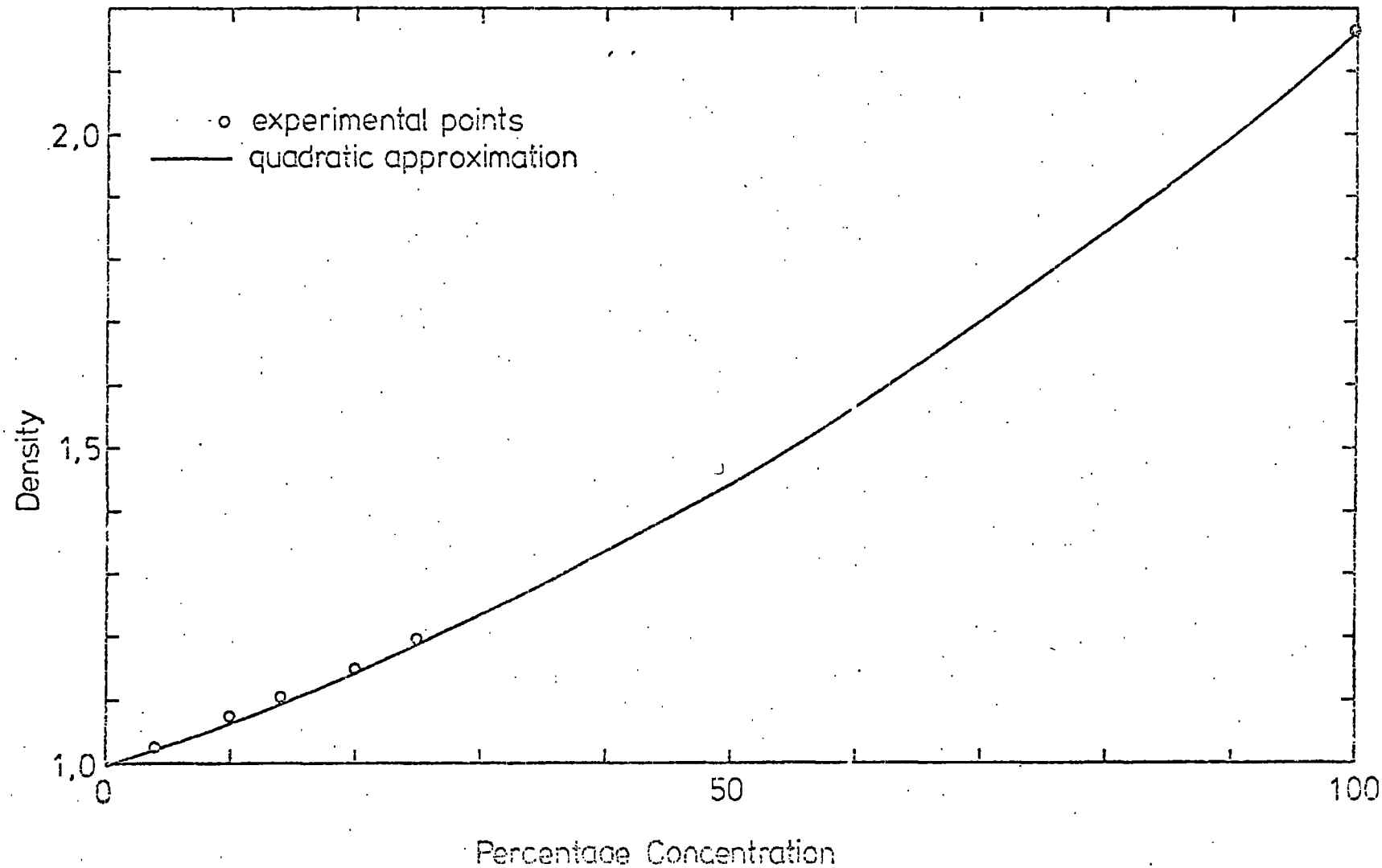

Figure 2,2 Density as a Function of Solution Concentration $(NH_4)_2SO_4$

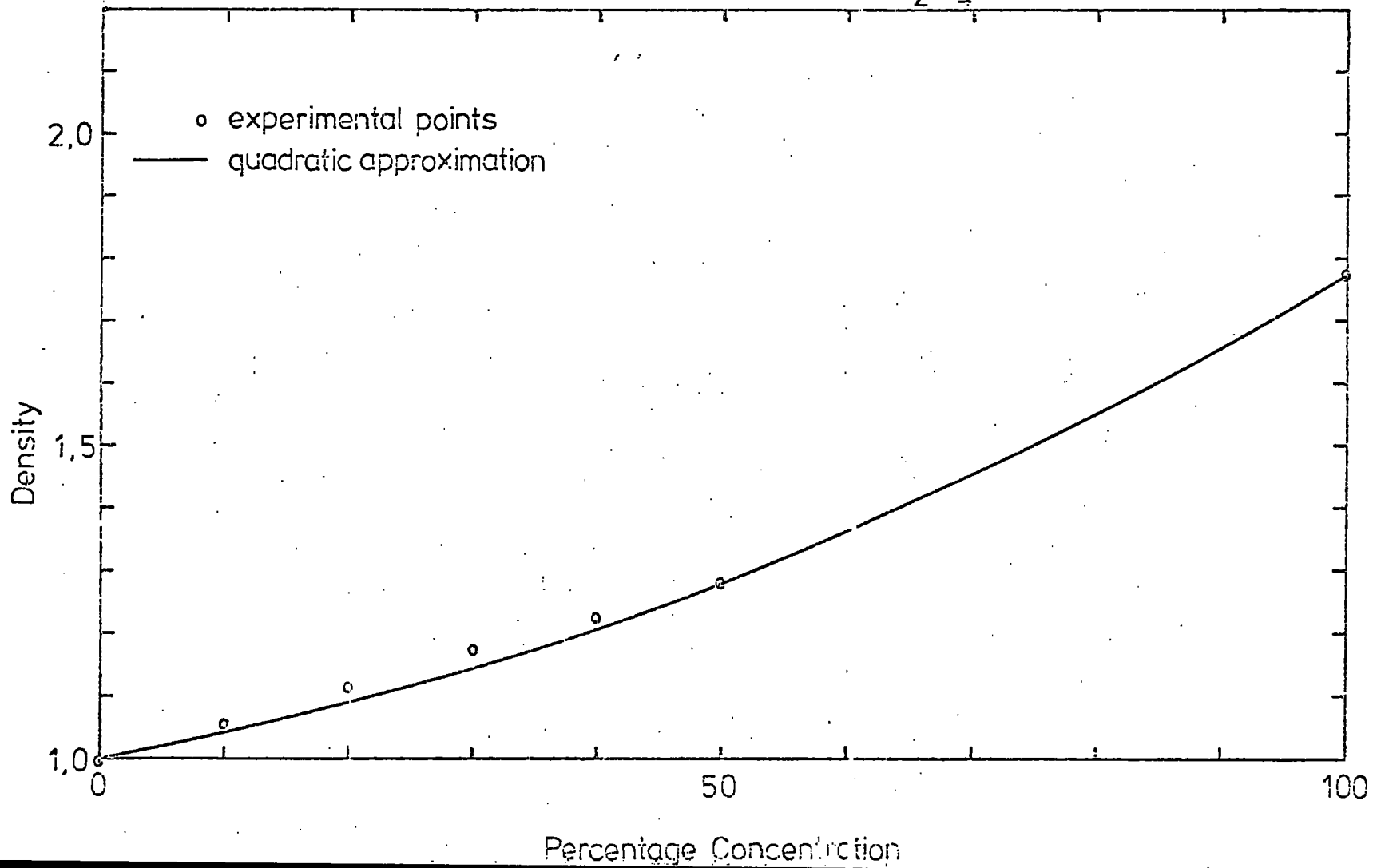

Figure 2,3 Percentage Concentration Versus $(r/r_o)^3$ (NaCl)

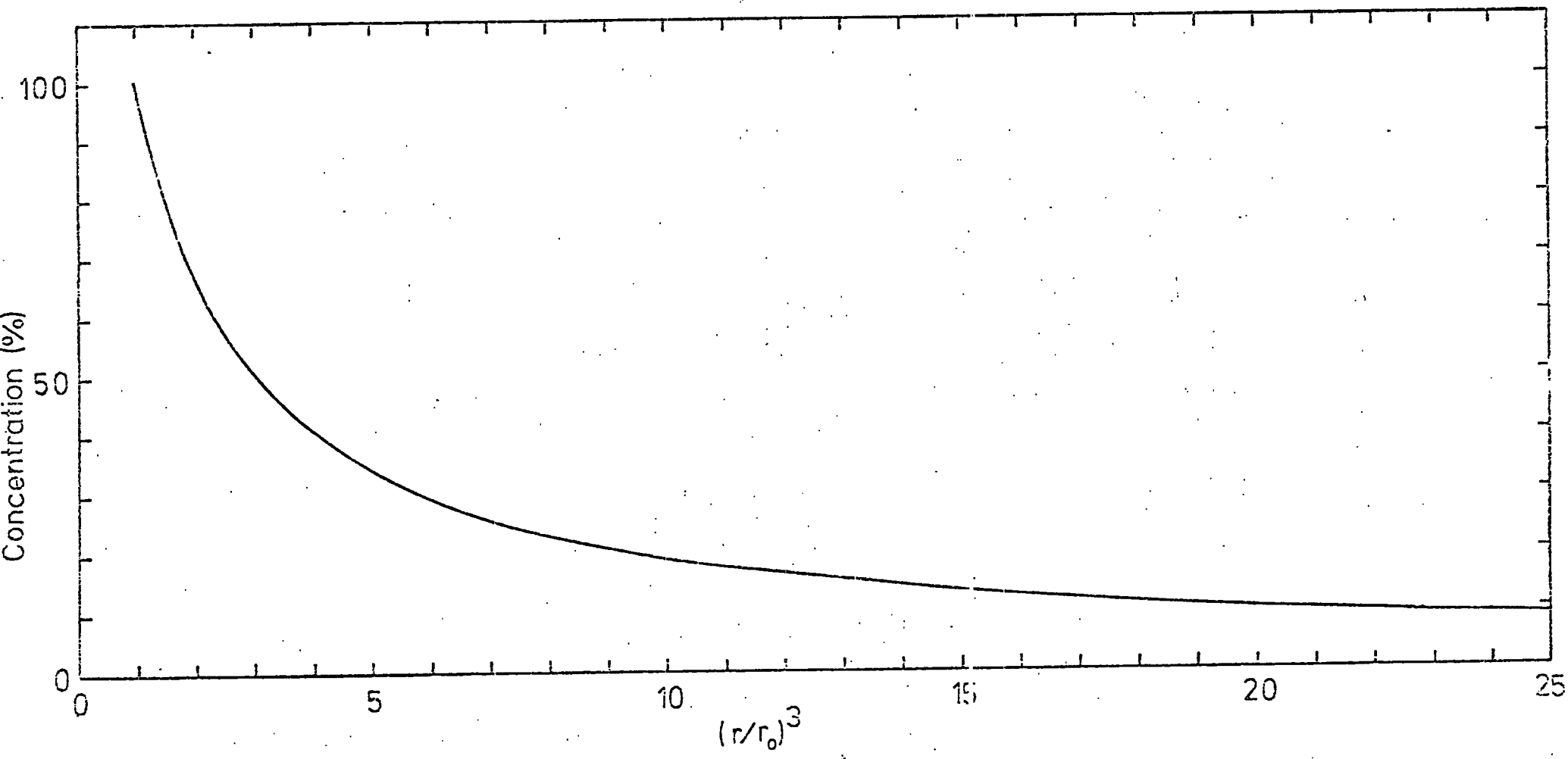

$$\rho' = 5{,}45\times10^{-5}\,p^2 + 6{,}20\times10^{-3}\,p + 0{,}999 \qquad (2.21)$$

$$\rho' = 4{,}08\times10^{-5}\,p^2 + 3{,}61\times10^{-3}\,p + 0{,}999 \qquad (2.22)$$

Given a quadratic fit of the form

$$\rho' = Ap^2 + Bp + C$$

Equation 2.20 assumes the form

$$\left(\frac{r'}{r_o}\right)^3 = \frac{100\,\rho_o}{Ap^3 + Bp^2 + Cp}$$

or

$$Ap^3 + Bp^2 + Cp - 100\rho_o\left(\frac{r_o}{r'}\right)^3 = 0 \qquad (2.23)$$

so the solution concentration can be evaluated if the droplet radius, r', is known. The relationship between the solution concentration, p, and $\left(\frac{r'}{r_o}\right)^3$, where r_o is the radius of the dry particle, is shown in Figure 2.3 for sodium chloride, for which ρ_o is equal to 2.165g cm^{-3}.

(c) The surface tension as a function of molality

Linear equations of the form given below for sodium chloride (Equation 2.24) and ammonium sulphate (Equation 2.25) were found to fit the curves of the variation of surface tension with molality given by Low (1969a).

$$\sigma' = 1{,}623m + 72{,}78 \qquad (2.24)$$

$$\sigma' = 2{,}165m + 72{,}78 \qquad (2.25)$$

(d) The van't Hoff factor, i

Low (1969a) has tabulated the van't Hoff factor, i, as a function of molality in the range 0.0001 to 6 for sodium chloride and 0.0001 to 5.5 for ammonium sulphate. At lower molalities i tends towards the value 2.0 for sodium chloride and 3.0 for ammonium sulphate.

The highest molality tabulated in both cases corresponds to the saturated solution. In order to attempt to describe the properties of the supersaturated solution it is necessary to assume that the experimental data can be extrapolated. Cubic equations of the form given below were found to be a good approximation to the data at the higher concentrations. It is assumed that they continue to describe the behaviour of the solutions up to molalities

of the order of 20.

For sodium chloride the cubic equation, fitted to Low's data at molalities of 1, 2, 4 and 6, is

$$i = 1{,}81736 + 6{,}13368 \times 10^{-2} m + 2{,}61582 \times 10^{-2} m^2 - 9{,}33083 \times 10^{-4} m^3 \qquad (2.26)$$

The equation for ammonium sulphate, using molalities of 3, 4, 5 and 5.5 is

$$i = 1{,}74017 + 5{,}77993 \times 10^{-2} m + 1{,}19040 \times 10^{-2} m^2 - 5{,}25333 \times 10^{-4} m^3 \qquad (2.27)$$

A good fit was obtained using these equations as can be seen in Figures 2.4 and 2.5, where the van't Hoff factor, i, is plotted as a function of molality, m, for sodium chloride and ammonium sulphate respectively. The use of the extrapolated values obtained from Equations 2.26 and 2.27 is fully justified since the particle growth curve indicates a smooth variation as low as 40% relative humidity as seen in Figures 2.6 to 2.9. The following procedure for solving the growth equation for a salt solution at a particular radius, r', for selected values of density, ρ_o, and initial dry particle radius, r_o, using the described interpolation equations, was adopted:

(i) The percentage concentration, p, of the solution was evaluated using the cubic equation 2.23.

(ii) The density of the salt solution was calculated from expressions 2.21 and 2.22.

(iii) The molality of the solution was calculated using Equation 2.19.

(iv) The surface tension, σ', of the solution was obtained from Equations 2.24 and 2.25.

(v) The values of the van't Hoff factor, i, were taken from Low (1969a) up to a molality of 6.0 for sodium chloride and 5.5 for ammonium sulphate. For higher molality values i was obtained by the use of Equations 2.26 and 2.27 as described earlier in this section.

(vi) The above parameters were then substituted into Equation 2.13 which gives the humidity at which a particle of radius r' is in equilibrium with the surrounding atmosphere. An IBM 370/168 computer was used in the numerical side of the equation.

No attempt has been made to predict the recrystallisation of the droplets with decreasing humidity. The transition from solid to solution droplets has been considered by Orr et al. (1958) but

Figure 2,4 The van't Hoff factor for sodium chloride as a function of molality

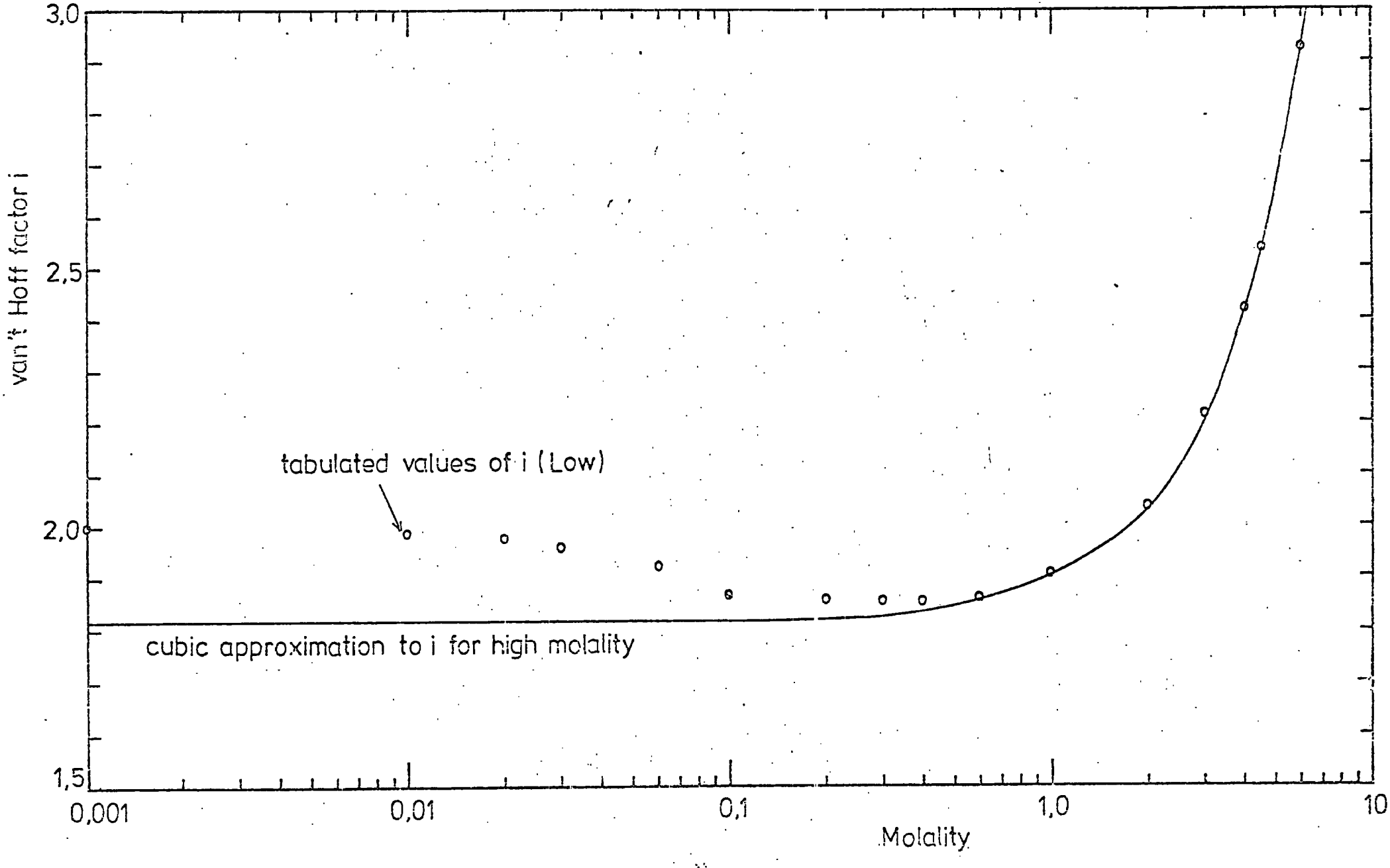

Figure 2,5 The van't Hoff factor for ammonium sulphate as a function of molality

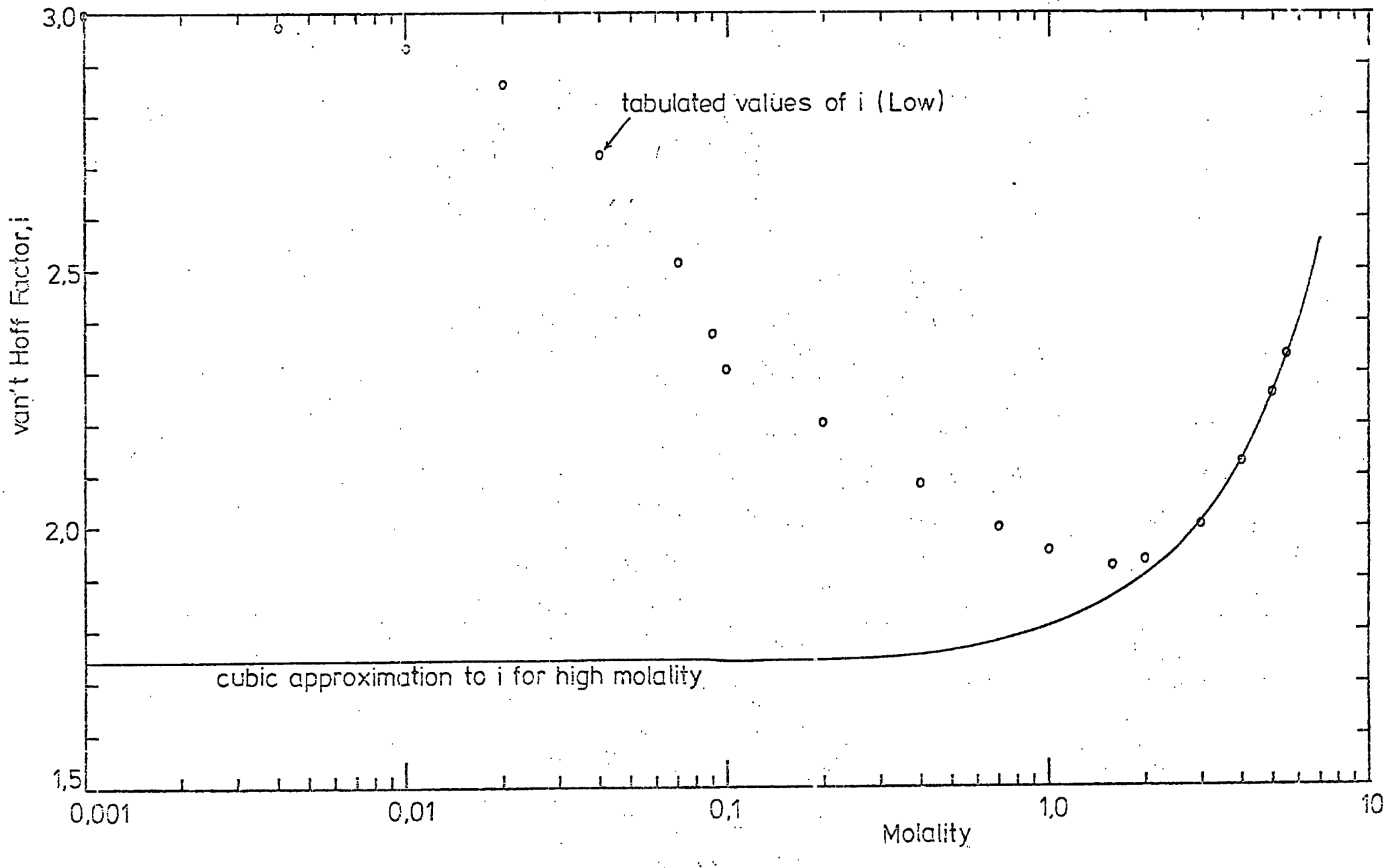

no satisfactory theory of the recrystallisation point has yet been evolved.

The growth curves for sodium chloride and ammonium sulphate obtained by the above procedure are shown in Figures 2.6 to 2.9. The growth of dry sodium chloride particles with humidity over the initial radius ranges of 1.5×10^{-6}cm to 1.5×10^{-5}cm and 1.5×10^{-5}cm to 1.5×10^{-4}cm can be seen in Figures 2.6 and 2.7 respectively. Similar curves over the same two initial radius ranges are drawn for ammonium sulphate nuclei as shown in Figures 2.8 and 2.9. Good agreement was found to exist between the growth curves derived for the sodium chloride particles with those calculated by Mason (1971). The extent of the agreement in evident in the comparison of the tabulated values of particle radius versus humidity obtained from the analysis outlined in Sections 2.2 and 2.3 with those obtained by Mason (Table 2.2). The solute mass was chosen as 10^{-15}gm which corresponds to a dry particle radius of 4.8×10^{-6}cm. It can be seen that the agreement is within 0.5% over the range of humidity shown.

Good agreement is also found between the growth curves computed here for ammonium sulphate and those plotted in Figure 1 of Garland (1969).

Particle radius (μm)	Relative humidity (%)		Difference (%)
	Equation 2.13	Mason	
0.084	72.9	72.6	0.31
0.096	83.7	83.6	0.18
0.108	89.5	89.4	0.12
0.120	92.9	92.8	0.07
0.144	96.2	96.2	0.03

Table 2.2 Comparison of the growth curves computed using Equation 2.13 with those due to Mason. A solute mass of 10^{-15}gm has been used.

2.4 The effect of particle growth on visibility

It is clear that the presence of suspended matter will affect the transmission of light through a medium. In the case of an aerosol the nature of the effect depends on the particle size in relation to the wavelength of light. A convenient

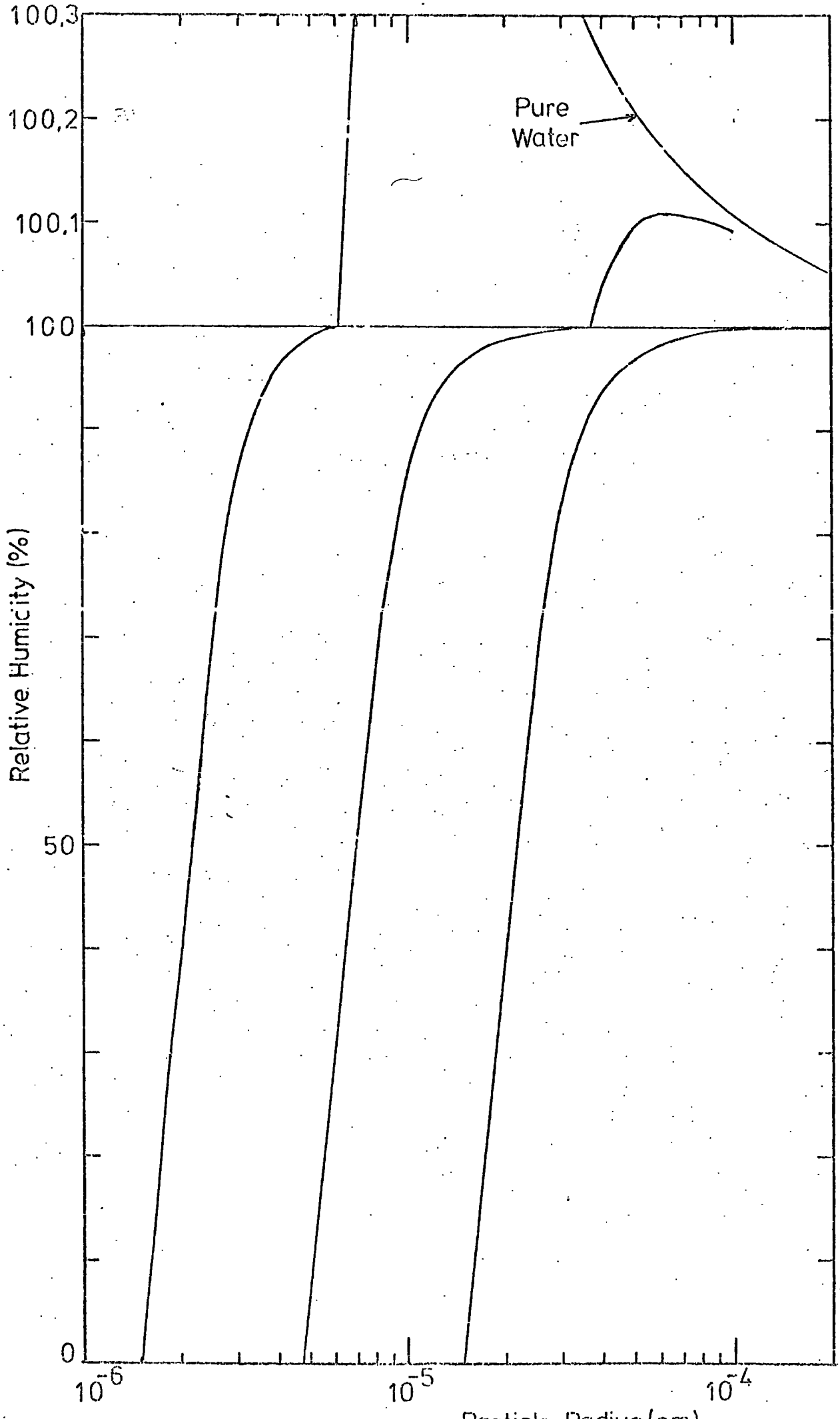

Figure 2.6 Selected theoretical growth curves of sodium chloride.

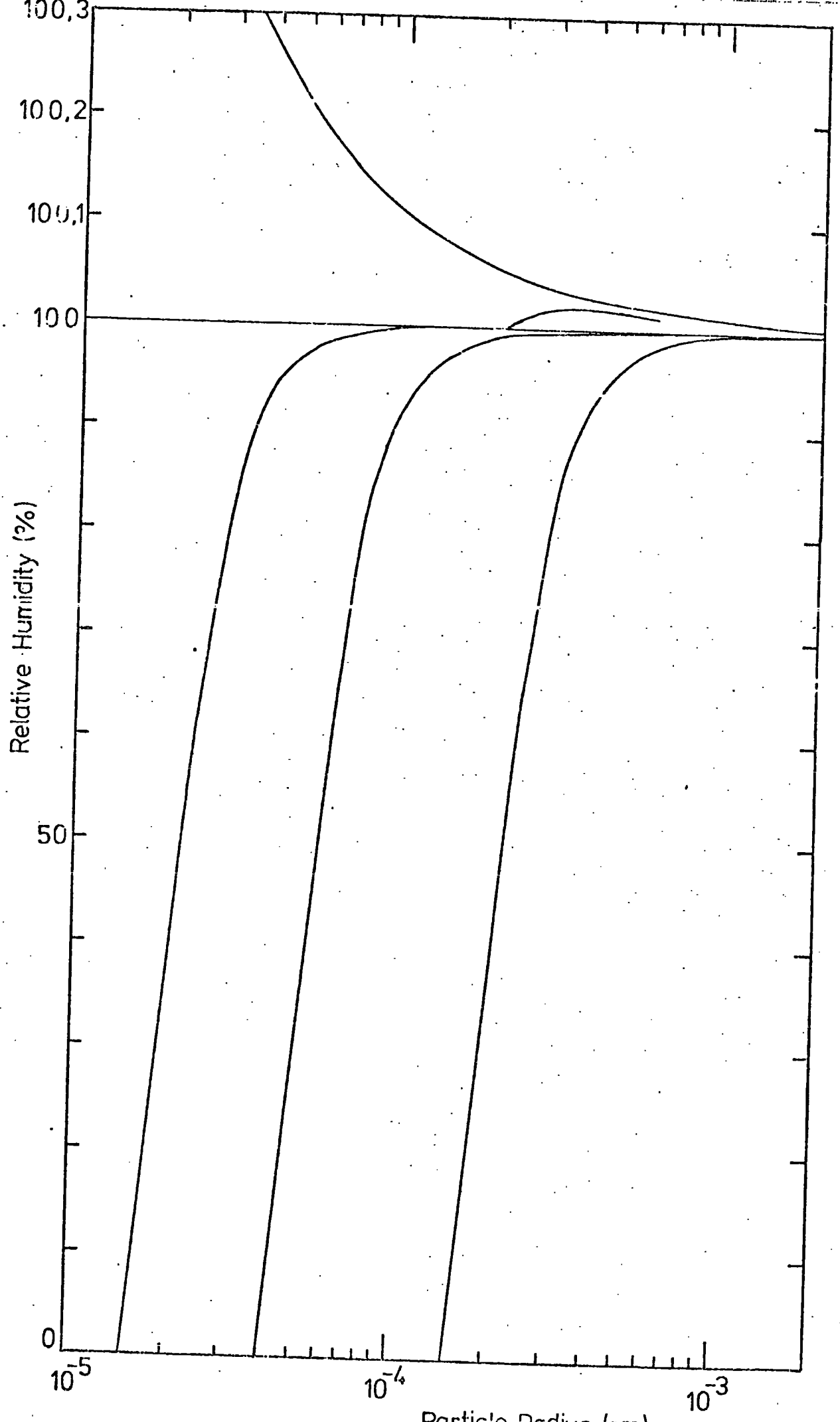

Figure 2.7 Selected theoretical growth curves of sodium chloride.

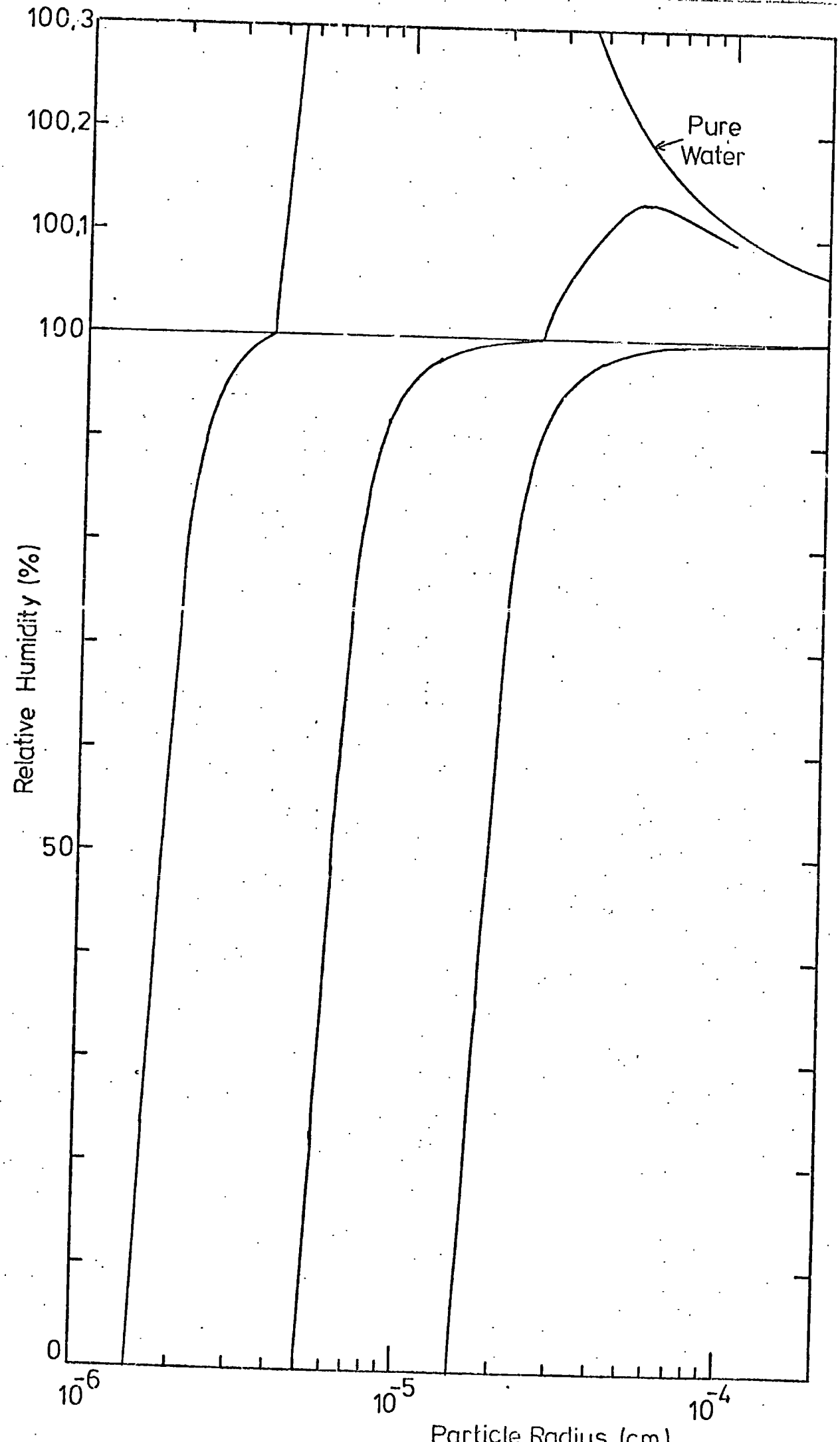

Figure 2.8 Selected theoretical growth curves of ammonium sulphate

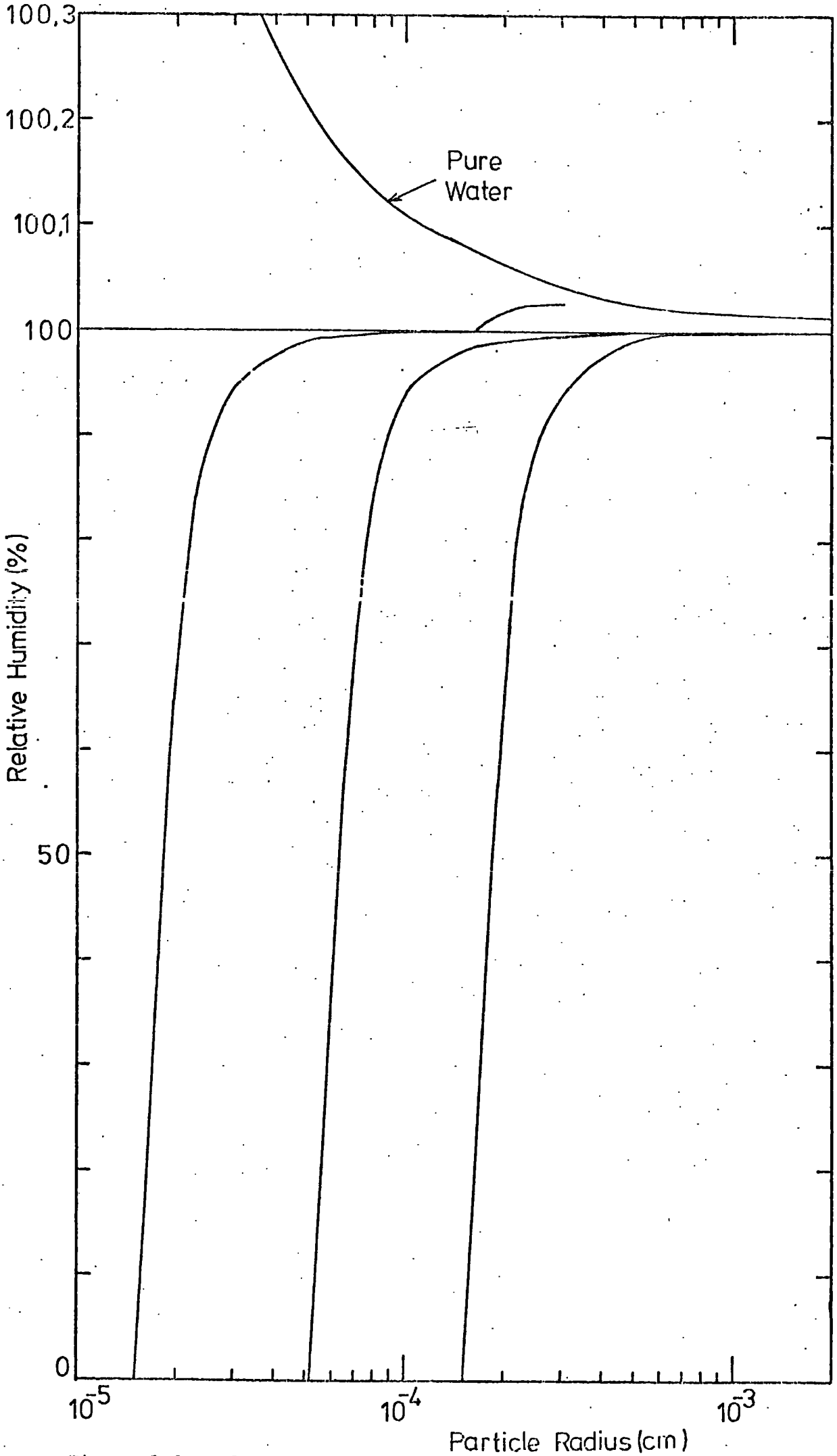

Figure 2.9 Selected theoretical growth curves of ammonium sulphate

parameter that can be used in consideration of this relationship is defined by the following relation

$$\alpha = \frac{2\pi r}{\lambda} \tag{2.28}$$

α is known as the size parameter, r is the particle radius and λ is the wavelength of light.

When $\alpha \ll 1$ light scattering through an aerosol can be described by the Rayleigh law, which is of the form:

$$\beta'(\phi,\lambda) = A\,\lambda^{-4}(1+\cos^2\phi) \tag{2.29}$$

that is to say, that the light scattered in any direction, ϕ, is proportional to the inverse fourth power of the wavelength. A is a constant in the above equation and β' is known as the volume scattering function (Middleton, 1952).

When $\alpha \sim 1$ that is, when the particle radius is about the same size as the wavelength of light, it is necessary to consider the variation of the electromagnetic fields inside and outside a small sphere and solve the differential equations that this treatment yields. This has been done by Mie (1908) and subsequently by several other workers, for example Stratton and Houghton (1931) and Sinclair (1947).

In view of the complexity of the analytical treatment, approximations to Mie's results will be used in the following treatment of light extinction.

Following the procedure outlined by Middleton (1952), the extinction coefficient, σ, can be expressed as

$$\sigma = N\pi r^2 K \tag{2.30}$$

for a monodisperse aerosol of particle radius r and N particles per unit volume. K is known as the scattering area ratio since it is the ratio of the area of the wavefront acted upon by the particle to the area of the particle itself. If the aerosol is polydisperse the extinction coefficients of all the monodisperse components can be added together with the result that the extinction coefficient is given by the relation

$$\sigma = \sum_{i=1}^{n} N_i \pi r_i^2 K_i \tag{2.31}$$

where n is the number of different particle sizes and N_i is the particle number concentration of particles of radius r_i.

If the extinction coefficient can be found, a value of the visibility can be obtained using the visual range, V, which is defined by Middleton (1952) as

$$V = \frac{3.912}{\sigma} \tag{2.32}$$

Solution of Equation 2.31 is straightforward if K is known. Tabulated values of K as a function of α and the refractive index may be used but these are only available for refractive indices with the values 1.33, 1.44, 1.55 and 2.00. Approximate equations for K have been derived by Penndorf (1962) and Diermendjian (1960) and are used in the following calculations.

If the refractive index, μ, of the material under consideration is expressed in the complex form

$$\mu = n + ik \tag{2.33}$$

then the approximation of Diermendjian can be written as

$$K_i = (1+D)\left\{2 - \frac{4\cos g}{\rho}\exp(-\rho\tan g)\sin(\rho-g) + 4\left(\frac{\cos g}{\rho}\right)^2\left[\cos 2g - \exp(-\rho\tan g)\cos(\rho-2g)\right]\right\} \tag{2.34}$$

where

$$\rho = \frac{4\pi r_i}{\lambda}(n_i-1), \qquad g = \arctan\left(\frac{k_i}{n_i-1}\right)$$

$$D = \frac{(n_i-1)^2}{1.632 n_i}\left[f(g)+1\right] + \frac{0.2\rho - (n_i-1)}{f(g)(n_i-1)} \qquad \text{for } \rho \leq 5(n_i-1)$$

$$D = \frac{(n_i-1)}{8.16 n_i}\left[f(g)+1\right]\rho \qquad \text{for } 5(n_i-1) \leq \rho \leq \frac{4.08}{1+3\tan g}$$

$$D = \frac{(n_i-1)[f(g)+1]}{2n_i(1+3\tan g)} \qquad \text{for } \frac{4.08}{1+3\tan g} \leq \rho \leq \frac{4.08}{1+\tan g}$$

$$D = \frac{2.04(n_i-1)[f(g)+1]}{n_i \rho f(g)} \qquad \text{for } \rho > \frac{4.08}{1+\tan g}$$

and $f(g) = 1 + 4\tan g + 3\tan^2 g$

Penndorf's approximation, given below, is used when $\alpha_i = \frac{2\pi r_i}{\lambda} \leq 1$

$$K_i = A\alpha_i + B\alpha_i^3 + C\alpha_i^4 \tag{2.35}$$

where

$$A = \frac{24 n_i k_i}{Z_1}$$

$$B = \frac{4}{15} n_i k_i + \frac{20 n_i k_i}{3 Z_2} + \frac{24}{5} n_i k_i \frac{\left[7(n_i^2+k_i^2)^2 + (4n_i^2 - k_i^2 - 5)\right]}{Z_1^2}$$

$$C = \frac{8}{3}\left\{\left[(n_i^2+k_i^2)^2 + (n_i^2 - k_i^2 - 2)\right]^2 - 36 n_i^2 k_i^2\right\} / Z_i^2$$

$$Z_1 = (n_i^2 + k_i^2)^2 + 4(n_i^2 - k_i^2) + 4$$

$$Z_2 = 4(n_i^2 + k_i^2)^2 + 12(n_i^2 - k_i^2) + 9$$

2.5 Use of the Visibility equations

The calculations on the variation of visibility with relative humidity were performed using a wavelength of 0.55 micrometres for light. This corresponds to an average wavelength in the range over which the human eye is sensitive. It was assumed that the imaginary part of the refractive index was zero which means that absorption of light by the particles is not accounted for. This assumption is justified by the negligible or zero values of the imaginary part of the refractive index given by Hänel (1972) for bulk atmospheric aerosol. Linear approximations to the real part of the refractive indices for sodium chloride and ammonium sulphate respectively are given below as functions of the percentage concentrations of the solutions

$$\mu = 0{,}00177p + 1{,}333 \qquad (2.36)$$

$$\mu = 0{,}00158p + 1{,}333 \qquad (2.37)$$

The approximation relations are plotted in Figures 2.10 and 2.11 and show good agreement with the tabulated values given in the Handbook of Chemistry and Physics, 50th. ed., published by the Chemical Rubber Co., 1969. The values of the extinction coefficient were calculated as a function of relative humidity and particle mass by means of a computer program. The particle number concentration was chosen to correspond to one microgram of salt per cubic metre which means that the curves for ammonium sulphate can be compared with those of Garland (1969).

The extinction coefficient, σ, of an atmosphere containing one microgram of ammonium sulphate per cubic metre is plotted in Figure 2.12 for the following size distributions:

a) A monodisperse aerosol at the mass median radius of 0.21 micrometres of an idealised Junge type distribution shown in Figure 2.13

b) A monodisperse aerosol at the mass median radius of 0.3 micrometres of a distribution measured by Heard and Wiffen (1969)

Figure 2,10 Refractive Index as a Function of Solution Concentration (NaCl)

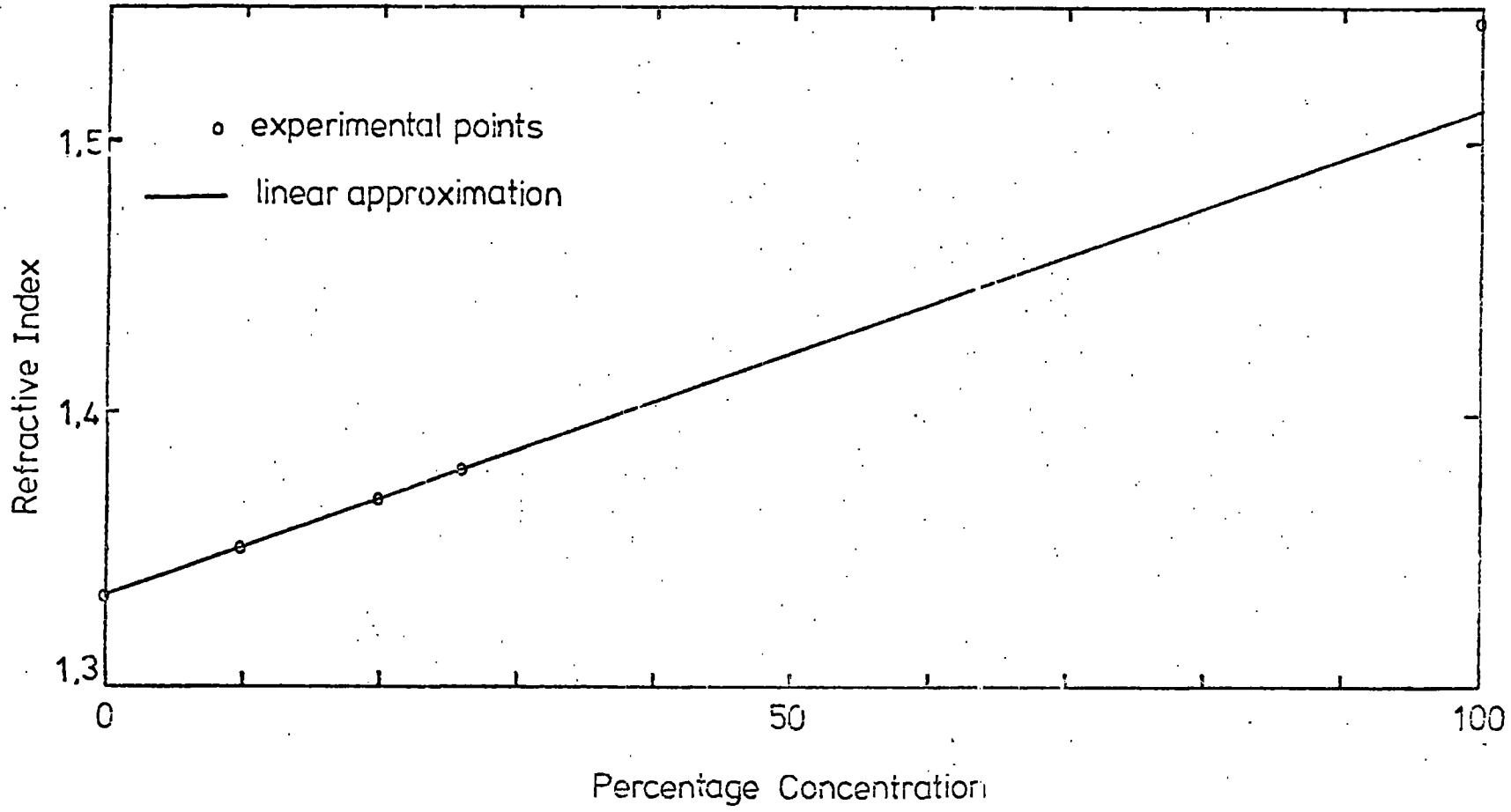

Figure 2,11 Refractive Index as a Function of Solution Concentration $(NH_4)_2SO_4$

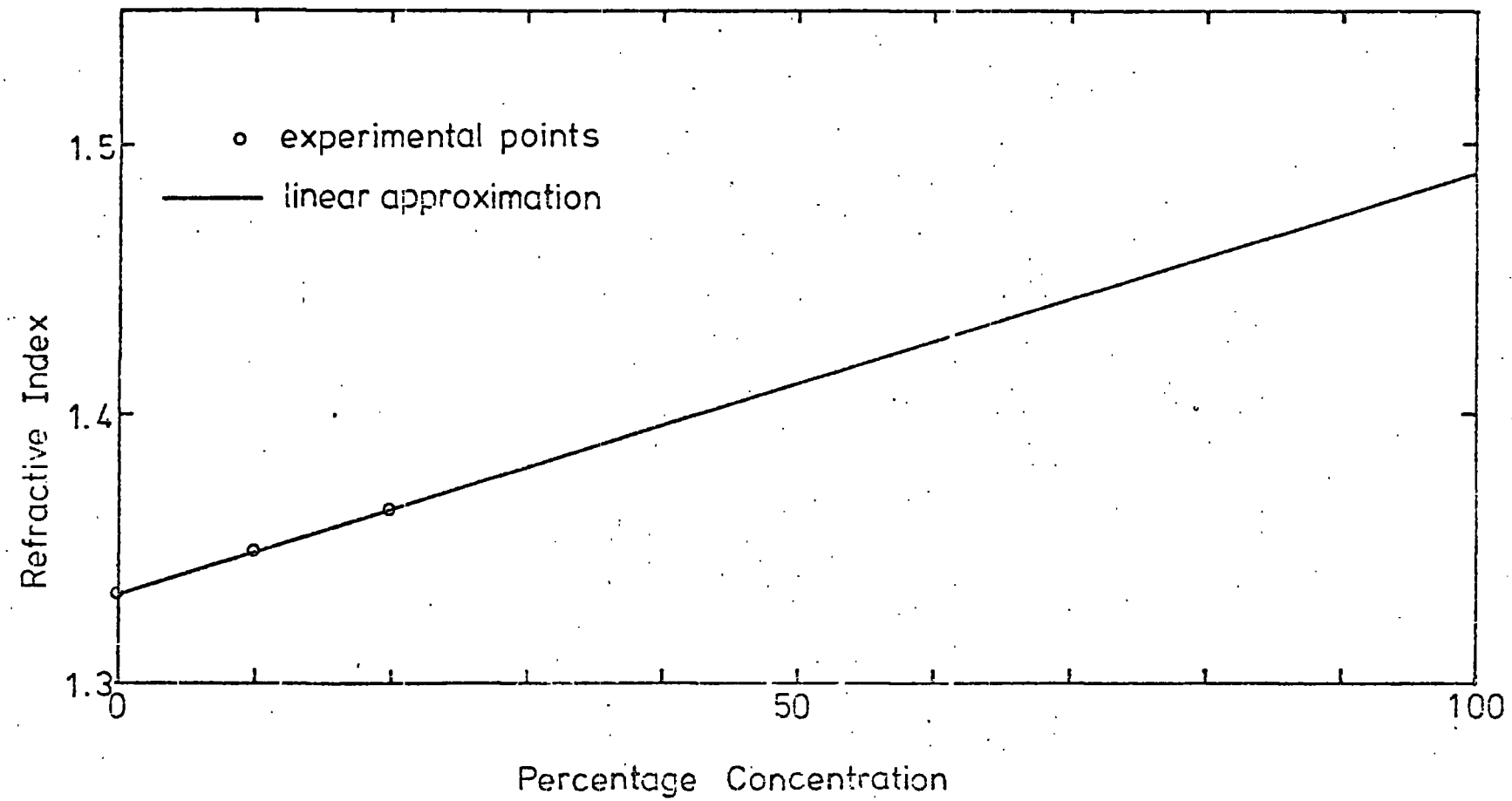

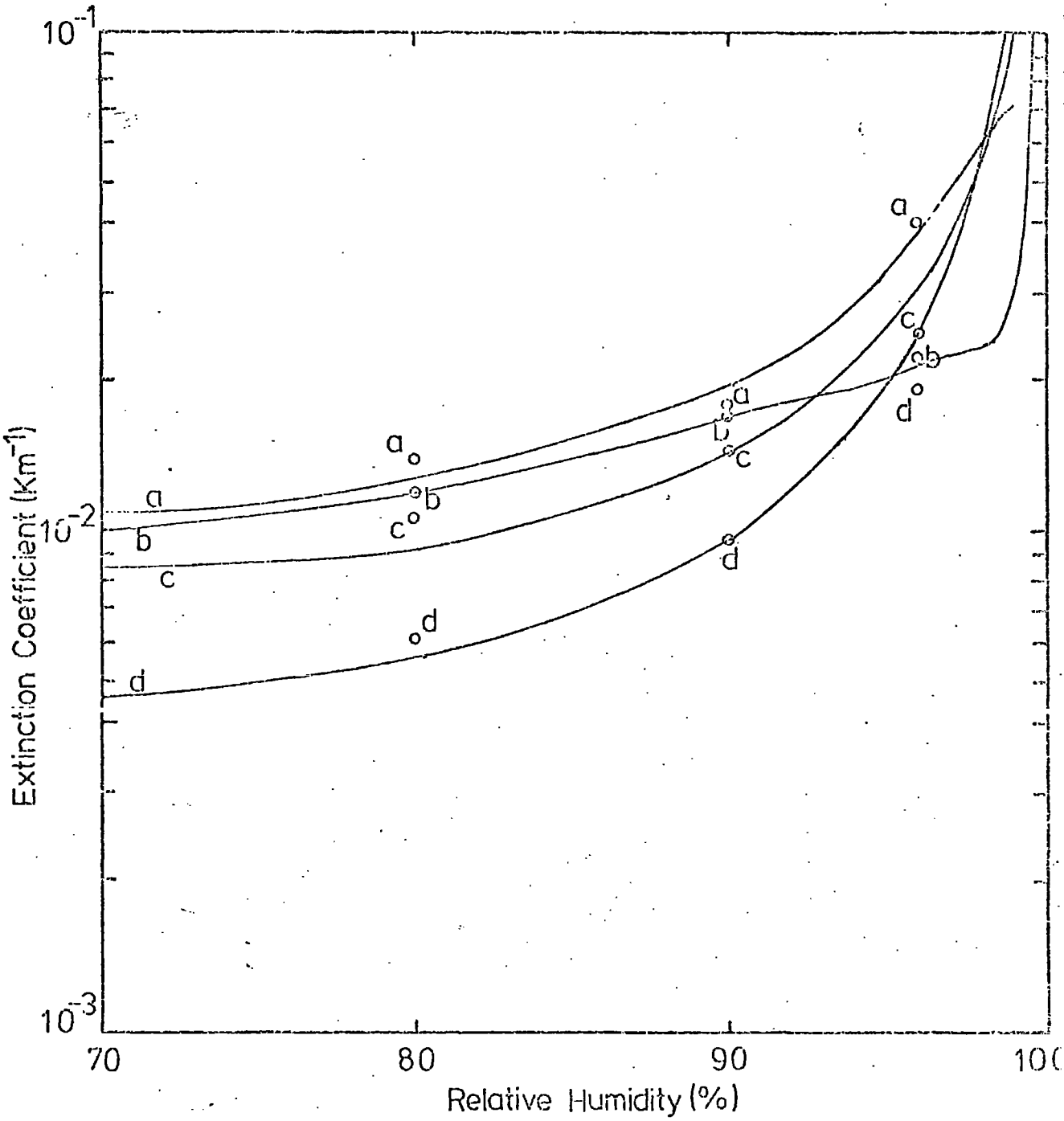

Figure 2.12 The extinction coefficient of an atmosphere containing 1 $\mu g/m^3$ of ammonium sulphate with the following size distributions:

a monodisperse aerosol at the mass median radius, 0.21 μm, of the Junge distribution.

b monodisperse aerosol at the mass median radius, 0.3 μm, of Heard and Wiffen's distribution.

c distribution measured by Heard and Wiffen.

d distribution of the Junge type illustrated in Figure 2.13.

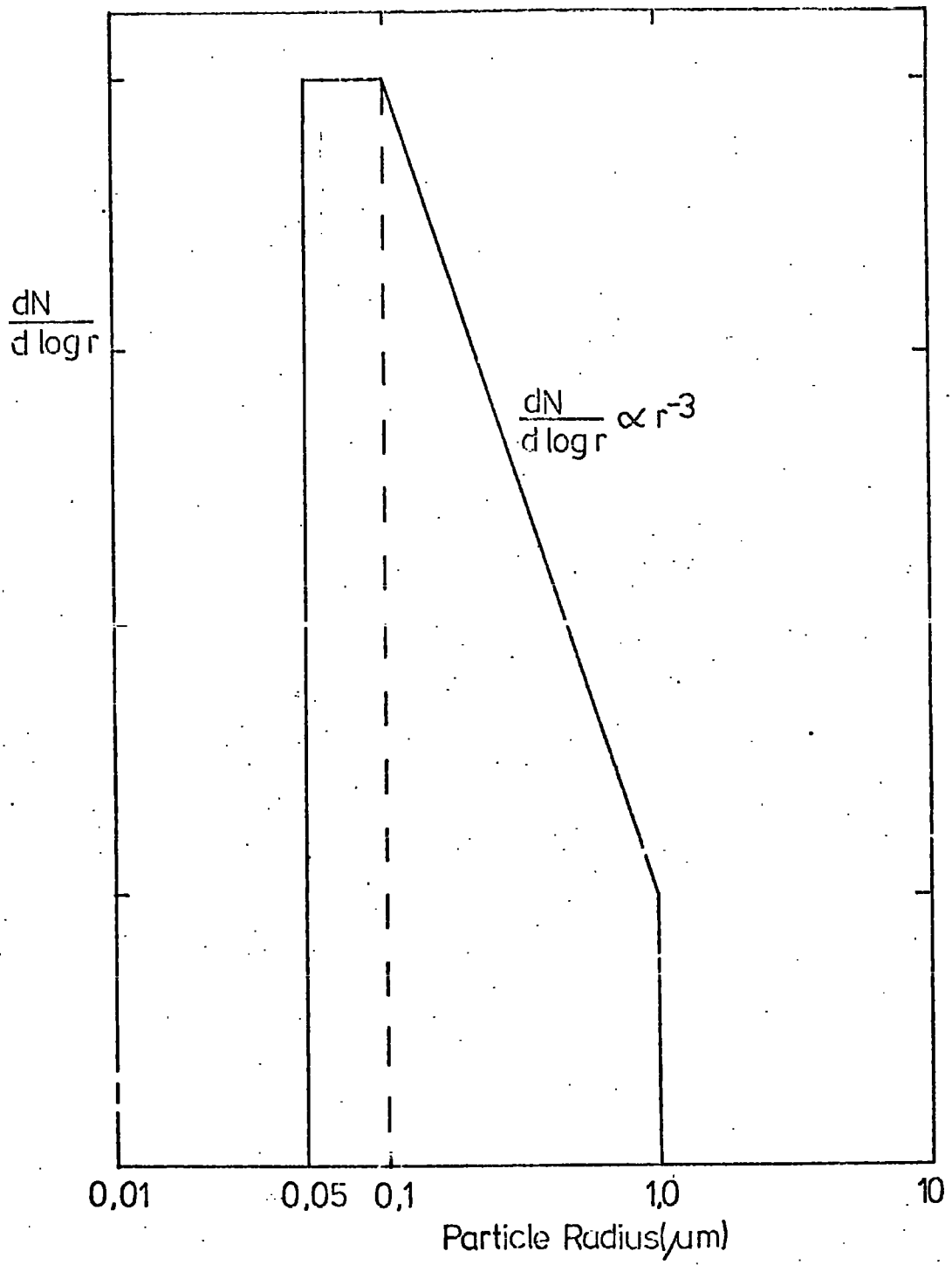

Figure 2.13 Simplified Size Distribution, after Junge

c) An atmospheric ammonium sulphate particle size distribution measured by Heard and Wiffen (1969) using electron microscope techniques. This distribution is shown in Table 2.3

d) A Junge type particle size distribution as shown in Figure 2.13.

It can be seen that good agreement was obtained between the results using approximations to Mie's theory and the results of Garland (1969) who used an interpolation formula to calculate the scattering area ratio, K, for each particle size. Some of Garland's calculated points are shown in Figure 2.12 to illustrate the agreement between the two sets of results.

Figure 2.14 shows the variation of the extinction coefficient with humidity and dry particle mass over a range from 3×10^{-17}gm to 3×10^{-11}gm for ammonium sulphate in an atmosphere containing one microgram of salt per cubic metre. It can be seen that maximum

Radius (μm)	Dry particle mass (gm)	Percentage of the total number concentration
0.060 - 0.105	4.30×10^{-15}	22.9
0.105 - 0.145	1.45×10^{-14}	25.7
0.145 - 0.185	3.43×10^{-14}	13.5
0.185 - 0.230	6.70×10^{-14}	14.8
0.230 - 0.270	1.16×10^{-13}	7.67
0.270 - 0.310	1.84×10^{-13}	6.40
0.310 - 0.350	2.74×10^{-13}	5.14
0.350 - 0.395	3.90×10^{-13}	2.56
0.395 - 0.435	5.36×10^{-13}	1.28

Table 2.3 The size distribution of ammonium sulphate particles in the atmosphere on 23.8.67 reported by Heard and Wiffen.

extinction occurs for the highest value of 99% relative humidity for a dry particle mass of 10^{-14}gm corresponding to a radius of 1.2×10^{-5}cm. It is also clear that visibility is reduced by approximately an order of magnitude over the whole range of particle mass as the humidity is increased from 80% to 99%.

The corresponding curves for sodium chloride are shown in

Figure 2,14 The extinction coefficient as a function of dry particle mass-$(NH_4)_2SO_4$

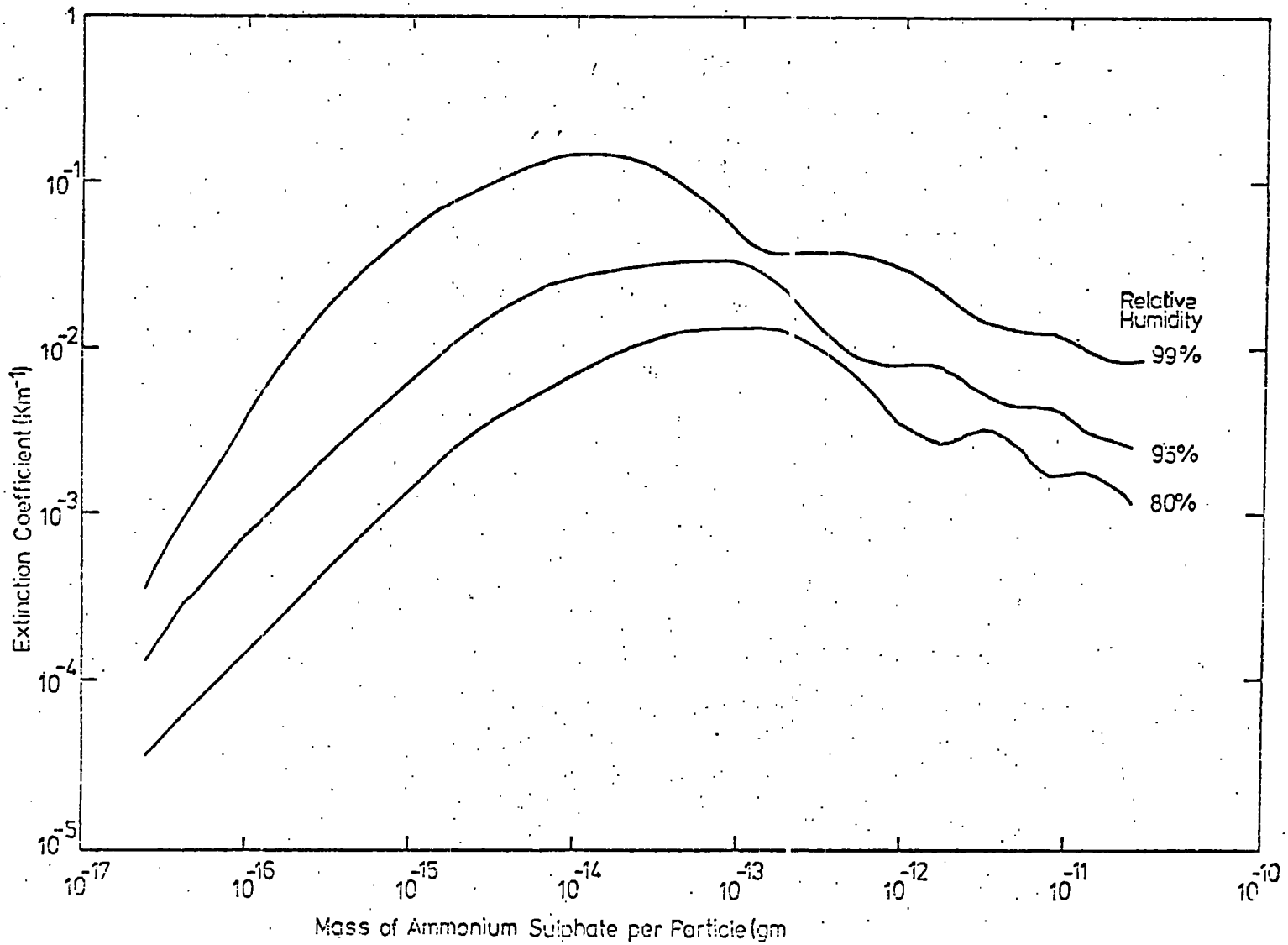

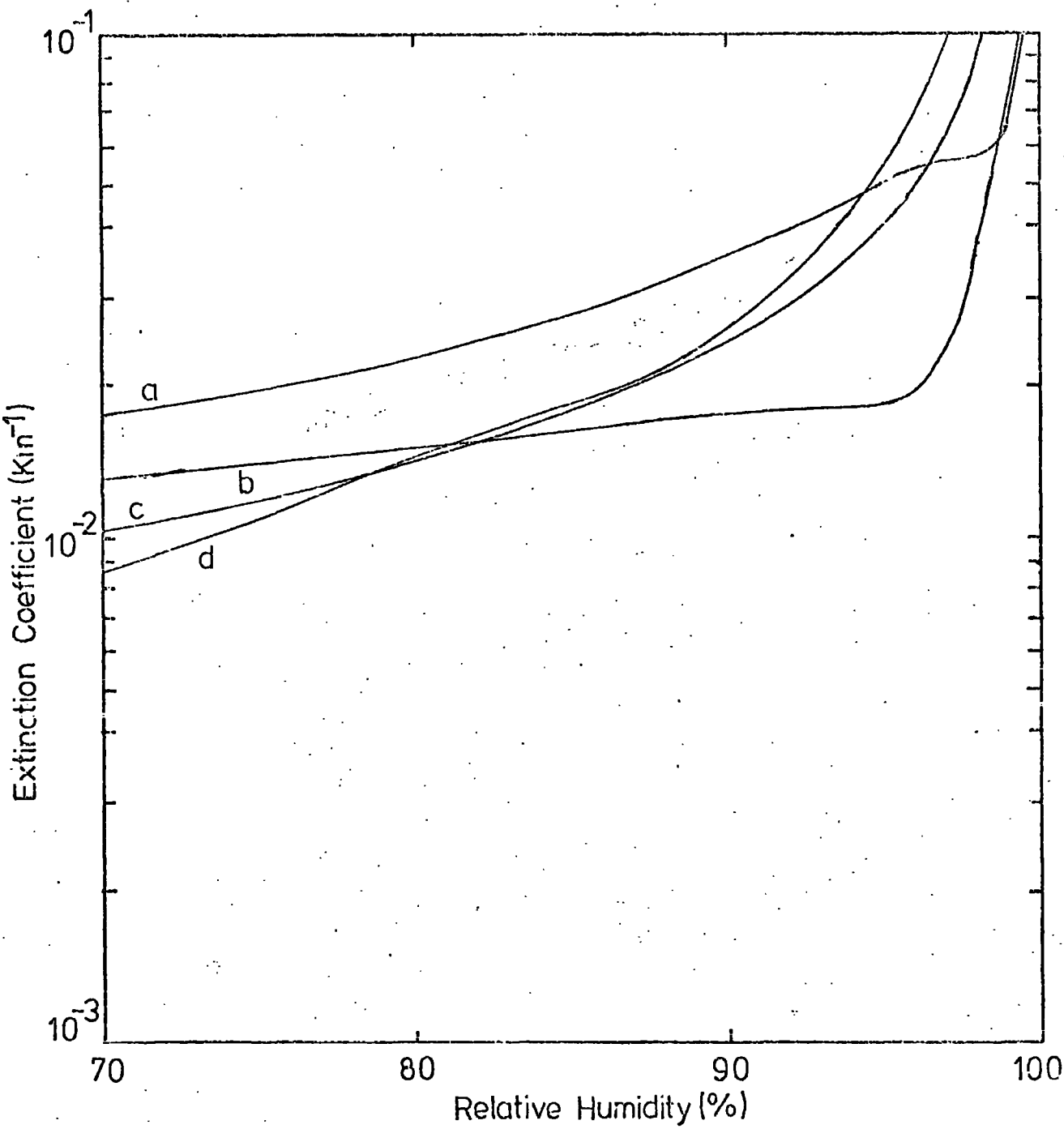

Figure 2.15 The extinction coefficient of an atmosphere containing 1 $\mu g/m^3$ of sodium chloride with the following size distributions:

a monodisperse aerosol at the mass median radius, 0.21μm, of the Junge distribution.

b monodisperse aerosol with particle radius 0.3μm.

c sea spray distribution shown in Figure 2.17.

d distribution of the Junge type illustrated in Figure 2.13.

Figure 2,16 The extinction coefficient as a function of dry particle mass- NaCl

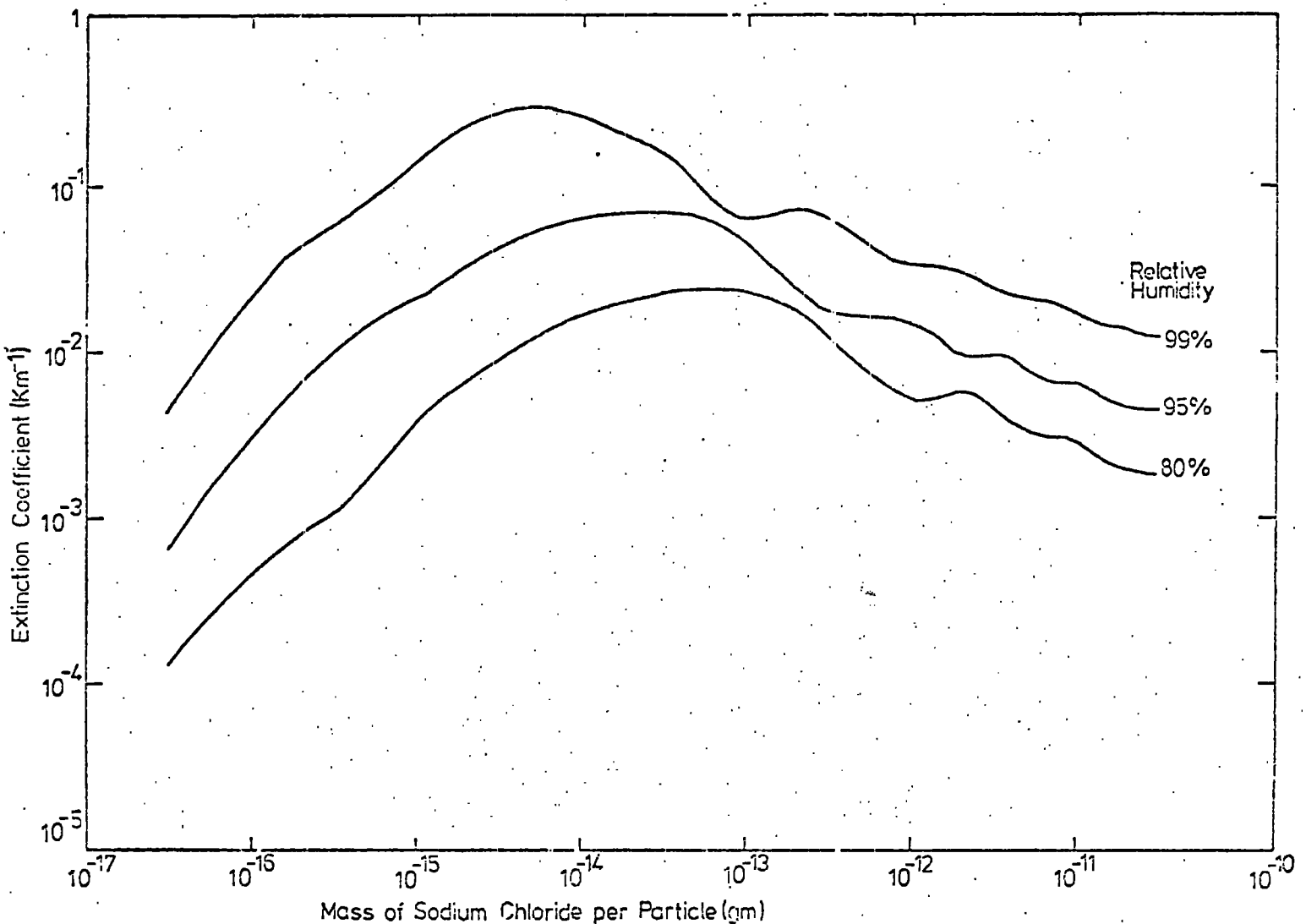

Figures 2.15 and 2.16. The distributions used are identical to those described above with the exception of the Heard and Wiffen values (distribution (c)) which are replaced by a sea spray distribution similar to that used by Hänel (1972). The sea spray particle size distribution is shown in Figure 2.17. It is clear by comparing the plots of extinction coefficient with relative humidity for the two salts, Figures 2.12 and 2.15, that the extinction coefficient is generally greater in the case of sodium chloride particles for the three chosen distributions (a), (b) and (d).

It can be seen from Figure 2.16, the extinction coefficient plotted against dry particle mass for sodium chloride, that for 99% relative humidity, maximum extinction occurs at a dry particle radius of 8.2×10^{-6} cm. The shapes of the curves are similar to those for ammonium sulphate although important differences between the two sets of results will be discussed in the next section.

A comparison was made between the extinction coefficient at selected values of humidity H, $\sigma(H)$, with the extinction coefficient at a value of humidity k, $\sigma(k)$, where k was chosen to be a humidity value at which it could be assumed that the particle was dry. The values used for k were taken as 48.4 and 53.7 per cent for ammonium sulphate and sodium chloride respectively which correspond to the lowest values of humidities calculated using the particle growth equation. A graph of the ratio $\sigma(H)/\sigma(k)$ is is plotted against the relative humidity, H, in Figures 2.18 and 2.19. The curves for both ammonium sulphate and sodium chloride are computed for a Junge distribution, shown in Figure 2.13, and for a monodisperse aerosol of particle radius 0.21 micrometres, corresponding to the mass median radius of the Junge distribution.

It can be seen from the curves for the monodisperse aerosols of particle radius 0.21 micrometres that the ratio $\sigma(H)/\sigma(k)$ attains a value of 2.0 at a relative humidity of 86% and 6.0 at 97% for ammonium sulphate. In the case of the monodisperse aerosol of sodium chloride particles of radius 0.21 micrometres, the ratio $\sigma(H)/\sigma(k)$ is equal to 2.4 and 4.7 at 86% and 97% relative humidity respectively.

The curves of $\sigma(H)/\sigma(k)$ versus relative humidity, H, for the Junge distributions indicate that this form of distribution is more effective at reducing visibility than the monodisperse aerosol. The ratio of $\sigma(H)/\sigma(k)$ attains a value of 2.0 at 77% and

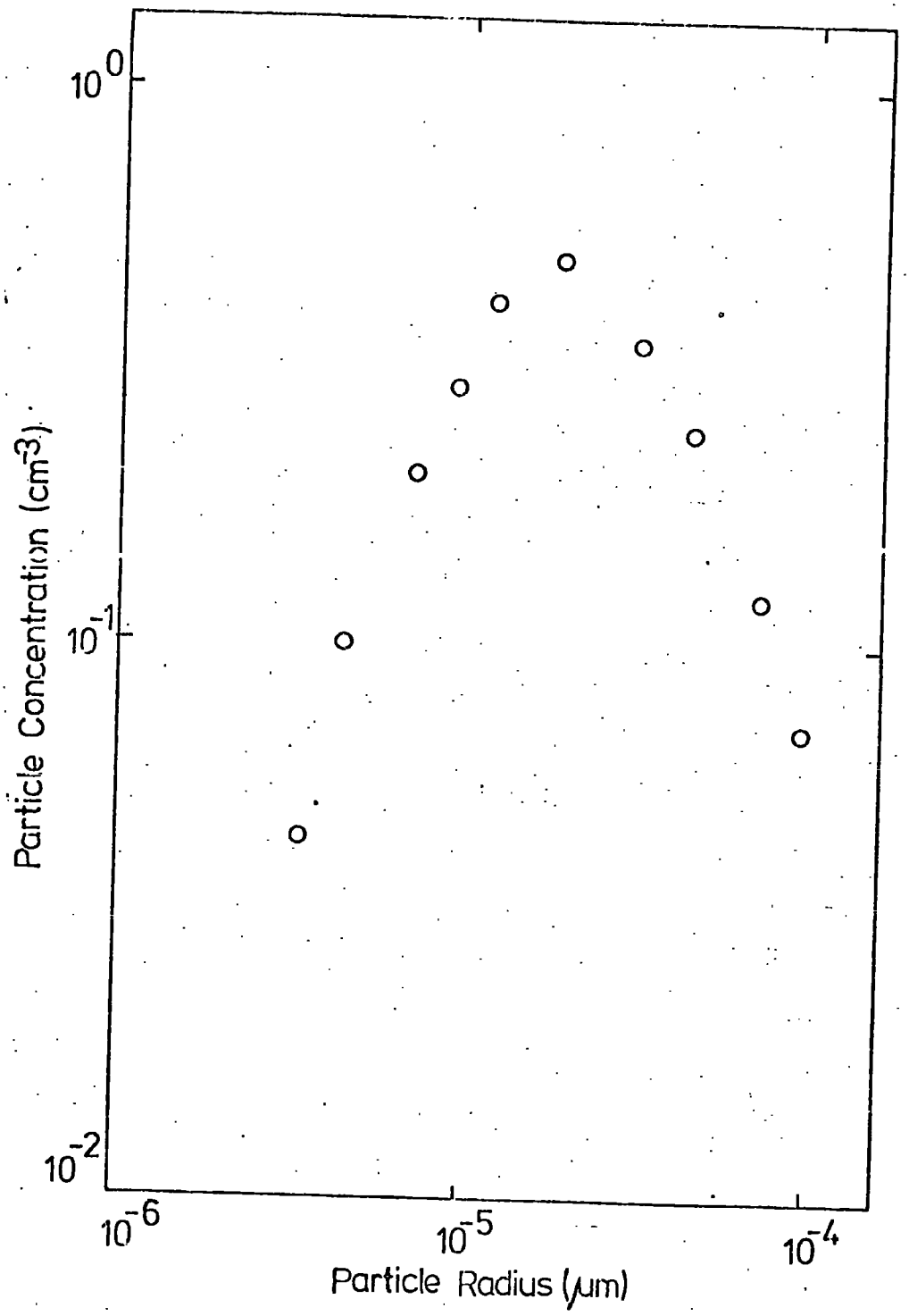

Figure 2.17 Sea Spray Size Distribution used by Hänel

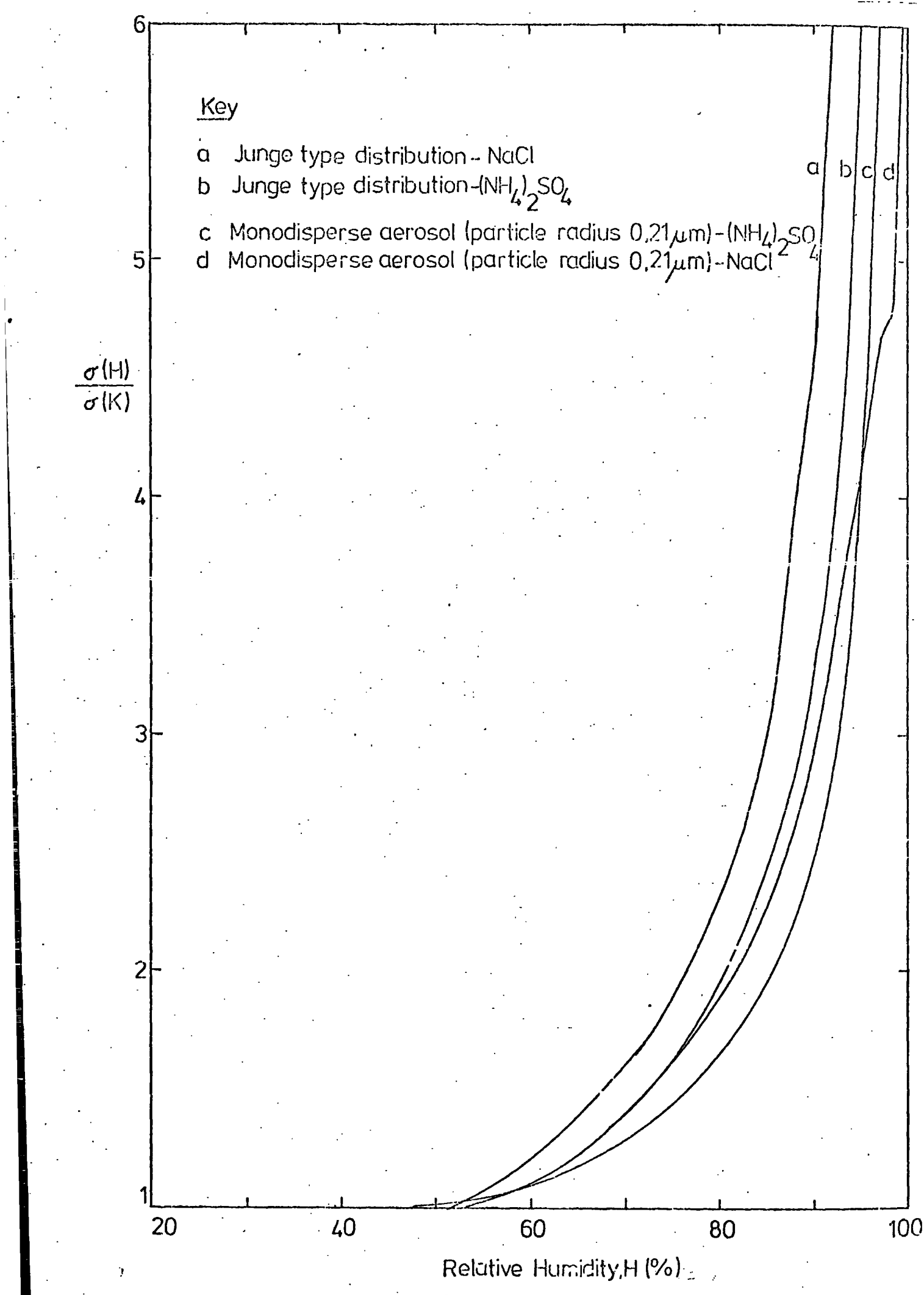

Figure 2.18 The ratio $\sigma(H)/\sigma(K)$ as a function of relative humidity.

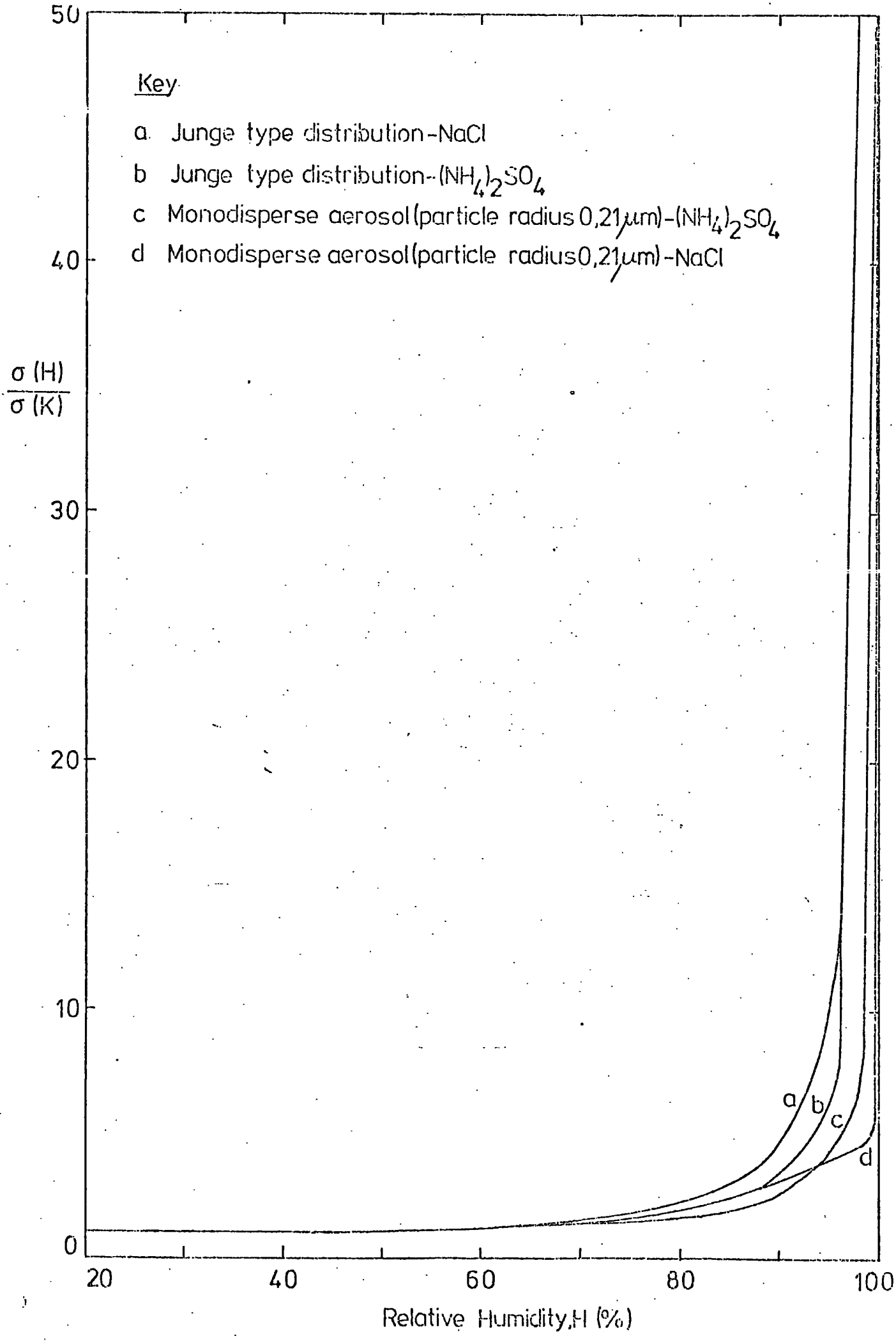

Figure 2.19 $\sigma(H)/\sigma(K)$ as a function of relative humidity.

6.0 at 92% relative humidity for the sodium chloride aerosol and the same values at 81% and 95% respectively for the ammonium sulphate particles.

2.6 Discussion of the Results

An equation has been derived relating the size of a solution droplet, which is in equilibrium with the atmosphere, to the relative humidity. The equation is based on that derived by Mason (1971) but novel approximations are incorporated in its application to the growth of solution droplets. Values of the van't Hoff factor tabulated by Low (1969) have been used. These values are given for a range of molalities up to 5.5 and 6.0 for ammonium sulphate and sodium chloride respectively. Cubic approximations to these values were used to predict the van't Hoff factor for higher values. Quadratic equations were derived to relate the density of the salt solution to solution concentration and linear approximations were used to describe the variation of surface tension with solution concentration. These approximations gave good agreement with the tabulated values and were assumed to be valid in the regions of supersaturation for which no measurements have been published.

Good agreement was found between the growth curve derived for sodium chloride particles over the dry particle mass range from 3×10^{-17} to 3×10^{-11} gm and values quoted by Mason (1971). A comparison between the values for a solute mass of 10^{-15} gm derived from the two forms of the growth curve is shown in Table 2.2 which indicates agreement better than 0.5%. Good agreement was also found between the completed growth curves of ammonium sulphate and those derived by Garland (1969).

An expression has been derived for the extinction coefficient, σ, for both a homogeneous and a non-homogeneous source of aerosol particles. This has involved the use of approximations for the scattering area ratio, K, based on the equations of Diermendjian (1960) and Penndorf (1962). K is a function of the particle radius, the wavelength of the incident light and the refractive index of the particle. The variation of refractive index with humidity was taken into account by means of a linear approximation equation relating the refractive index to the percentage concentration of the salt solution in the droplet. The two linear approximations

for ammonium sulphate and sodium chloride give good agreement with tabulated values.

The effect of relative humidity on the extinction coefficient for a monodisperse aerosol of sodium chloride and ammonium sulphate over a range of particle mass of 3×10^{-17} to 3×10^{-11} gm is shown in Figures 2.16 and 2.14 respectively. The particle number concentration was chosen to correspond to one microgram of salt per cubic metre. It can be seen that the shapes of the curves are quite similar for both sets of results. The smooth variation of the curves below a mass of about 10^{-15} gm indicates the region over which Rayleigh's scattering law, for particle size much less than the wavelength, can be regarded as a good approximation to the more precise Mie theory. The undulations in the curves can be attributed to the oscillatory variation of the scattering area ratio with the particle radius. The oscillations are most pronounced for values of particle radius less than about 10 micrometres.

Values of the maximum extinction coefficient obtained for sodium chloride and ammonium sulphate at relative humidities of 80%, 95% and 99% are shown in Table 2.4. The sodium chloride aerosol yields a value of extinction coefficient greater than ammonium sulphate by a factor of about two for the three humidity values. Maximum contribution to the extinction coefficient

Relative Humidity (%)	Sodium Chloride		Ammonium Sulphate	
	Dry particle radius (cm)	σ (km^{-1})	Dry particle radius (cm)	σ (km^{-1})
80	1.90×10^{-5}	0.024	2.40×10^{-5}	0.013
95	1.30×10^{-5}	0.075	2.04×10^{-5}	0.034
99	7.90×10^{-6}	0.295	1.20×10^{-5}	0.150

Table 2.4 Maximum values of the extinction coefficient, σ, for monodisperse aerosols with number concentration corresponding to 1 microgram per cubic metre.

is made by a dry particle radius of 1.90×10^{-5} and 2.4×10^{-5} cm for sodium chloride and ammonium sulphate respectively when the relative humidity is 80%. These values are shifted to the lower values of 7.9×10^{-6} cm and 1.2×10^{-5} cm respectively as the humidity is increased to 99%.

	Dry Particle Radius (μm)	Solute Mass per Droplet (gm)	Particle number concentration (cm^{-3})	Extinction Coefficient (km^{-1})		
				Relative Humidity (%)		
				80	95	99
ammonium sulphate	0.0238	10^{-16}	10,000	1.4×10^{-4}	7.0×10^{-4}	4.0×10^{-3}
	0.0513	10^{-15}	1,000	1.4×10^{-3}	6.2×10^{-3}	5.4×10^{-2}
	0.111	10^{-14}	100	7.0×10^{-3}	2.6×10^{-2}	1.5×10^{-1}
	0.238	10^{-13}	10	1.3×10^{-2}	3.3×10^{-2}	4.7×10^{-2}
	0.513	10^{-12}	1	3.5×10^{-3}	8.0×10^{-3}	3.1×10^{-2}
	1.11	10^{-11}	0.1	1.6×10^{-3}	4.0×10^{-3}	1.1×10^{-2}
sodium chloride	0.0223	10^{-16}	10,000	4.4×10^{-4}	3.0×10^{-3}	2.2×10^{-2}
	0.0480	10^{-15}	1,000	4.0×10^{-3}	2.2×10^{-2}	1.4×10^{-1}
	0.103	10^{-14}	100	1.6×10^{-2}	6.4×10^{-2}	2.5×10^{-1}
	0.223	10^{-13}	10	2.3×10^{-2}	4.3×10^{-2}	6.5×10^{-2}
	0.480	10^{-12}	1	5.4×10^{-3}	1.5×10^{-2}	3.3×10^{-2}
	1.03	10^{-11}	0.1	3.0×10^{-3}	6.3×10^{-3}	1.6×10^{-2}

Table 2.5(a) Selected values of the extinction coefficient as a function of particle size and relative humidity.

Humidity (%)	Particle Mass(gm)					
	10^{-16}	10^{-15}	10^{-14}	10^{-13}	10^{-12}	10^{-11}
80	3.14	2.85	2.29	1.77	1.54	1.38
95	4.29	3.55	2.46	1.30	1.88	1.58
99	5.50	2.59	1.67	1.38	1.06	1.45

(b) The ratios of extinction coefficients for sodium chloride to the corresponding values for ammonium sulphate.

Individual values of the extinction coefficient as a function of solute mass and relative humidity are shown in Table 2.5(a) for the two salts. The ratio of the extinction coefficient due to a monodisperse aerosol of sodium chloride to the corresponding values for a similar aerosol of ammonium sulphate at the selected values of dry particle mass from 10^{-15}gm to 10^{-11}gm for the values of relative humidity 80%, 95% and 99% are tabulated in Table 2.5(b). It can be seen that for the lower values of solute mass of 10^{-15}gm to 10^{-14}gm the sodium chloride particles are more efficient in reducing visibility by factors ranging from 1.7 to 5.5. The sodium chloride aerosol particles possess larger values of extinction coefficient by an average factor of 1.54 for the remaining three solute masses of 10^{-13}gm, 10^{-12}gm and 10^{-11}gm.

Results of the extinction coefficient due to selected particle size distributions for ammonium sulphate and sodium chloride as a function of relative humidity in the range 70 to 99% are presented in Figures 2.12 and 2.15 respectively. It can be seen that the extinction coefficient for the two monodisperse aerosol particles of ammonium sulphate of radius 0.21 and 0.3 micrometres labelled curve (a), (b) respectively in Figure 2.12 exceeds the values of extinction coefficient due to the distribution measured by Heard and Wiffen (1969) and a typical Junge distribution (Figure 2.13) represented by curves (c) and (d) in Figure 2.12 for values of humidity less than about 92%. For values of humidity greater than 98.5% the contribution to the extinction coefficient is greater for the non-homogeneous Junge distribution. The values of the extinction coefficient are tabulated in Table 2.6 for the four particle size distributions of ammonium sulphate for values of relative humidity ranging from 70% to 99%.

The corresponding curves for sodium chloride are plotted in Figure 2.15 for initial particle size distributions with the exception of distribution (c) which replaces the measured distribution of Heard and Wiffen. Distribution (c) is chosen to be a sea spray distribution over the radius range from 2×10^{-6}cm to 1×10^{-4}cm as shown in Figure 2.17. It can be seen that the Junge distribution causes the largest extinction for values of humidity greater than 94%. The sea spray aerosol has approximately the same effect on the extinction values as the Junge distribution up to about 90% relative humidity. The extinction coefficient for a Junge distribution exceeds that due to the

Distribution	Relative Humidity (%)				
	70	80	90	95	99
(a)	1.10×10^{-2}	1.30×10^{-2}	1.97×10^{-2}	3.35×10^{-2}	7.08×10^{-2}
(b)	1.00×10^{-2}	1.21×10^{-2}	1.70×10^{-2}	2.03×10^{-2}	3.16×10^{-2}
(c)	8.40×10^{-3}	9.31×10^{-3}	1.47×10^{-2}	2.59×10^{-2}	1.00×10^{-1}
(d)	4.64×10^{-3}	5.62×10^{-3}	9.72×10^{-3}	1.94×10^{-2}	1.22×10^{-1}

Table 2.6 The extinction coefficient of an ammonium sulphate aerosol as a function of relative humidity for the following distributions:

a) A monodisperse aerosol of particle radius 0.21 micrometres

b) A monodisperse aerosol of particle radius 0.30 micrometres

c) A Heard and Wiffen distribution

d) A Junge type distribution

Distribution	Relative Humidity (%)				
	70	80	90	95	99
(a)	1.73×10^{-2}	2.24×10^{-2}	3.55×10^{-2}	5.01×10^{-2}	6.88×10^{-2}
(b)	1.30×10^{-2}	1.50×10^{-2}	1.78×10^{-2}	1.86×10^{-2}	7.94×10^{-2}
(c)	1.03×10^{-2}	1.41×10^{-2}	2.48×10^{-2}	4.21×10^{-2}	1.34×10^{-1}
(d)	8.66×10^{-3}	1.45×10^{-2}	2.55×10^{-2}	5.31×10^{-2}	2.37×10^{-1}

Table 2.7 The extinction coefficient of a sodium chloride aerosol as a function of relative humidity for the following distributions:

a) A monodisperse aerosol of particle radius 0.21 micrometres

b) A monodisperse aerosol of particle radius 0.30 micrometres

c) A sea spray aerosol

d) A Junge type distribution

sea spray distribution by an average value of 35% for the relative humidity range between 90% and 99%.

Selected values of the extinction coefficient from Figure 2.15 for the four size distributions for a range of relative humidity from 70% to 99% are shown in Table 2.7. A comparison of the extinction coefficients shown in Tables 2.6 and 2.7 indicates that the extinction coefficient due to the sodium chloride particle distributions exceeds that due to the ammonium sulphate distributions for all the distributions considered. Average values over the relative humidity range from 70% to 99% of the ratio of the extinction coefficients for sodium chloride and ammonium sulphate for the three distributions (a), (b) and (d) are equal to 1.60, 1.35 and 2.25 respectively.

The rate of increase of extinction coefficient at particular values of humidity is compared to the extinction coefficient at a humidity, k, considered sufficiently low to assume that the salt nucleus is dry. Values of $\sigma(H)/\sigma(k)$ shown in Figures 2.18 and 2.19 indicate that the extinction coefficient increases more rapidly for a sodium chloride monodisperse aerosol of particle radius 0.21 micrometres than for an ammonium sulphate source up to a value of 95% relative humidity. The rate of rise of $\sigma(H)/\sigma(k)$ is greater for the two salts for a non-homogeneous Junge type distribution than for the monodisperse aerosol of particle size equivalent to the mass median radius of the Junge distribution as seen in Figure 2.13. It can be seen from Figure 2.19 that the extinction coefficient for a Junge distribution for both sodium chloride and ammonium sulphate approaches the same rate of increase with increasing values of humidity.

CHAPTER 3

THE EXPERIMENTAL APPARATUS

3.1 Introduction

The experimental apparatus described in this chapter was designed to investigate the effect of reative humidity on the mean size of aerosol particles of sodium chloride and ammonium sulphate. A schematic diagram of the apparatus used is shown in Figure 3.1. It can be divided into three major sections. The aerosol generator system constitutes the first section followed by a storage vessel in which the aerosol is stored whilst the humidity is altered and monitored. Finally the apparatus used to measure the mean particle size is described. This consists of a photoelectric nucleus counter operated in conjunction with an ion tube. Details of the instrumentation used is given in the following subsections.

3.2 The Aerosol Generator

A nebulizer based on the Collison type (May, 1973) was constructed as shown in Figure 3.2 in order to generate the aerosol particles. The Nebulizer is shown in Figures 3.3 and 3.4. The reservoir of volume 560cm^3 was sufficiently large so that the solution concentration remained approximately constant during use. Three jets, 0.0343cm in diameter, were drilled in the spray head assembly and the atomiser was carefully sealed. Wire mesh formed a protective shield around the nebulizer reservoir.

The nebulizer was operated at a pressure of 35lb in^{-2}. The atomised spray leaves the device through a heated vertical tube in order to vaporise the water from the salt droplets; this process is similar in principle to that described by Liu et al., 1966. The particles then enter the storage vessel.

3.3 The Storage Vessel

The base of the vessel consisted of a standard glove box with a volume of about 450 litres. The top of this box was removed and a flexible 'Mylar' reservoir, with a maximum volume of 550 litres, was attached to the box instead.

This vessel proved a convenient particle reservoir since its volume was variable. It also possessed an observation window and the gloves facilitated access to the interior during experiments.

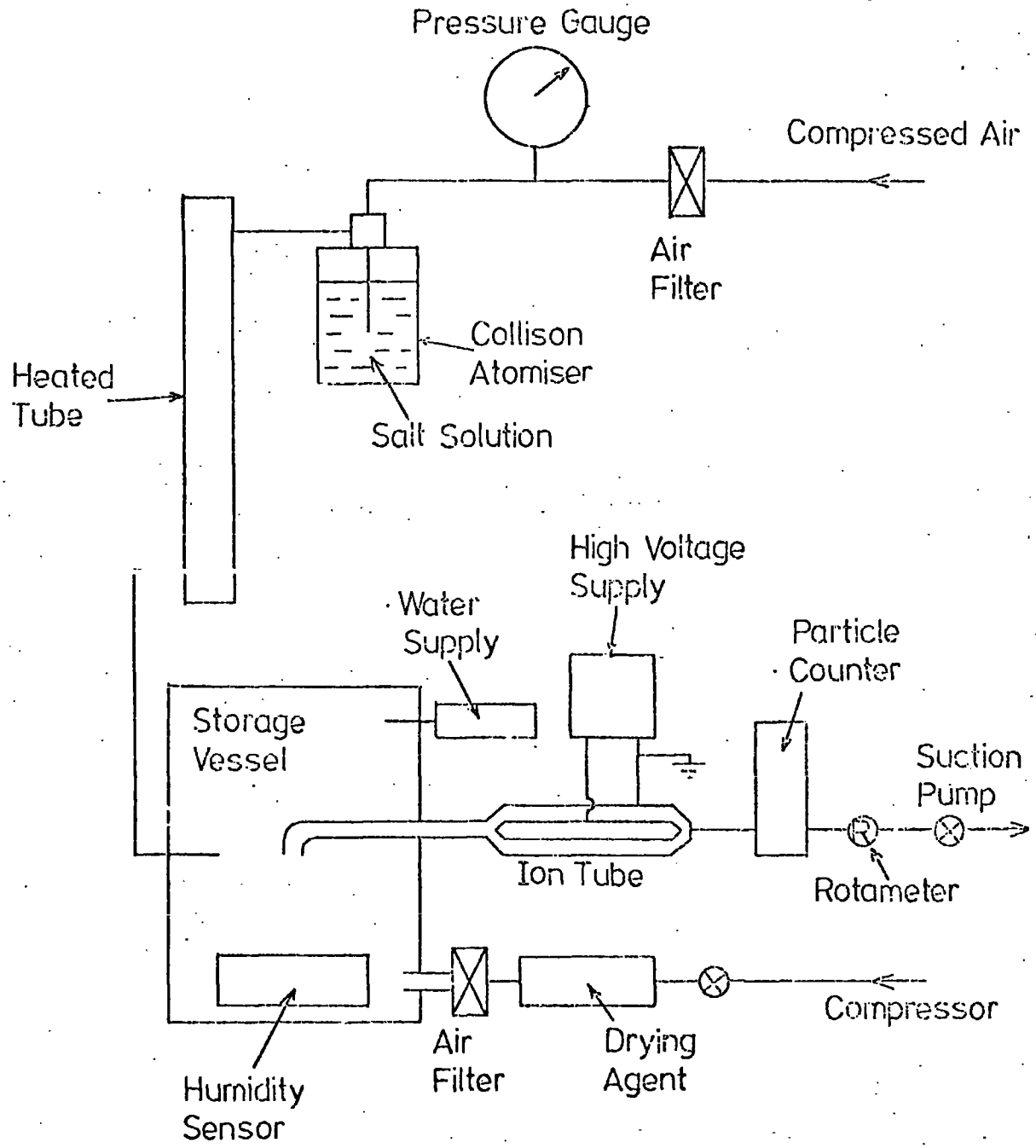

Figure 3.1 Schematic Diagram of the Apparatus

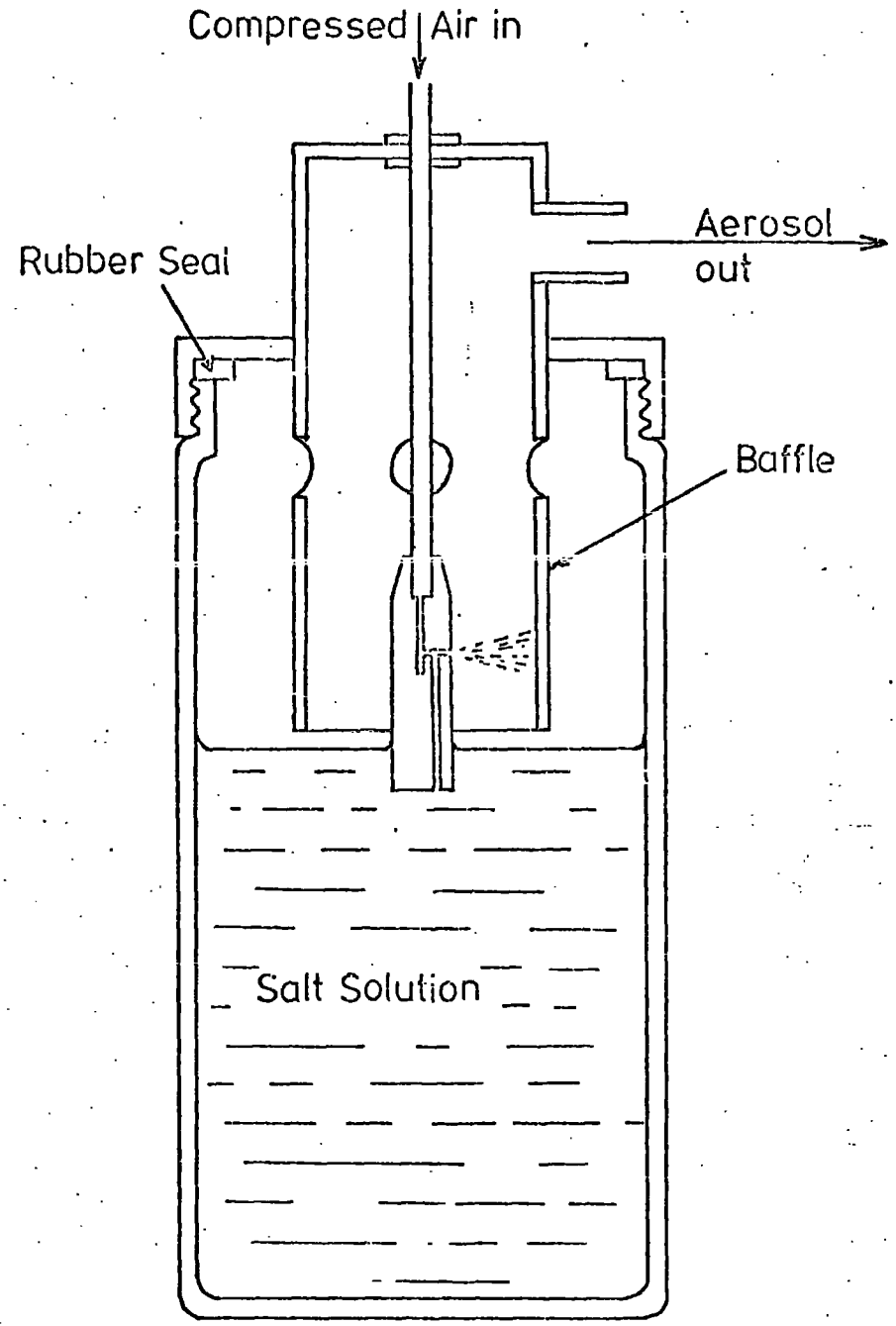

Figure 3,2 Schematic Diagram of the Nebulizer

Figure 3.3
The Collison Nebulizer.

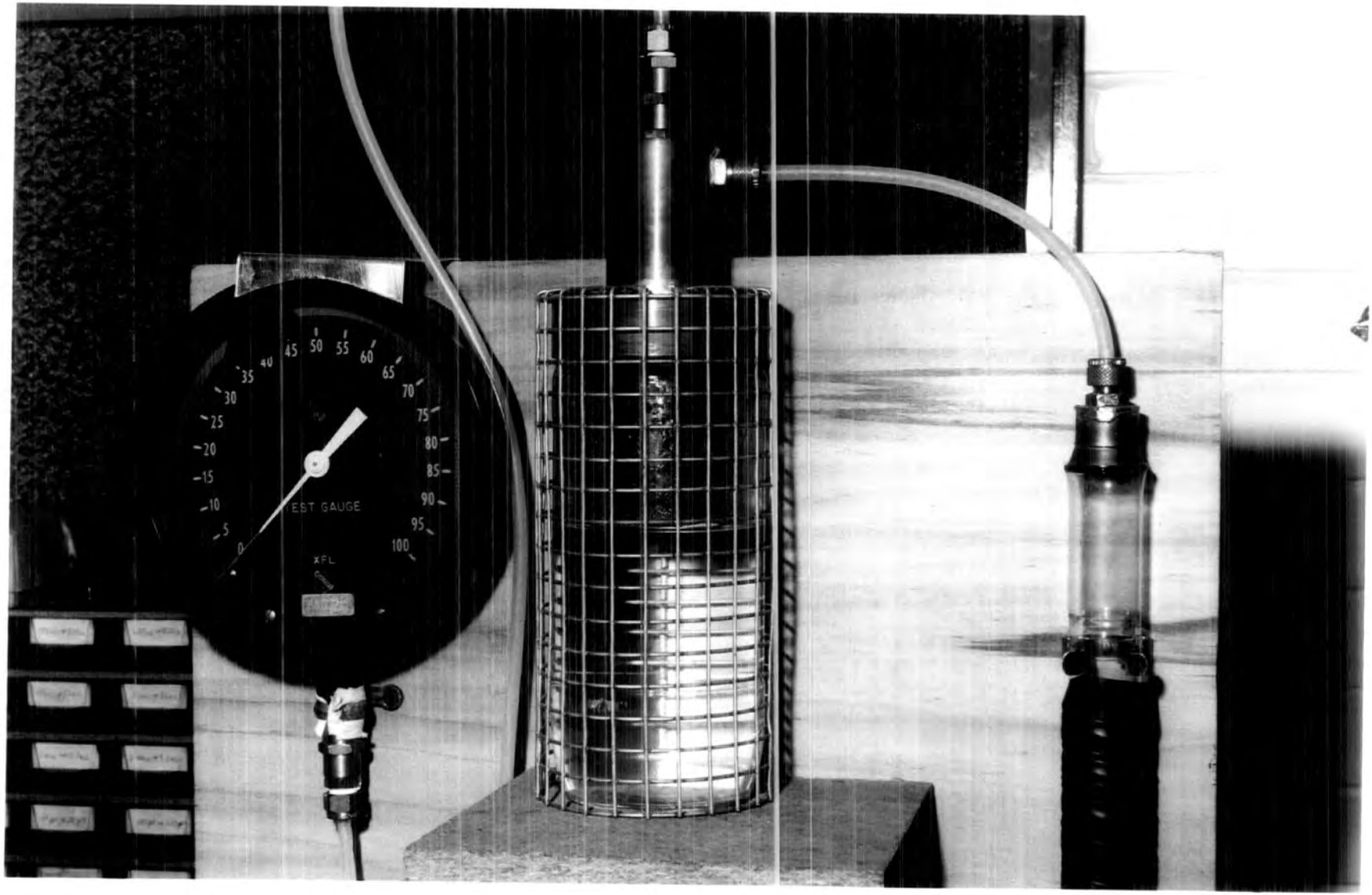
TEST GAUGE
XFL

Figure 3.4
The Aerosol Generator Unit.

A photograph of the storage vessel is shown in Figure 3.5.

Existing inlet holes on the box were used to :-

a) introduce the aerosol direct from the heating tube

b) introduce dry, filtered air from a compressor to dilute the aerosol

c) introduce water to vary the humidity

d) support the sampling tube (of internal diameter 1.905cm and length 50cm) to the ion tube.

A large area (approximately $1.7m^2$) of the internal walls of the vessel was covered with blotting paper. Water was introduced through a flexible tube to wet the paper and cover the floor of the storage vessel ($0.6m^2$). The rate of rise of the relative humidity could be controlled by wetting only part of the blotting paper thus reducing the exposed wet area. A check was made to ensure that the process of introducing water into the storage vessel did not produce nuclei. It was found that no particles were produced by this process. The diluting air was first dried in a tube of length 1 metre containing calcium chloride and filtered before entering the storage vessel. It usually took about 10 minutes to fill the storage vessel using a flow rate of about 50 l min^{-1}.

3.4 The Psychrometer

The relative humidity in the chamber was measured by wet and dry bulb thermometers over which air was drawn by means of a small fan as shown in Figure 3.6. The relative humidity was found from Hygrometric Tables published by the Meteorological Office (Met.O.265b). The air speed as measured with a hot wire anemometer was $1.2 \pm 0.2 m\ s^{-1}$, which is within the recommended range.

A check was made to ensure that the psychrometer assembly did not produce particles.

3.5 The Photoelectric Nucleus Counter

A schematic diagram of the photoelectric nucleus counter is shown in Figure 3.7. It consists of a vertical tube 60cm in length and 3.85cm in diameter lined with wet blotting paper. The glass discs at both ends are treated with an antimist coating to prevent condensation on them. A parallel beam of light from a small P.O. 40 mA bulb powered by a constant current circuit was directed down

Figure 3.5
The Storage Vessel.

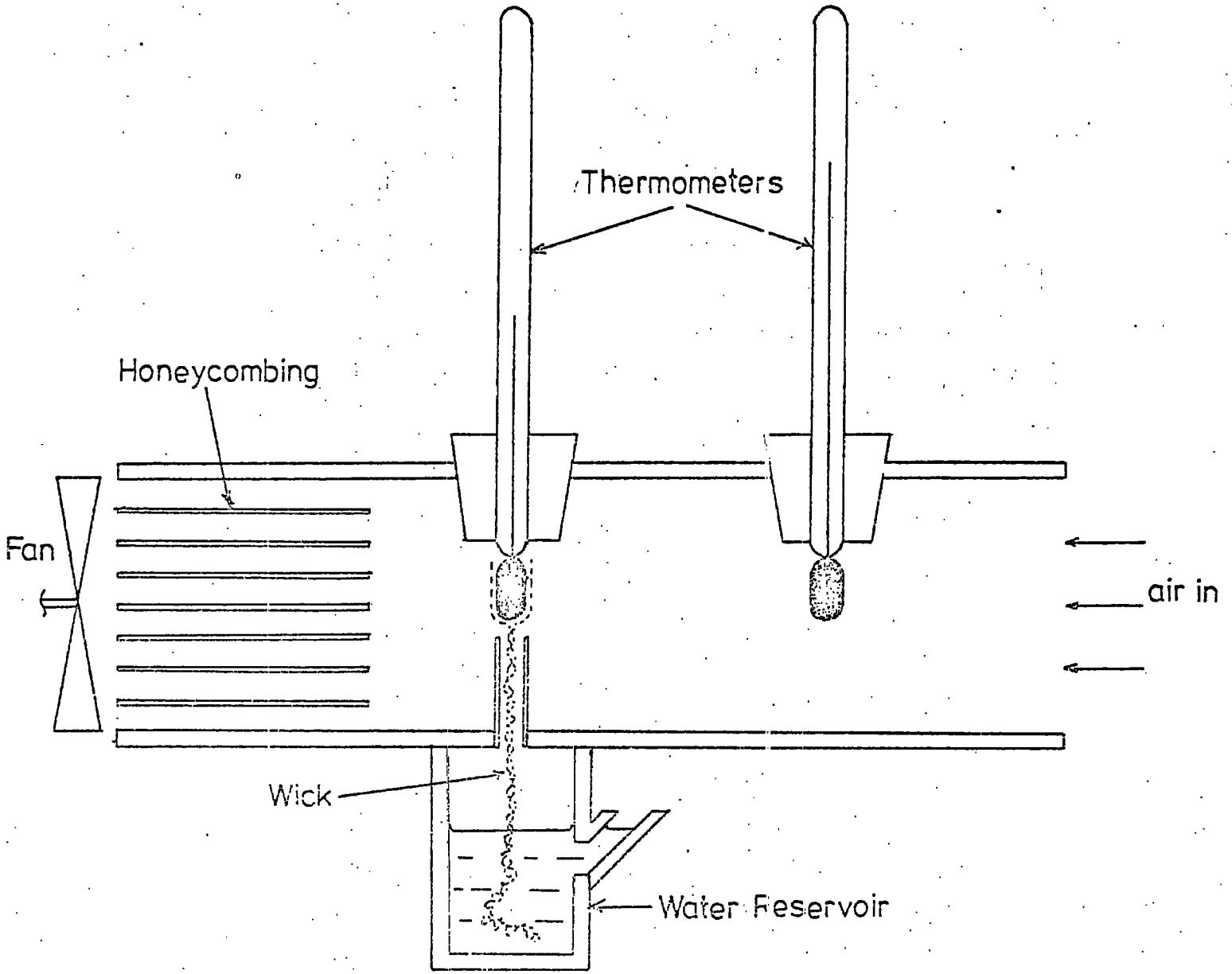

Figure 3.6 Schematic Diagram of the Psychrometer

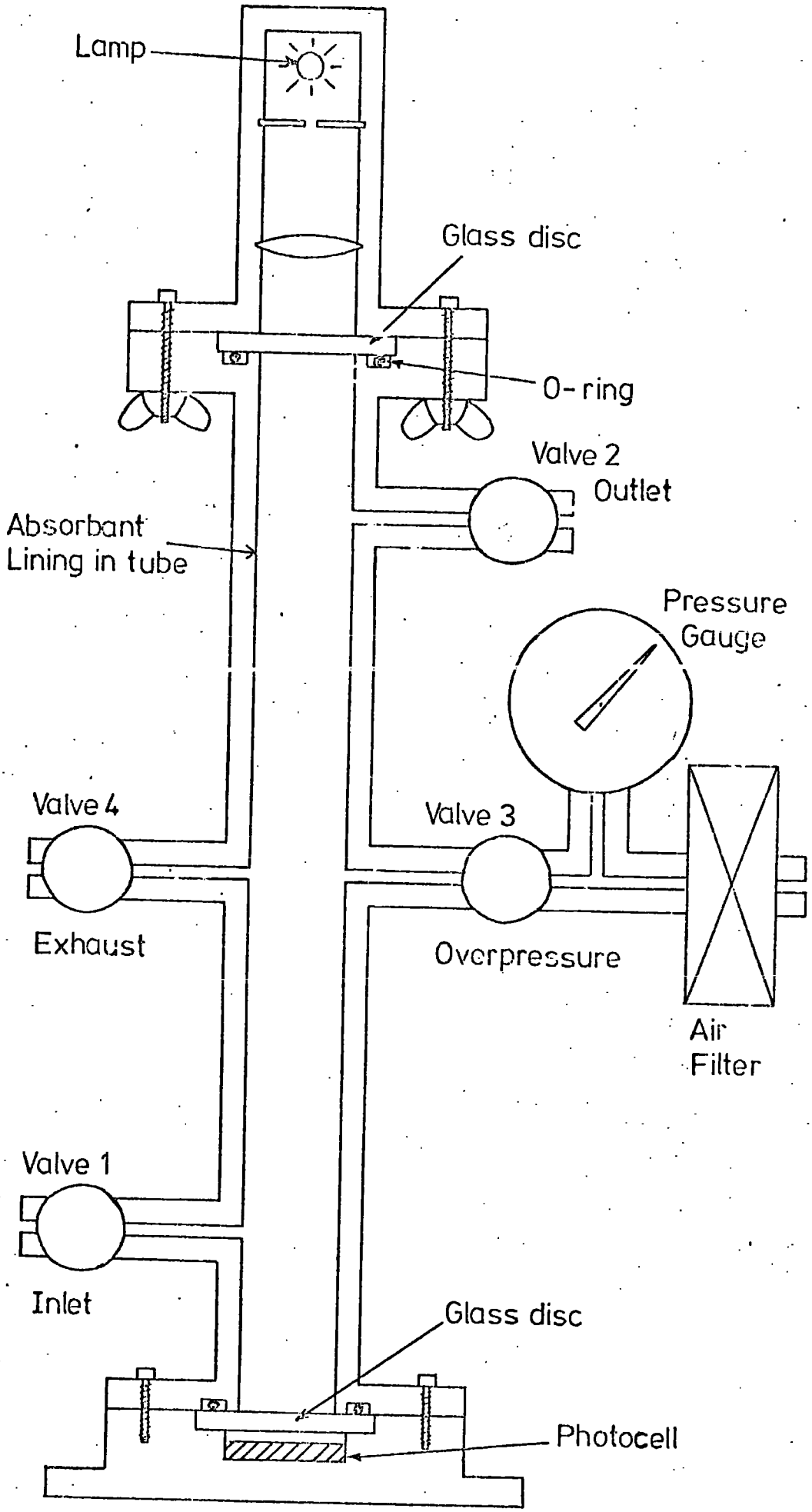

Figure 3.7 Schematic diagram of the photoelectric nucleus counter.

the tube and the resulting light intensity was detected by a barrier layer photocell, which was connected to a suitable circuit, described below. A photograph of the photoelectric counter assembly is shown in Figure 3.8.

Air containing the particles under investigation was drawn through the tube via valves 1 and 2 at a flow rate of between 1 and 10 l min^{-1} (see Figure 3.7). An adequate time was allowed to flush out previous aerosol samples. Then the new aerosol was drawn through the counter and sampling took place by closing valves 1 and 2. Valve 3 was then opened to provide an overpressure of 160mm mercury in the tube. When this pressure was reached valve 3 was closed and after a few seconds valve 4 was opened to allow adiabatic expansion of the enclosed supersaturated air. Table 3.1 gives details of the timing sequence. Fog formed on the nuclei and the light intensity decreased.

The ratio of the current from the photocell before expansion to that after expansion is directly related to the particle number concentration, as shown by Nolan and Pollak (1946). Calibration tables (Metnieks and Pollak, 1959) were used to deduce the number of particles present per cm^3 in the sample.

TIME (SECONDS)	OPERATION
0	Inlet (1) and outlet (2) valves are opened.
0 - 60	Valves (1) and (2) remain open and air is drawn through the counters at a rate determined by the rotameter.
60	Valves (1) and (2) are closed and the overpressure valve (3) is opened for about 5 - 7 seconds during which time filtered air is pumped into the counter until the correct overpressure is obtained.
~66	Valve (3) is closed.
104	Photocell current is read.
105	Expansion valve (4) is opened.
109	Photocell current is read.
113	Valve (4) is closed.

Table 3.1 Details of the two minute operating cycle of the photoelectric counter.

Figure 3.8

The Photoelectric Nucleus Counter.

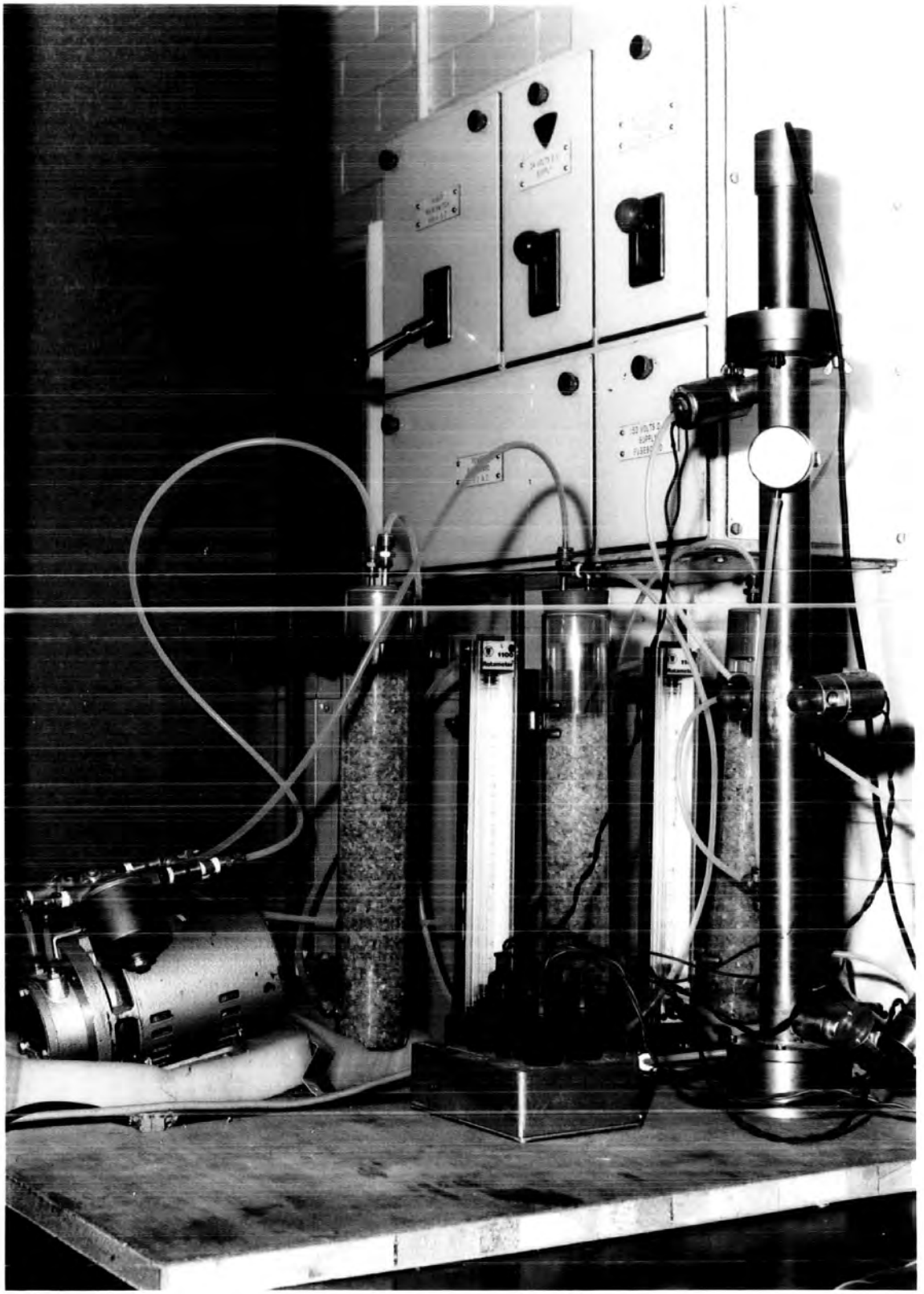

The sampling process was automated using electrically operated solenoid valves and an electric cam timer. The entire cycle took 2 minutes. A two way valve was inserted in the sampling line before valve 1 to direct the air flow whilst the photoelectric counter was sealed off. This provided a continuous flow through the ion tube.

The voltage produced by the photocell was amplified by means of the inverting amplifier shown in Figure 3.9. The gain of this circuit was set at about 150. A check was made on the linearity of the output signal from the amplifier and the original photocell current. The linearity was found to hold to within a few per cent as shown in Figure 3.10. The output voltage was fed into a digital voltmeter which possessed a print-out facility. The voltmeter was triggered just before the expansion of the air sample in the tube and again exactly 4 seconds after expansion had taken place. This conforms to the recommendation of Pollak and Metnieks (1959).

3.6 The Diffusion Battery

The diffusion battery consists of a number of parallel rectangular channels through which air was drawn as schematically shown in Figure 3.11. The ratio of the particle concentration emerging from the box (n) to that entering (n_o) has been calculated as a function of the air flow rate through the box by several workers for example Nolan, Nolan and Gormley (1938). The equation given in a form derived by Thomas and De Marcus (1952) is

$$\frac{n}{n_o} = 0{,}9149\, e^{-1{,}885\mu} + 0{,}0592\, e^{-22{,}3\mu} + 0{,}026 e^{-151\mu} \qquad (3.1)$$

where

$$\mu = \frac{lAD}{h^2 Q} = \frac{2blcD}{hQ} \qquad (3.2)$$

h = half the plate separation

b = the channel width

c = the number of channels

l = the length of the channels

A = the cross sectional area of all the channels

Q = the air flow rate

D = the diffusion coefficient of the particles.

The box constant, k, is given by the expression

$$k = \frac{h}{3{,}77blc} \qquad (3.3)$$

Figure 3,9 The Inverting Amplifier Circuit

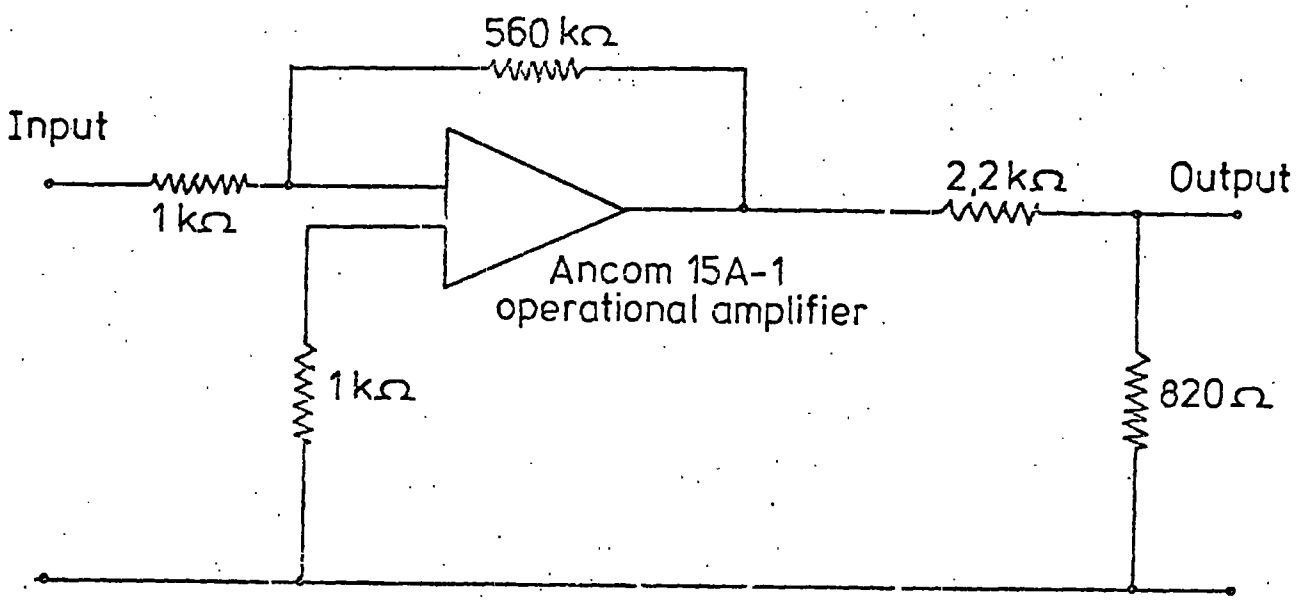

Figure 3,10 Test of the linearity of the amplifier output

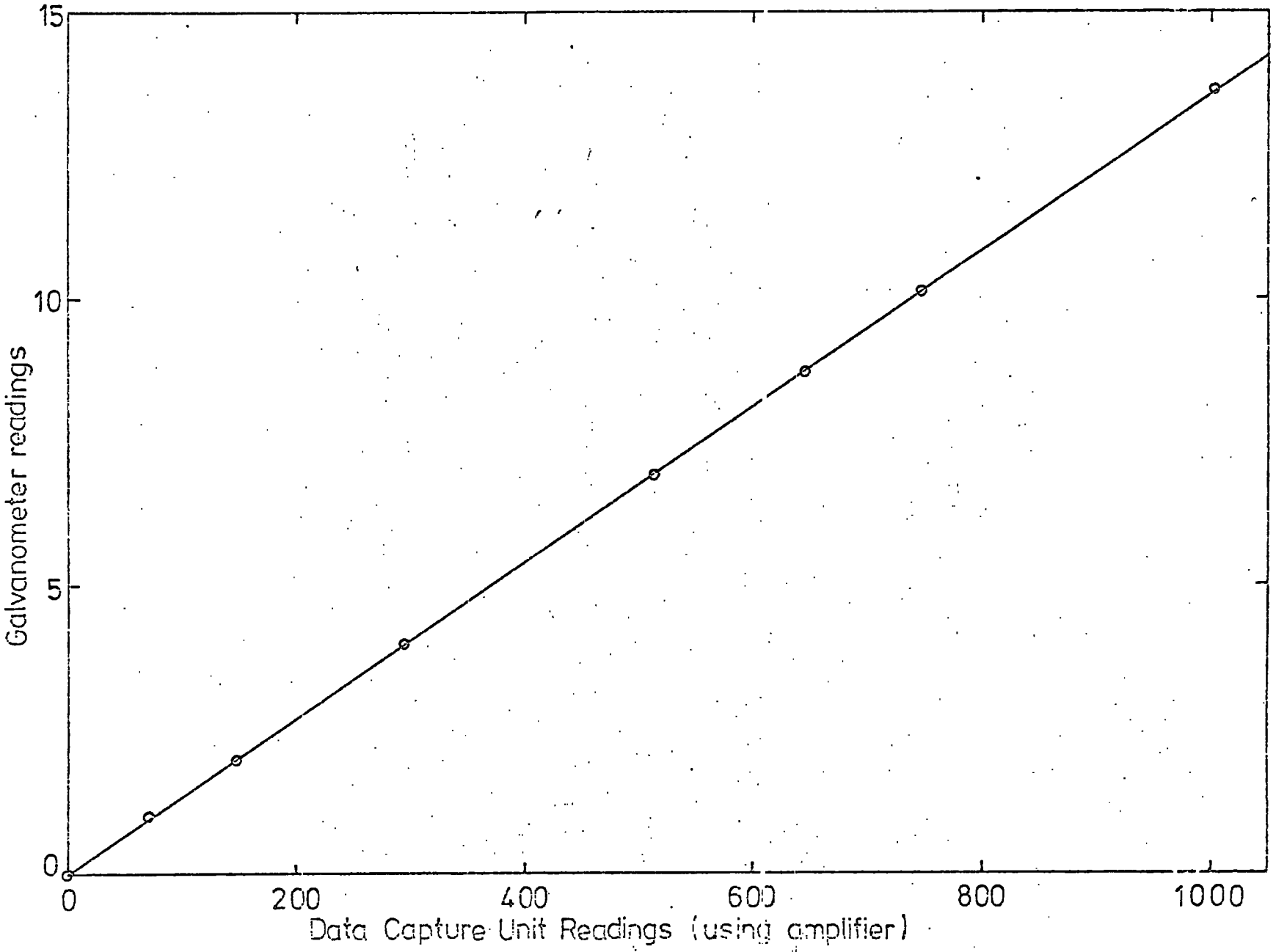

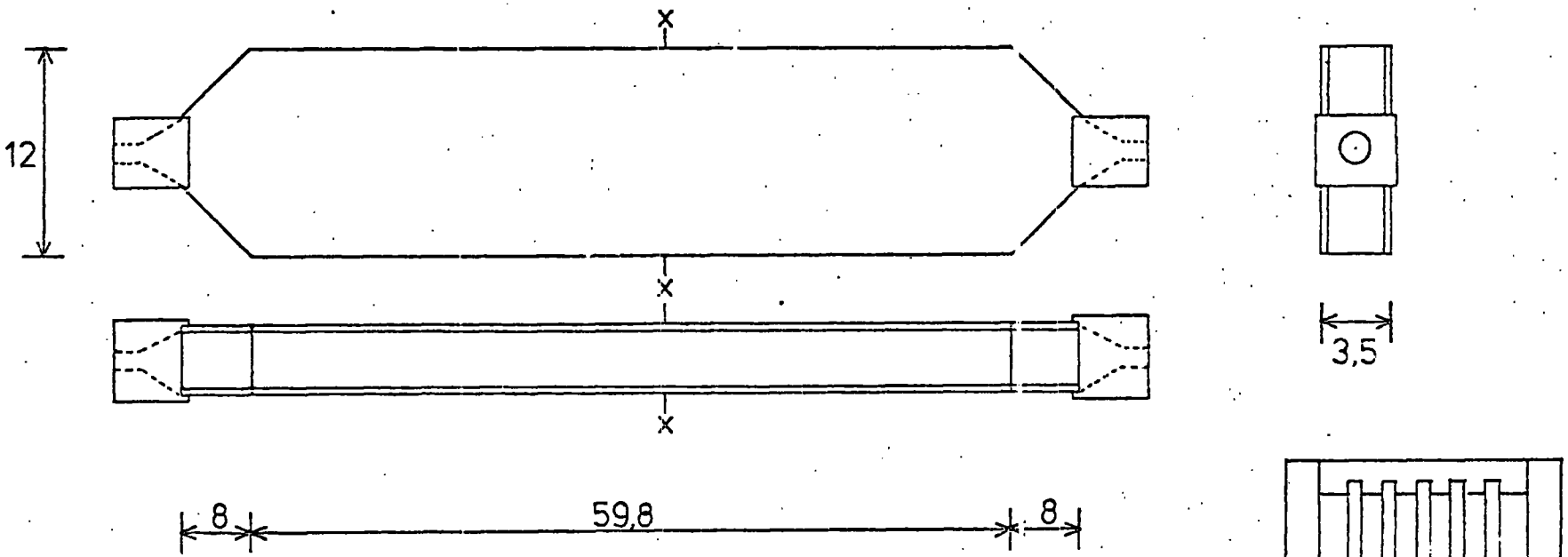

Diffusion Battery
Not to scale
Material: Brass except for
Internal sheets which
are Aluminium
Dimensions in cm.

Figure 3,11 The Diffusion Battery

The dimensions of the box used are given in Table 3.2 below. The box constant was calculated as $5.71 \times 10^{-7} cm^{-1}$.

Assuming a log-normal distribution it is possible to plot a series of curves from which the geometric mean radius, r_g, and geometric standard deviation, σ_g, can be estimated if n/n_o and Q, the flow rate, are known. The curves derived by Fuchs et al., (1962), are shown in Figure 3.12. Air was drawn through the equivolume tube to the counter. This gave a value for n_o. Then the air was diverted

Plate separation (2h)	0.0578cm
Effective area of one plate ($\simeq$ bl)	$840cm^3$
Number of channels (c)	16

Table 3.2 Dimensions of the Diffusion Battery

to flow via the diffusion battery to the counter which gave a value for n.

The air was drawn through the equivolume tube for three consecutive concentration readings, through the diffusion battery for three readings and then again through the equivolume tube for another three readings. Interpolation is used to give direct comparison between the n and n_o values. The process was repeated at several flow rates between 1 and 10 min^{-1}.

Comparison of the experimental curves with the theoretical ones yields the geometric standard deviation, σ_g, of the distribution and the value of the geometric radius, r_g. The graph shown in Figure 3.13 was used to interpolate between Fuchs' values of radius.

3.7 The Large Ion Tube

A cocylindrical condenser was used to measure the mean radius of the particles as the humidity was altered. It was found to be a more convenient and quicker way of measuring the mean radius than the diffusion battery. Comparison of the two methods of size measurement showed very close agreement, the meaurements only differing by a few per cent.

The ion tube, shown in Figure 3.14, is a concentric tube capacitor. The dimensions of the ion tube are given in Table 3.3 overleaf. A potential difference is applied across the air gap to remove all charged particles with mobility greater than some critical value.

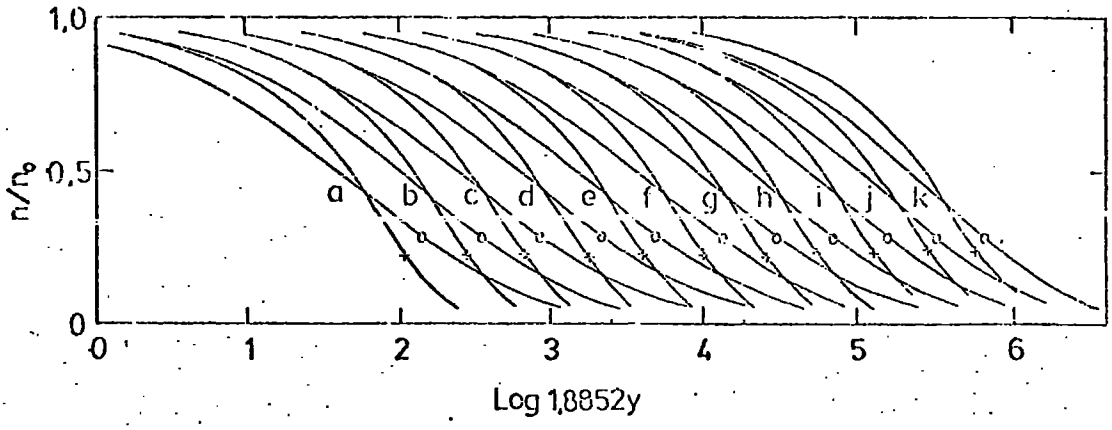

Figure 3.12 Penetration curves of polydisperse aerosols through a parallel-walled channel.

Curves	a	b	c	d	e
r_E(cm)	10^{-7}	1.6×10^{-7}	2.5×10^{-7}	4×10^{-7}	6.3×10^{-7}
	f	g	h	i	j
	10^{-6}	1.6×10^{-6}	2.5×10^{-6}	4×10^{-6}	6.3×10^{-6}
	k				
	10^{-5}				
Symbols	+	o			
Log β_E	0	0.4			

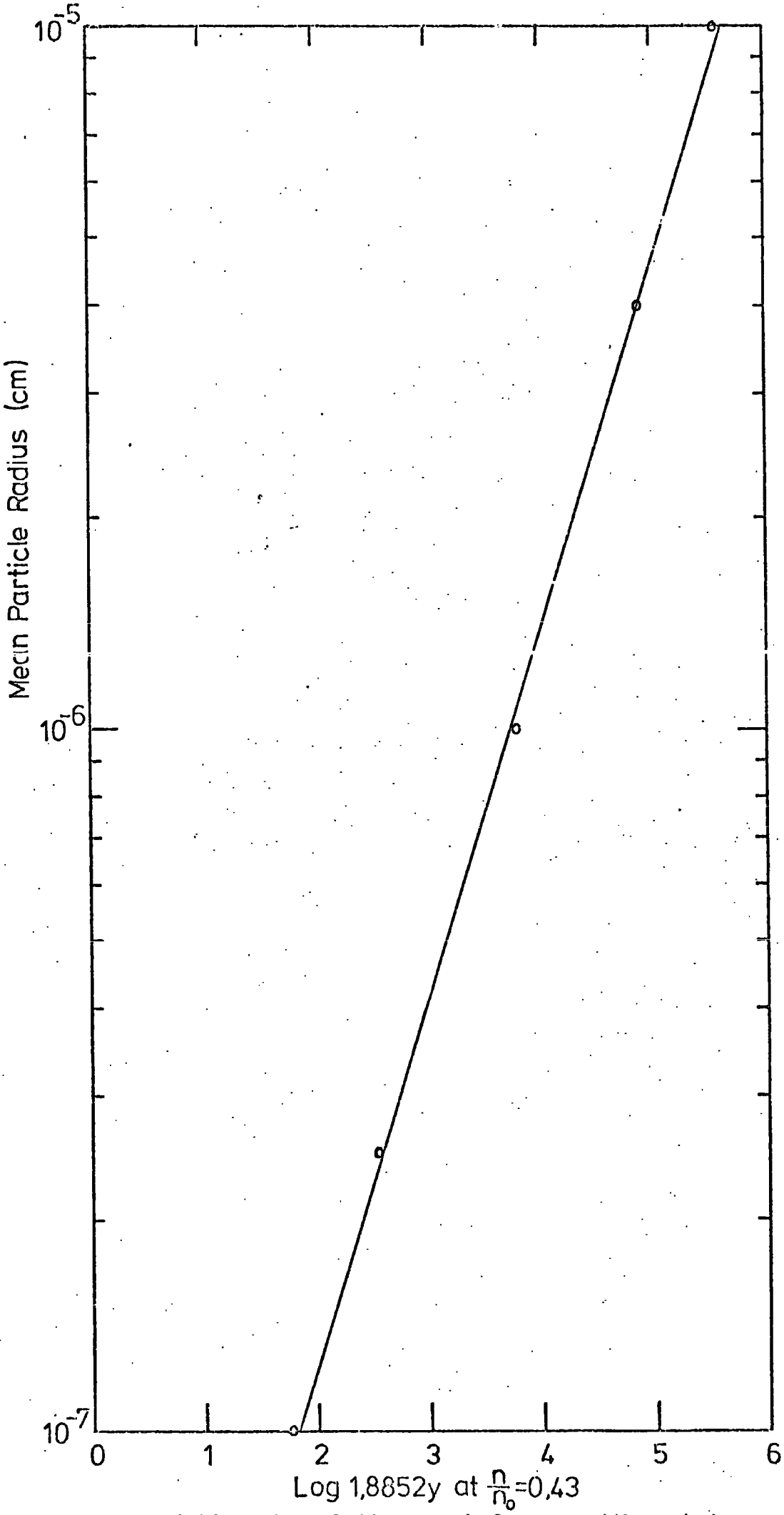

Figure 3.13 Interpolation graph for use with Fuchs' curves.

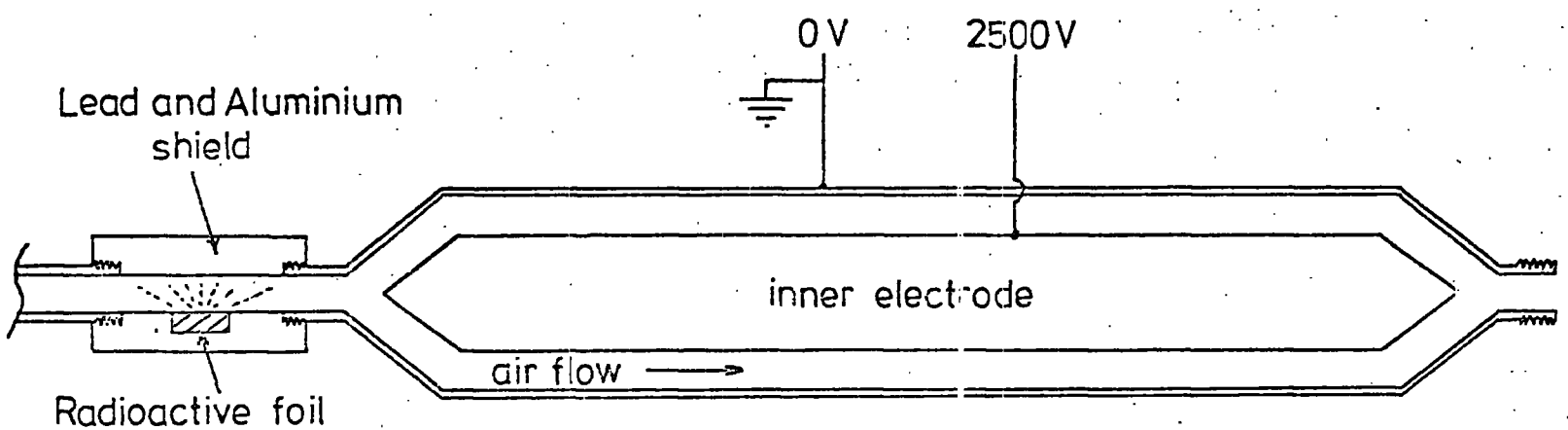

Figure 3.14 Schematic Diagram of the Large Ion Tube

Particles entering the tube are brought to electrical equilibrium by a radioactive Americum foil of strength 125μC. A check was made to ensure that this source did not produce particles. The ratio of the concentration of uncharged particles (N_o) to the concentration of all the particles (Z) has been related to an equivalent size, r, by Keefe, Nolan and Rich (1959) who assumed that the charge distribution on the aerosol obeys a Boltzmann law when the aerosol is in electrical equilibrium. Values of r as a function of N_o/Z have benn tabulated by Metnieks and Pollak (1961).

The number of particles passing through the tube was measured with and without the high voltage applied using a sequential measurement procedure similar to that used with th diffusion battery.

Mean circumference of the airgap (b)	12.95cm
Length of the ion tube (l)	86.36cm
Spacing between the tubes (h)	0.3175cm

Table 3.3 Dimensions of the ion tube

It was necessary to use a high airflow rate of about 8 l min^{-1} in order to avoid appreciable diffusion loss. A voltage of 2500V was used to ensure complete removal of the charged particles as shown below. A convenient voltage source was the Brandenburg model 512 which was driven by a D.C. input voltage of 10 – 30V. This has the advantage that it can be switched off immediately with a simple cam switch.

The mobility of a particle is given by the equation

$$\omega = v/E \qquad (3.4)$$

where v is the velocity of the particle and E is the applied field. So its longitudinal transit time down the tube $= \frac{lA}{Q} = \frac{lbh}{Q}$ (3.5)

where l is the length of the tube, b is the mean circumference of the airgap, h is the spacing between the tubes and Q is the air flow rate. A is the area of the annulus ($\simeq$ bh).

The radial velocity of the particle is given by

$$\omega E = \frac{\omega V}{h} \qquad (3.6)$$

where V is the applied voltage and the radial transit time is given by

$$\tau = \frac{h^2}{\omega V} \qquad (3.7)$$

For a critical mobility (ω_c), above which all particles are caught:

$$\frac{h^2}{\omega_c V} = \frac{lbh}{Q} \qquad \Longrightarrow \qquad \omega_c = \frac{Qh}{lbV} \tag{3.8}$$

So, for a flow rate of 8 litres min^{-1} and an applied voltage of 2500 V the critical mobility is $1.5 \times 10^{-5} cm^2 V^{-1} s^{-1}$. This corresponds to a radius of about 4 micrometres using tables due to Metnieks and Pollak (1961). This indicates that all particles smaller than 4 micrometres in radius were captured when the voltage was applied. It was necessary to dry the ion tube thoroughly after use as condensing water was apt to cause electrical breakdown across the necessarily narrow spacing if allowed to accumulate.

CHAPTER 4

THE EXPERIMENTAL PROCEDURE AND RESULTS

4.1 The Experimental Procedure

The following experimental procedures were normally adopted in the course of an experimental run:

The storage vessel was first filled with dry, filtered air by means of a compressor pump. The system was then tested for filtered by means of the photoelectric counter through the observation of the "scintillation effect". When the storage vessel was free from nuclei, aerosol particles generated by the Collison atomizer were introduced into the storage vessel continuously. The particle concentration was allowed to rise to about 5×10^4 particles cm^{-3} before generation was stopped. It was found that, at higher concentrations, rapid growth of the particles by coagulation occurred. Measurements of particle number concentration were taken every 2 minutes throughout each experiment, beginning as soon as the aerosol generator was switched on. The psychrometer fan was switched on at the start of an experimental run and the wet and dry bulb readings were taken throughout the experiment at 2 minute intervals.

A typical variation of particle number concentration with time from the initial introduction of the particles is shown in Figure 4.1. Equivalent size measurements were made, when the particle concentration became steady, using an ion tube. This technique has already been described in section 3.7. The size measurements were taken continuously throughout the experiment.

Once the initial size was established, the humidity in the chamber was raised by introducing water into the storage vessel. Selected parts of the walls were wetted in order to obtain size measurements at intermediate humidity values. It was found that the relative humidity remained quite stationary over a size measurement. For example, in the range of humidity between 70 and 80%, the humidity rose by only 3% during the course of a complete size measurement.

The rate of rise of humidity could be increased by introducing additional water to the vessel. During a complete experimental run, at least five size measurements could be made at different humidity values. In general the lowest humidity attained was about

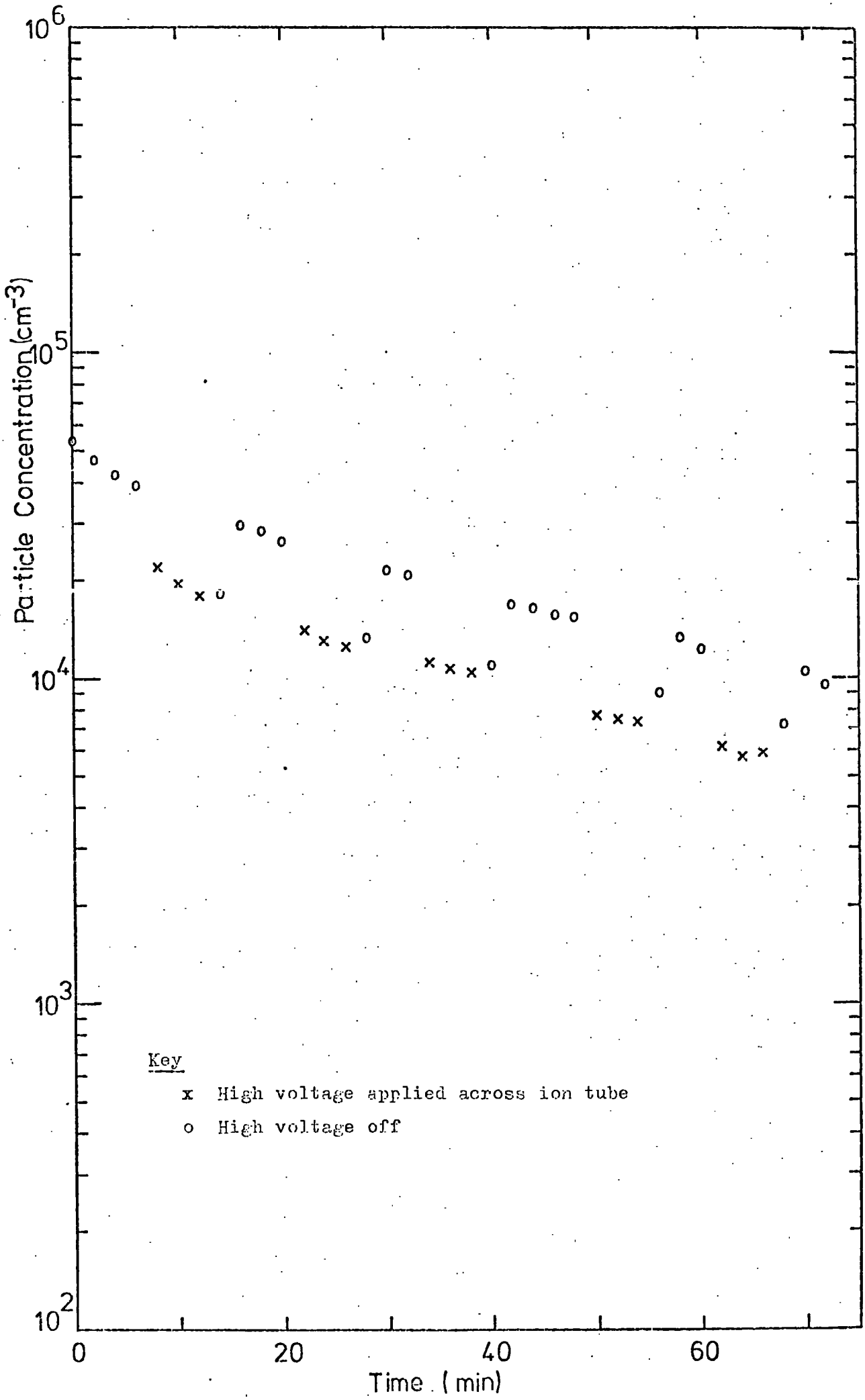

Figure 4.1 Typical variation in particle concentration during experiment.

50 per cent whilst the highest value was usually of the order of 92 per cent.

4.2 The Generated Aerosol

A solution concentration of about 0.005% by weight in the Collison atomizer was found to produce particles of about 2×10^{-6}cm mean radius. Analysis of the size distribution was carried out using the diffusion battery as described in section 3.6. Typical results, shown in Figures 4.2 and 4.3, indicate that the distribution was approximately log normal with a geometric mean radius and geometric standard deviation of 2.44, 3.16 and 2.78, 2.51 for sodium chloride and ammonium sulphate particles respectively. A graph of n/n_o at 0.43 plotted against log 1.8852y using Fuchs' data was used to interpolate between Fuchs' curves in order to obtain values of the geometric mean radius at intermediate points. This graph is shown in Figure 3.13 and the theory is explained in section 3.6.

4.3 Coagulation Effects

A typical experiment took approximately one and a half hours to perform during which time one would expect some coagulation and an increase in the mean particle size to occur. To check on this, experimental runs were carried out in which the humidity was not altered but the particle size was monitored continuously. In a typical experiment the humidity changed from 62% to 64%. Five size measurements were made which showed no systematic increase with time. The mean and standard deviation of the 5 measurements were 3.047×10^{-6}cm and 0.1407×10^{-6}cm respectively. The standard error was 0.0704×10^{-6}cm or about 2.3% which suggests that the contribution of coagulation to the particle growth can be regarded as negligible.

4.4 The Experimental Results and Discussion

The measurements of particle size as the relative humidity was increased are shown in Figures 4.4 and 4.5 for both ammonium sulphate and sodium chloride particles. The measurements for ammonium sulphate represent the growth for three initial dry radii of 2.8×10^{-6}cm, 2.9×10^{-6}cm and 3.1×10^{-6}cm. It can be seen that the smallest particle size grows to 4.0×10^{-6}cm as the humidity is increased from 61% to 89%, which represents a size increase of 43%.

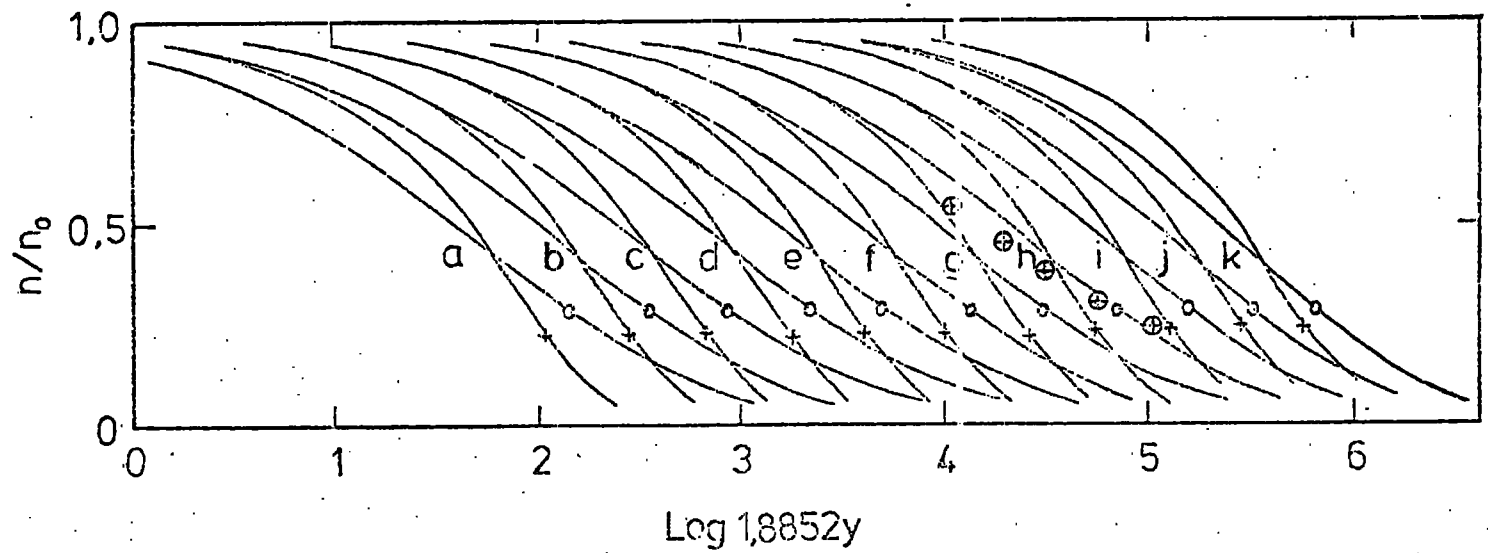

Figure 4.2 Experimental measurements of the size distribution of the generated sodium chloride aerosol.

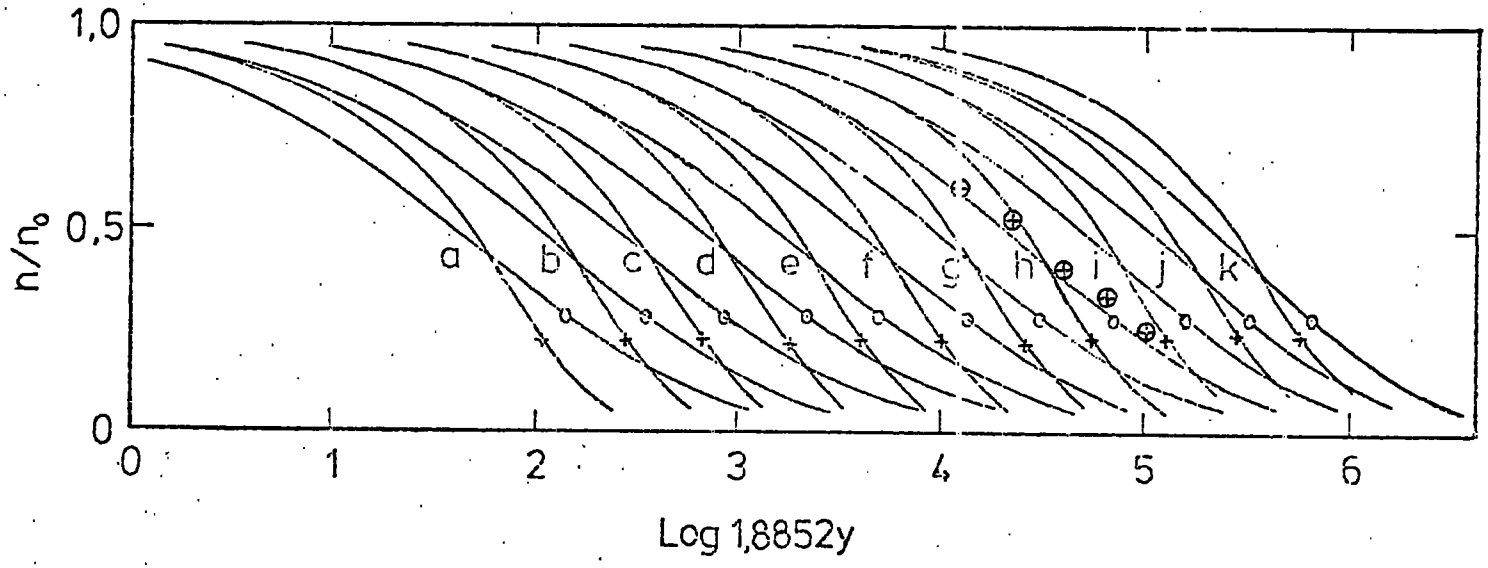

Figure 4.3 Experimental measurements of the size distribution of the generated ammonium sulphate aerosol.

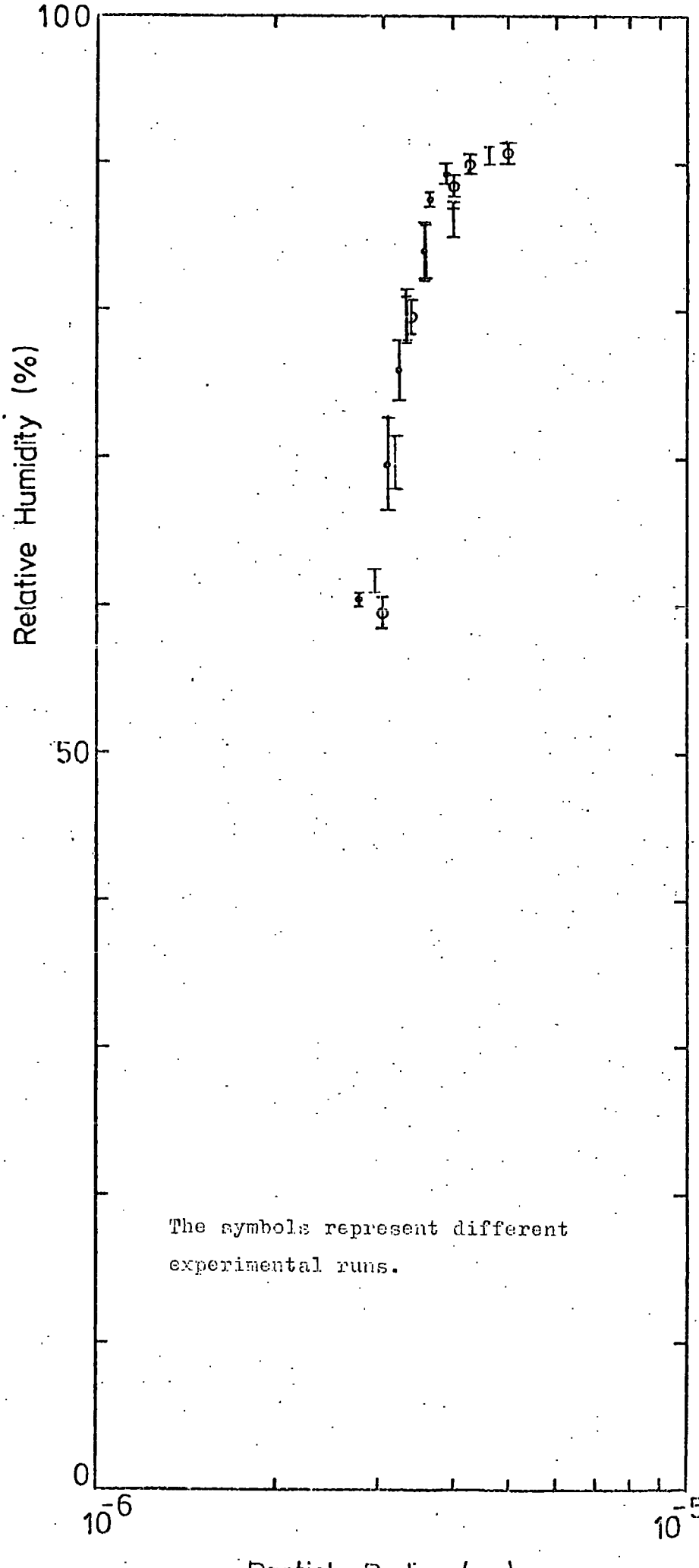

Figure 4.4 Experimental growth of ammonium sulphate.

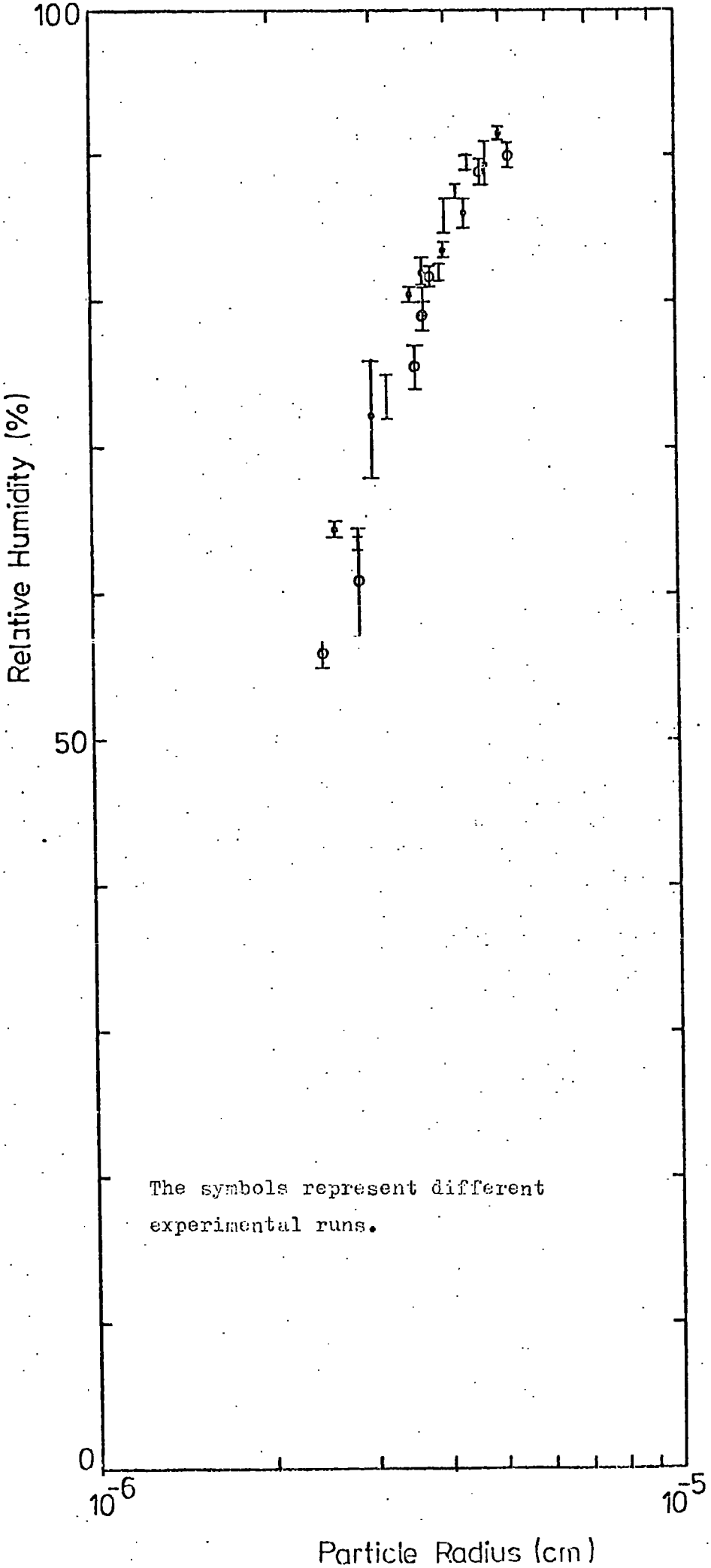

Figure 4.5 Experimental growth of sodium chloride.

The largest particle size of 3.1×10^{-6}cm is increased to a value of 5.0×10^{-6}cm which is an increase of 61%. The growth of sodium chloride particles of initial radius 2.5×10^{-6}cm, 2.7×10^{-6}cm and 2.8×10^{-6}cm as the humidity is increased from about 60% to about 92% is shown in Figure 4.5. The smallest particles increase in size by a factor of two over this range. A summary of the fractional increase in particle size as the humidity is increased to the maximum value is given in Table 4.1 for both salts.

	Initial Humidity (%)	Radius ($\times 10^{-6}$cm)	Final Humidity (%)	Radius ($\times 10^{-6}$cm)	Fractional Size Increase
ammonium sulphate	62	2.8	89	3.9	0.39
	63	2.9	92	4.7	0.62
	59	3.1	92	5.0	0.61
sodium chloride	56	2.5	90	5.1	1.04
	64	2.7	92	5.0	0.85
	67	2.8	89	4.4	0.57

Table 4.1 Typical Experimental Growth of Ammonium Sulphate and Sodium Chloride particles.

A comparison is made between the experimental growth curves and the theoretical predictions according to Equation 2.13. Two theoretical curves for ammonium sulphate, between which the experimental points are approximately bounded, are drawn for initial dry particle radii of 2.4×10^{-6}cm and 2.6×10^{-6}cm in Figure 4.6. The comparison shows good agreement between the experimental values and the theoretical curves representing particle sizes of 3.1×10^{-6}cm and 3.3×10^{-6}cm at 60% relative humidity. Similar theoretical curves are drawn for sodium chloride in Figure 4.7 for initial dry particle radii of 1.8×10^{-6}cm and 2.0×10^{-6}cm. These yield values of the theoretical radii at 60% relative humidity of 2.8×10^{-6}cm and 3.1×10^{-6}cm which compare favourably with the initial experimental values.

The experimental points lie very close to the predicted lines with some variation which may be explained in terms of the particles going into solution and recrystallising before entering the humidity chamber. When the particles are generated by the nebulizer they are droplets of solution. Since they are dried to about 55% relative

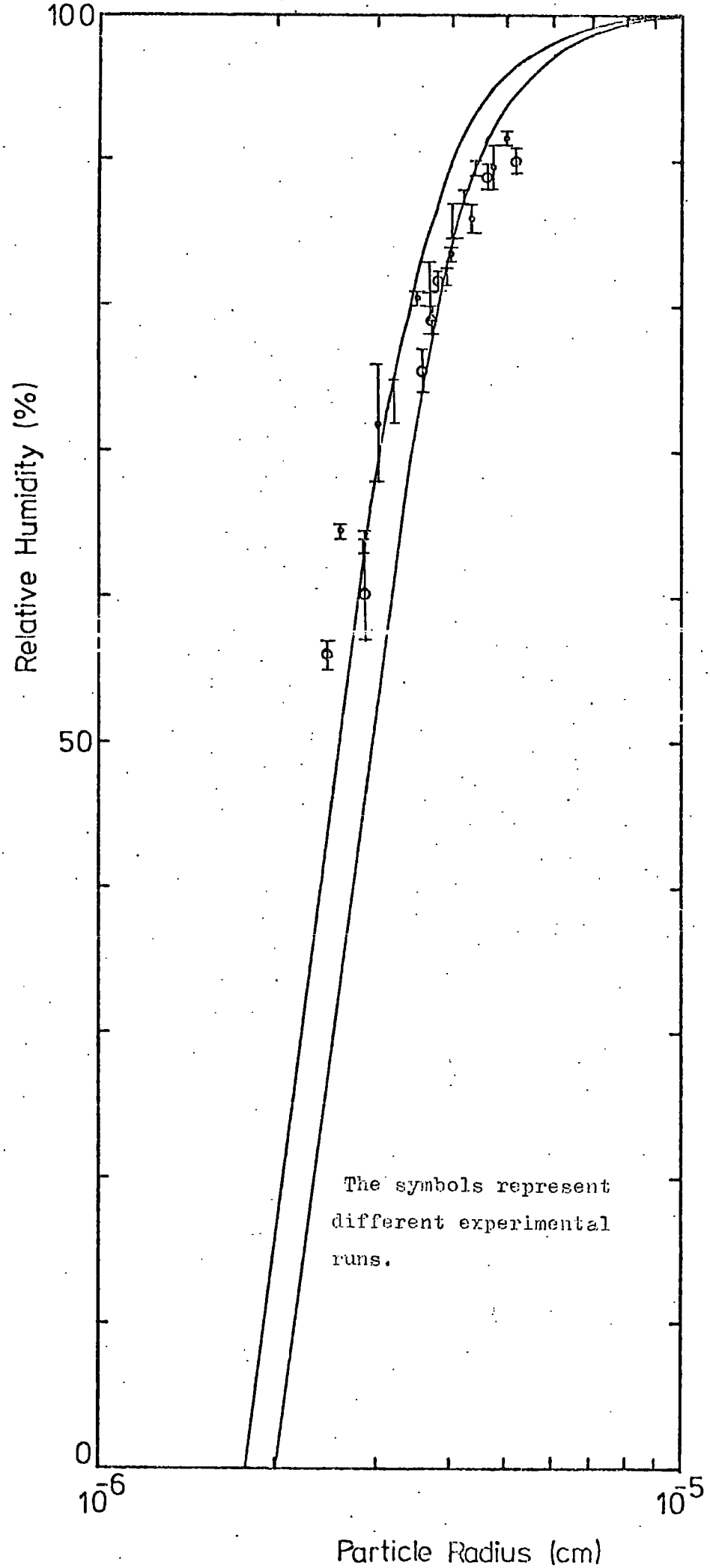

Figure 4.6 Comparison of theory with experiment (NaCl).

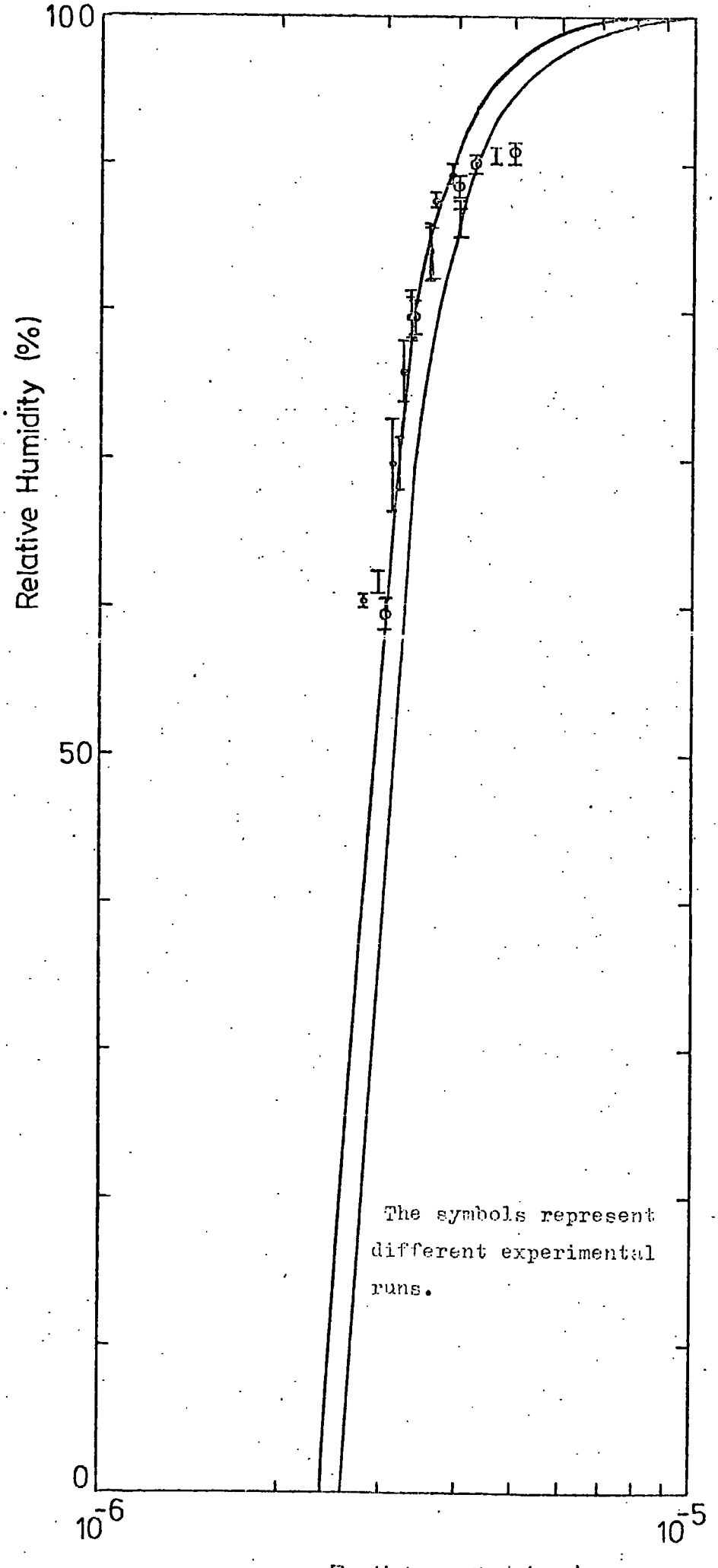

Figure 4.7 Comparison of theory with experiment ($(NH_4)_2SO_4$).

humidity a proportion will recrystallise but some will remain in a supersaturated solution form. This mixture of particles is then introduced to the storage chamber where the humidity is increased. The supersaturated droplets would be expected to follow a curve similar to the theoretical curve as shown by curves (a) in Figures 4.6 and 4.7 but the dry particles, on reaching a critical humidity, will go into solution and grow significantly over a very small range of humidity. At this point some spreading of the points will start to occur. Work by Orr et al. (1956) indicates that particles tend to dissolve at a precise value of the humidity but recrystallisation can occur over a much wider range and cannot yet be satisfactorily predicted. The same work suggests that sodium chloride and ammonium sulphate particles with initial radii of the order of 0.01 micrometres would completely dissolve at about 70% and 63% relative humidity respectively.

A spread of results is indeed observable in the sodium chloride curve at a value of 73% to 74% relative humidity. There appears to be a lack of spread in the experimental values for ammonium sulphate which probably indicates that only a small percentage of particles recrystallised after generation. It can be seen that maximum particle growth occurs for the two salts at the higher values of relative humidity. Experimental measurements at constant humidity indicate that coagulation plays little part in the growth of the aerosol particles compared with the growth due to the condensation of water vapour.

CHAPTER 5

AN ANALYSIS OF THE ATMOSPHERIC AEROSOL SAMPLED AT DURHAM UNIVERSITY

5.1 Introduction

In order to calculate the effect of relative humidity on the growth of atmospheric particles it is desirable to know the shape of the particle size distribution. Similarly, knowledge of the size distribution is essential in order to make accurate predictions of the effect of particle growth on the extinction coefficient.

Few particle size distribution measurements have been published which extend over periods longer than a few days. Measurements of the salt content of the air sampled between 100 and 1600 hours in July and August 1970 have been made by Blanchard and Syzdek (1972) at Oahu in Hawaii. Junge and Jaenicke (1971) have presented data collected over 24 days from 13 April 1969 during the Atlantic expedition of the R.V. Meteor and Whitby et al. (1975) have published data collected over 24 hours on 19 and 20 September 1972 along the Harbor Freeway in Los Angeles, California.

The results presented here are based on measurements of the natural aerosol size distribution in the radius range 0.25 to 5.0 micrometres radius over a 49 day period from 21 July to 8 September 1975 at Durham Observatory. An attempt is made to correlate the particle concentration in five size ranges with some common meteorological parameters, in particular humidity and wind speed.

5.2 The Instrumentation and Measurement Procedures

A Royco model 225 optical particle was used. It allowed the aerosol particle size range to be classified into five radius categories, viz. 0.25 - 0.35, 0.35 - 0.7, 0.7 - 1.5, 1.5 - 2.5 and 2.5 - 5.0 micrometres. The counter was precalibrated with homogeneous sources of Latex particles over the five ranges.

Measurements were made at Durham Observatory, situated about 2 km SSW of Durham City in the North of England. The city has a population of 28,250 and some light industry. Continuous records of windspeed, wind direction, temperature and humidity were available at the site.

Air was drawn in at a height of 4m above ground level. An oil free Diaphragm pump operating at a flow rate of 70 l min^{-1} was used

to draw the air through a mixing vessel from which a sample was drawn to the optical counter sensor head via a short piece of antistatic tubing at a constant flow rate of 2.83 l min^{-1}. Calculations showed, using the fractional loss formula for particles settling in a horizontal tube (Thomas, 1958), that negligible loss of particles occurred in the sampling tube. The number concentration for each size category was printed onto an automatically operating digital line printer and subsequent analysis of the measurements was carried out on an IBM 370/168 computer.

5.3 The Experimental Results

Results are described of continuous measurements over 49 days from 21 July to 8 September 1975 of the particle size distribution in the radius range 0.25 to 5 micrometres at Durham Observatory. In addition an analysis is made of aerosol particle size measurements taken continuously every minute over a 6 day period from 15 July to 21 July 1975 in Durham.

Measurements of the particle radius categories 0.25 - 0.35, 0.35 - 0.7, 0.7 - 1.5, 1.5 - 2.5 and 2.5 - 5.0 micrometres were taken successively over a period of ten minutes so that an entire sampling cycle took fifty minutes. The diurnal variation of the individual particle size categories averaged over the 49 continuous observational days is shown in Figure 5.1. It clearly shows maximum number concentration occurring in all size ranges, with the exception of the largest particles, during the period from 0200 to 0800 BST (British Standard Time). The afternoon period from 1400 up to about 2000 hours BST is characterised by a distinct minimum in particle concentration for the lower particle size categories.

The hourly variations of particle concentration in three of the size ranges is shown in Figure 5.2 over the total period of measurement. Two curves are omitted for clarity but they follow the same general pattern of variation shown by the 0.25 - 0.35 micrometre range. The increase in particle numbers at night followed by an afternoon decrease can be observed here. A general increase in the number concentration can be seen to occur from about the 3rd to the 15th of August which corresponds to a significant increase in the daily average temperatures for the period. This is reflected in the positive correlation coefficient values shown in Table 5.3 and probably indicates that photochemical reactions are making an important contribution to particle production.

Figure 5.1 Diurnal Variation of Particle Concentration

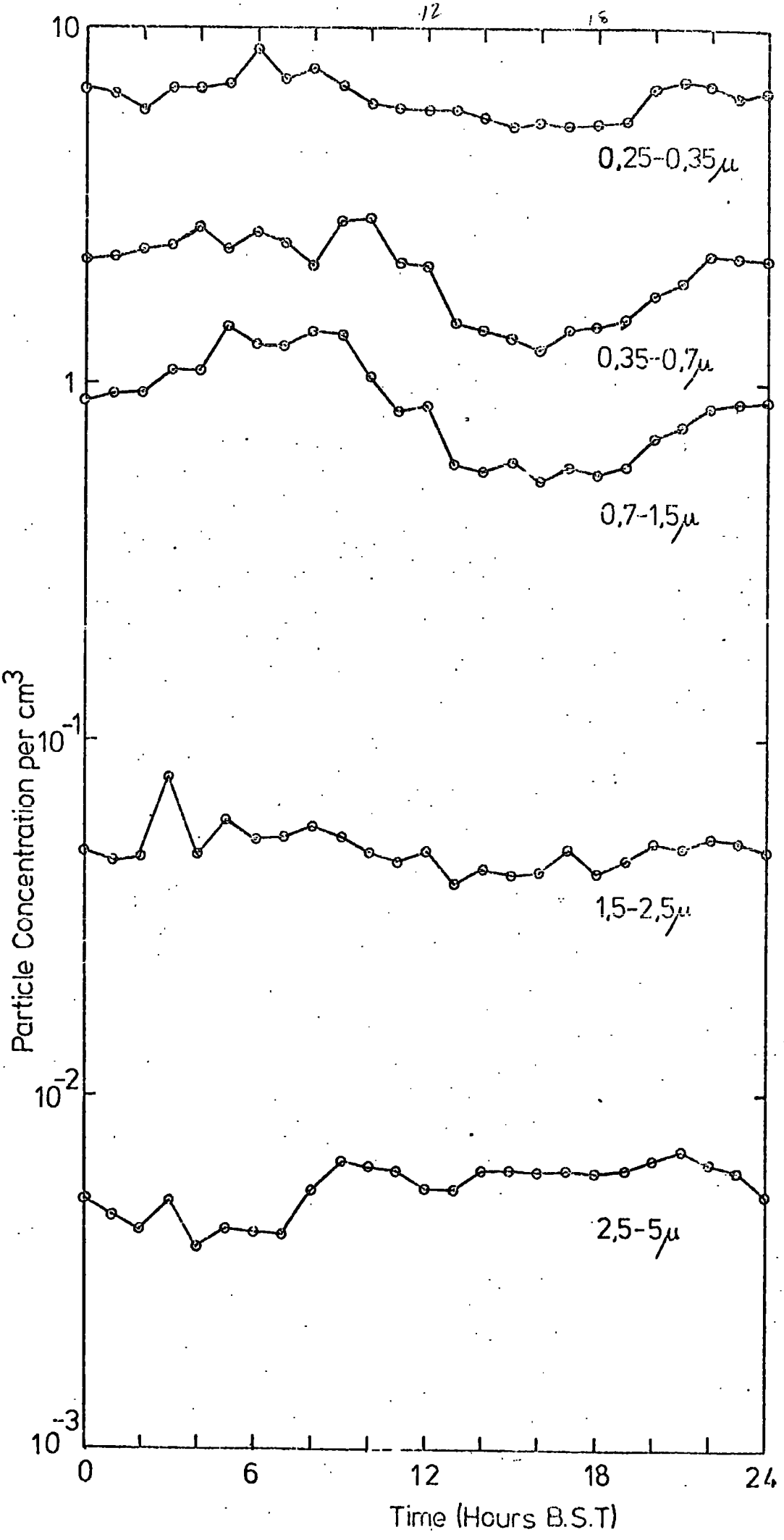

Figure 5.2 Hourly variation in particle concentration over 49 days

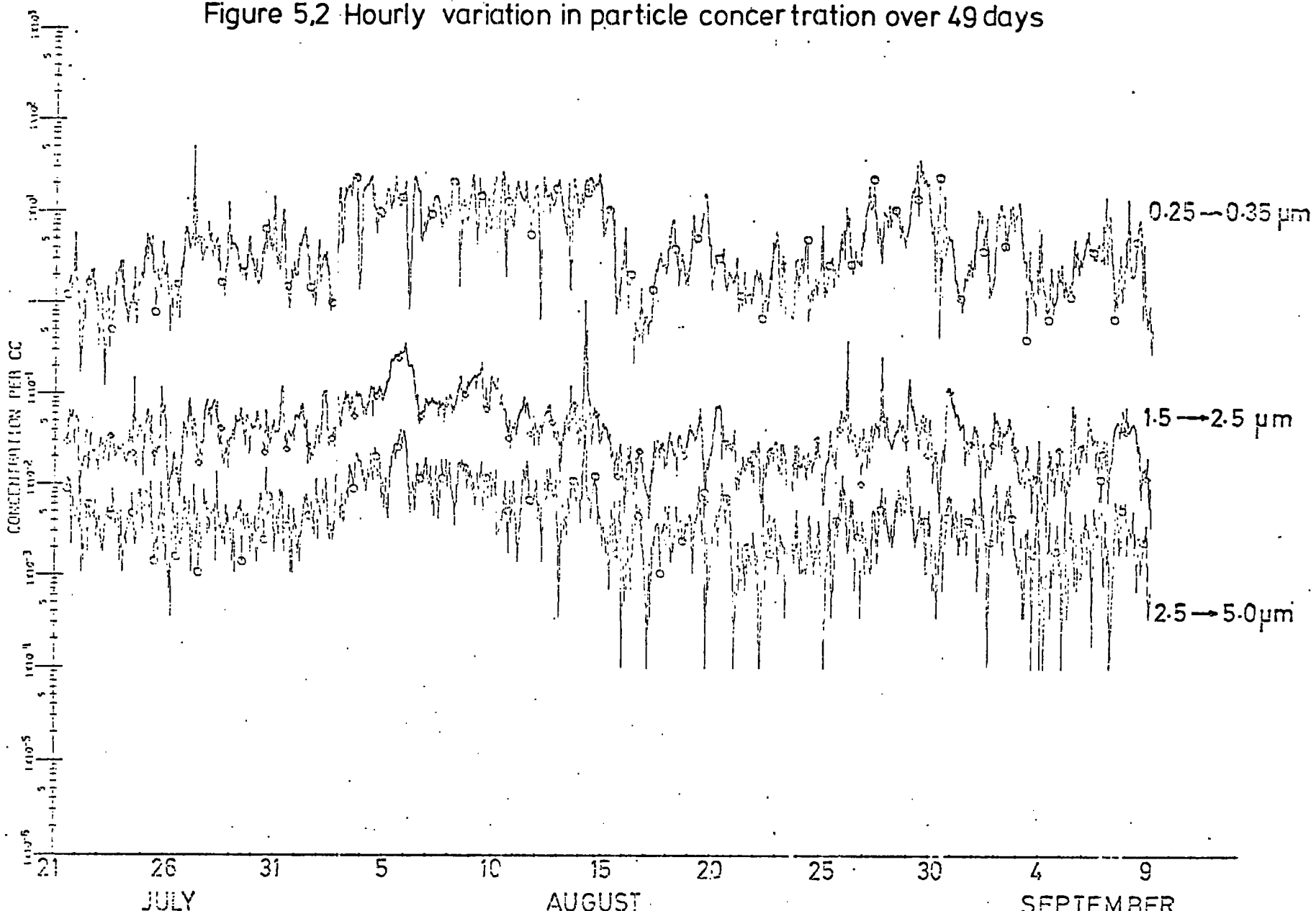

Table 5.1

Summary of Statistics of Particle Concentration

Diameter Range (μm)	0.5-0.7	0.7-1.4	1.4-3.0	3.0-5.0	5.0-10.0
Geometric Mean Radius of Interval (μm)	0.2958	0.4950	1.025	1.937	3.536
Arithmetic Mean of Concentration (cm^{-3})	6.372	2.065	9.036×10^{-1}	4.976×10^{-2}	5.555×10^{-3}
Arithmetic Standard Deviation (σ)	6.509	2.899	1.372	5.722×10^{-2}	5.480×10^{-3}
Arithmetic Standard Error ($\alpha = \frac{\sigma}{\sqrt{n-1}}$)	1.923×10^{-1}	8.459×10^{-2}	3.990×10^{-2}	1.669×10^{-3}	1.593×10^{-4}
Geometric Mean	3.853	1.084	5.178×10^{-1}	3.569×10^{-2}	3.891×10^{-3}
Median	3.647	9.569×10^{-1}	4.770×10^{-1}	3.531×10^{-2}	3.884×10^{-3}
Number of Cases	1147	1175	1184	1182	1184
Number of Cases > 0	1147	1175	1184	1182	1170
$\frac{dN}{d\log(r)}$	43.61	6.860	2.730	0.2243	0.01845
Standard Error on $\frac{dN}{d\log(r)}$	1.316	0.2810	0.1206	7.505×10^{-3}	5.292×10^{-4}
$\frac{dV}{d\log(r)}$ (r in μm)	4.727	3.485	12.30	6.822	3.416
Standard Error on $\frac{dV}{d\log(r)}$	0.1426	0.1428	0.5433	0.2283	0.09798

A frequency distribution of the individual observations over the 49 days sampling was calculated using suitable class intervals. The cumulative frequency distribution, Which expresses the percentage of observations less than a selected value of particle concentration N, was calculated and plotted on probability paper.

The results of the cumulative distribution of the five size ranges are shown in Figure 5.3. A line of best fit using the weighted least squares procedure which also allows for the exaggeration of the deviations due to probability scale is drawn in each case. This procedure was developed by Kottler (1950). It can be seen that the particle concentration follows closely a log normal distribution in each case.

The geometric mean, Z_g, and the geometric standard deviation, σ_g, can be obtained directly from the graph since Z_g corresponds to the 50% probability value and

$$\sigma_g = \frac{84\% \text{ number concentration}}{50\% \text{ number concentration}} = \frac{50\% \text{ number concentration}}{16\% \text{ number concentration}}$$

The values of Z_g and σ_g obtained from the curves of Figure 5.3 compare well with the computed values as seen in Table 5.2.

The particle size distribution, averaged over 49 days of continuous measurement, is presented in Figure 5.4 as a log-radius number distribution following Junge (1963). The graph suggests that the aerosol population may be formed of two separate components which would account for the slight deviation of the central size range. However five points are insufficient to resolve the components so a single distribution following a distribution described by Junge has been assumed. The equation used by Junge is

$$\frac{dN}{d \log r} = Ce^{-\beta} \qquad (5.1)$$

where dN is the number of particles per cm^3 in the range d log r and C is a constant depending on the total number, N, of particles per cm^3.

A weighted line of best fit yields a slope β of 3.04. A study of the effect of sampling frequency on the distribution of particle number concentration was made. Measurements of the particle concentration in the size range 0.25 - 0.35 micrometre radius were taken every minute for a 6 day period from 15 to 21 July 1975 giving a total of 7600 counts. There is an interval of 67 seconds between successive counts since an interval of 7 seconds is required for printout and resetting procedures. The cumulative percentage of

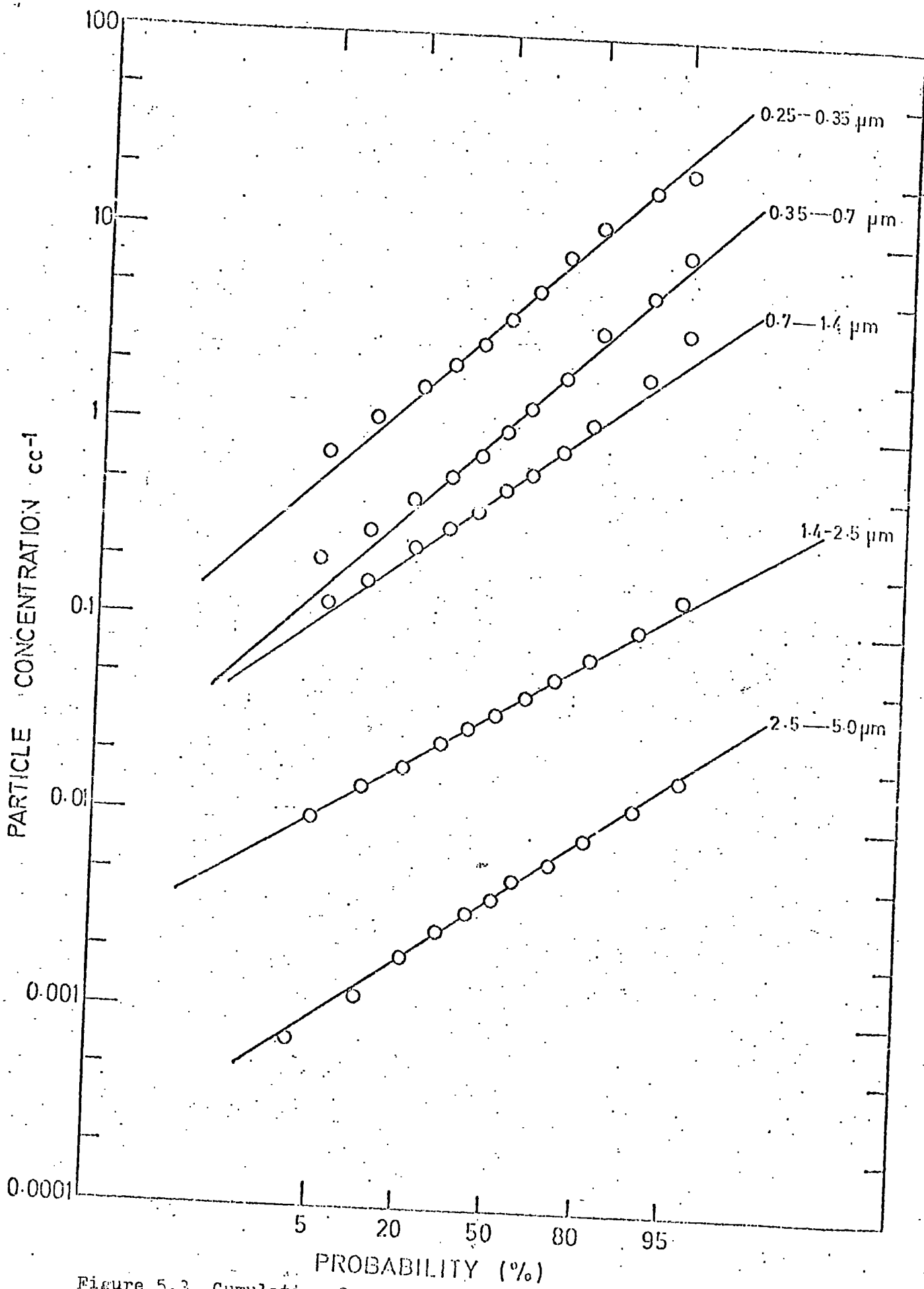

Figure 5.3 Cumulative frequency distribution.

Figure 5,4 Particle Size Distribution

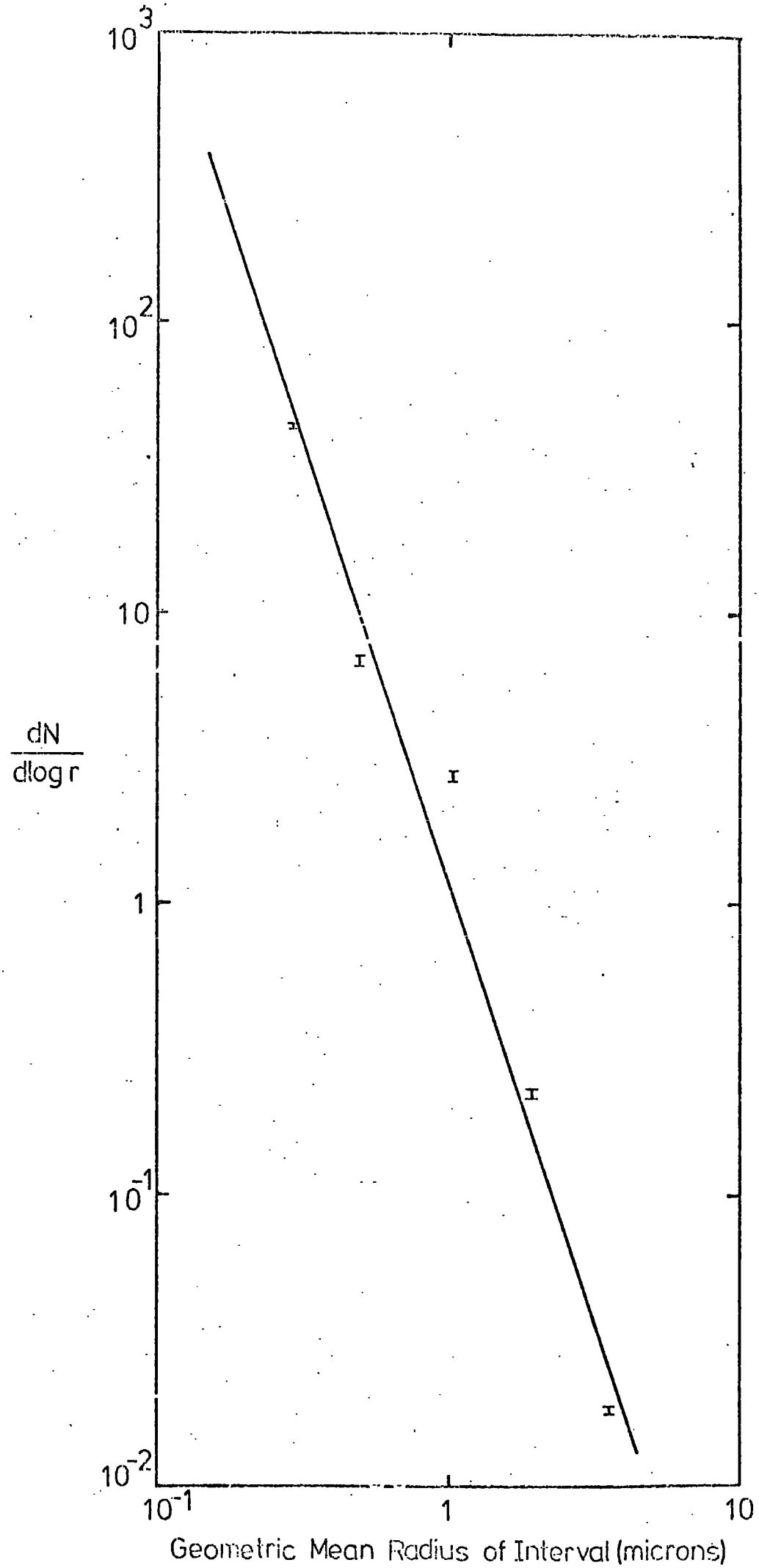

readings of particle number concentration which were less than selected values of the percentage deviation from the mean of all the measurements is shown in Figure 5.5. The solid line represents the one minute sampling measurements. The close proximity of the measured values for the ten and twenty minute intervals indicate that the sampling frequency may be increased by at least twenty-fold from a one minute sampling frequency without significant loss of information.

Particle Radius Range (μm)	0.25 - 0.35	0.35 - 0.7	0.7 - 1.5	1.5 - 2.5	2.5 - 5.0
Geometric mean Z_g of particle concentration cm^{-3} (from Fig. 5.6)	3.75	0.98	0.48	0.035	0.004
Computed value of Z_g from all measurements	3.85	1.08	0.52	0.036	0.0039
Computed value of the median	3.65	0.96	0.48	0.035	0.0039
Geometric Standard Deviation σ_g, of particle concentration (from Fig. 5.6)	3.13	3.19	2.52	2.11	2.37
Computed value of σ_g	2.84	3.05	2.67	2.21	2.44

Table 5.2 A comparison of the statistics obtained from the cumulative curves with the actual values obtained directly from the data.

This finding is reinforced by a similar analysis carried out on the measurements of particle concentration over the 49 days. In Figure 5.6 the solid lines represent the fifty-minute sampling measurements for the smallest and largest radius intervals. The relatively close proximity of the values for 150 and 250 minute

Figure 5,5 Cumulative Percentage Plot July 15-21)

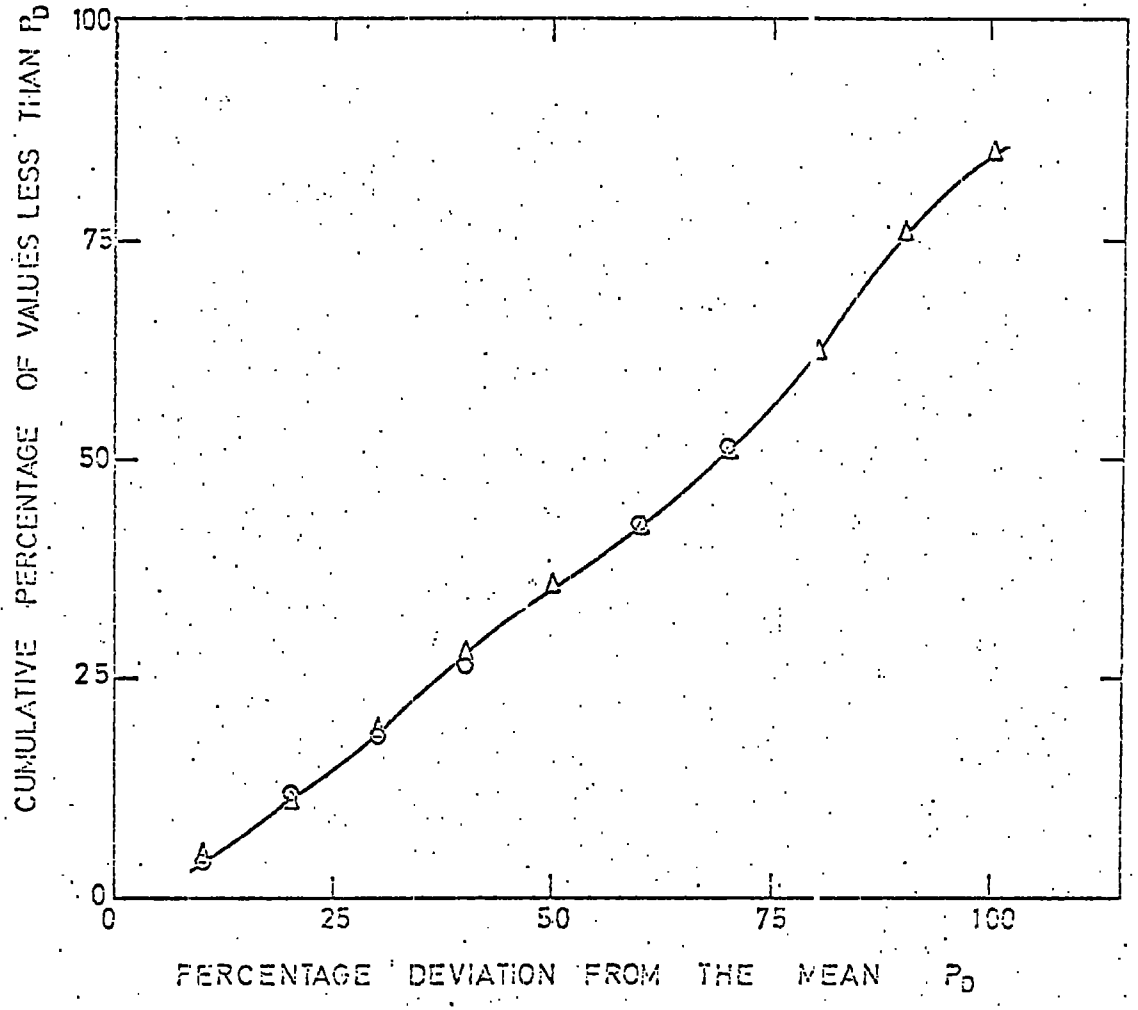

Figure 5,6 Cumulative Percentage Plot over 49 days

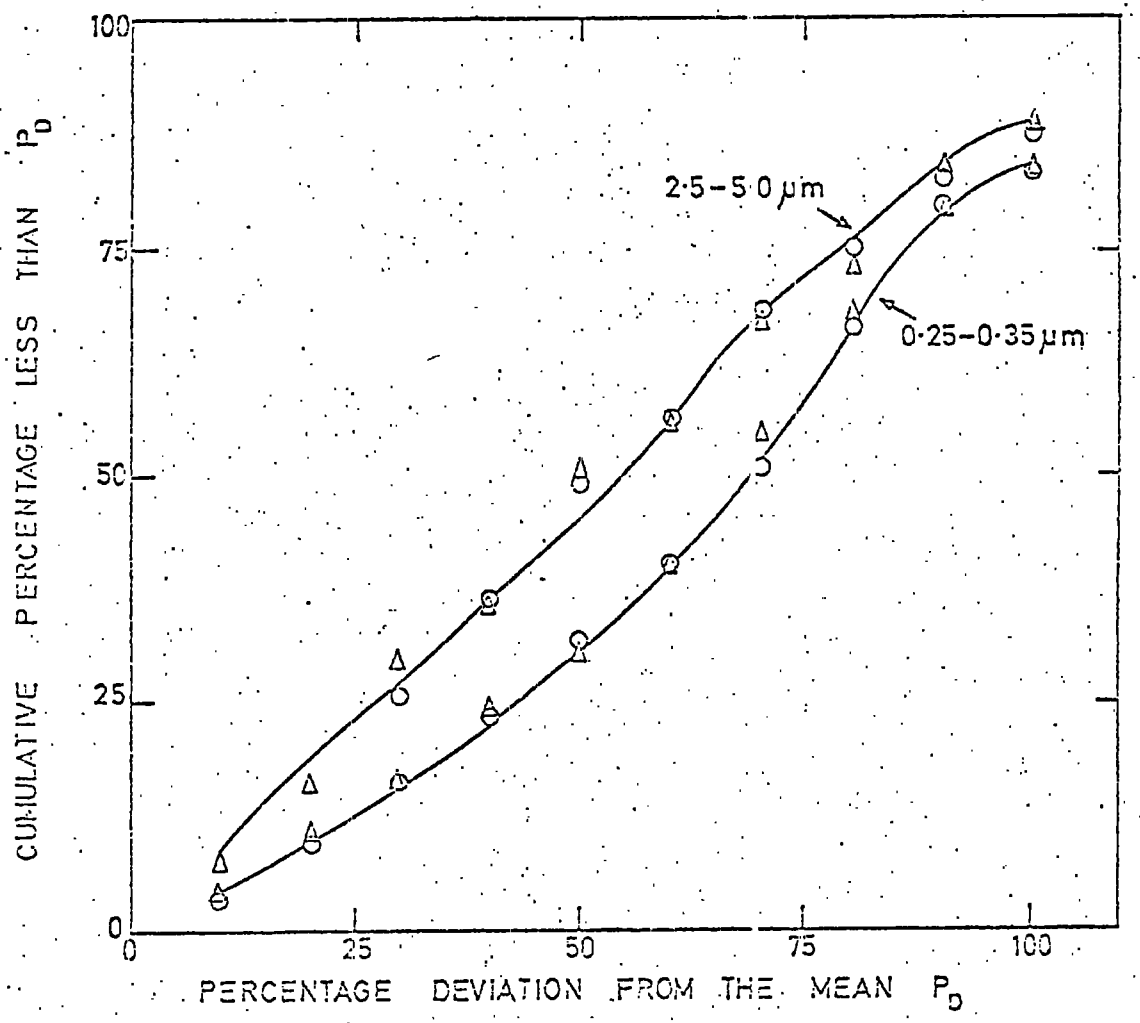

Particle Concentration	Radius Range 0.25-0.35μm	Radius Range 0.35-0.7μm	Radius Range 0.7-1.5μm	Radius Range 1.5-2.5μm	Radius Range 2.5-5.0μm	Wind Direction	Wind Speed	Humidity	Temperature
Radius Range 0.25-0.35μm	1	0.87	0.76	0.59	0.48	-0.33	-0.54	0.24	0.27
Radius Range 0.35-0.7μm		1	0.92	0.66	0.50	-0.36	-0.50	0.27	0.29
Radius Range 0.7-1.5μm			1	.73	0.51	-0.34	-0.44 (2.3%)	0.36	0.21
Radius Range 1.5-2.5μm				1	0.70	-0.36	-0.32	.16	.33
Radius Range 2.5-5.0μm					1	-0.30	-0.16	-0.04 (7.0%)	.45
Wind Direction						1	0.25	0.01	-0.25
Wind Speed							1	-0.26	-0.06
Humidity								1	-0.41
Temperature									1

Table 5.3 The Pearson product-moment correlation coefficient between the variables

sampling frequencies compared with the 50 minute solid curves illustrates the the sampling frequency can be extended to these large values particularly over long measurement periods. The curves indicate that about 30% of the total number of measurements are within 50% of the overall mean concentration value for the smallest particles and about 50% of the measurements lie within one standard deviation of the mean. Higher cumulative percentage values apply to larger particles.

A correlation analysis was carried out on the 49 day results. The Pearson product-moment correlation coefficients between the 5 particle concentrations and windspeed, wind direction, humidity and temperature are shown in Table 5.3. The coefficients have a significance level of 0.1% unless otherwise stated. The measurements of wind direction may not be sensitive enough to yield any detailed results since the wind was classified in quadrant intervals due to the scatter of the plots from the Dynes pressure tube anemomograph. There was insufficient rainfall during the period to include this as one of the parameters. There is high correlation between adjacent size ranges and, with the exception of the largest particles, a relatively high correlation of particle number concentration with windspeed was obtained.

A scatter diagram of windspeed in knots versus particle concentration in the range 0.25 - 0.35 micrometres is shown in Figure 5.7. The line of regression of the parameter Y{$\log_{10}$(particle concentration)} on X (windspeed) is

$$Y = -0{,}0588\,X + 0{,}8953 \qquad (5.2)$$

The decrease in particle concentration with increase in windspeed occurs for all size categories examined and can probably be attributed to increased vertical transportation of the particles due to an increase in atmospheric turbulence.

Figure 5.8 shows a scatter diagram of the relative humidity versus particle concentration in the same range. Poor correlation is obtained although an increase in concentration with humidity might be expected if the particles grow since there are more small particles than large ones.

Table 5.4 shows the percentage of particle counts made with the wind in each quadrant.

5.4 Discussion and conclusions

The diurnal variation of the natural aerosol particle size

FIGURE 5.7

Particle Number Concentration versus Windspeed

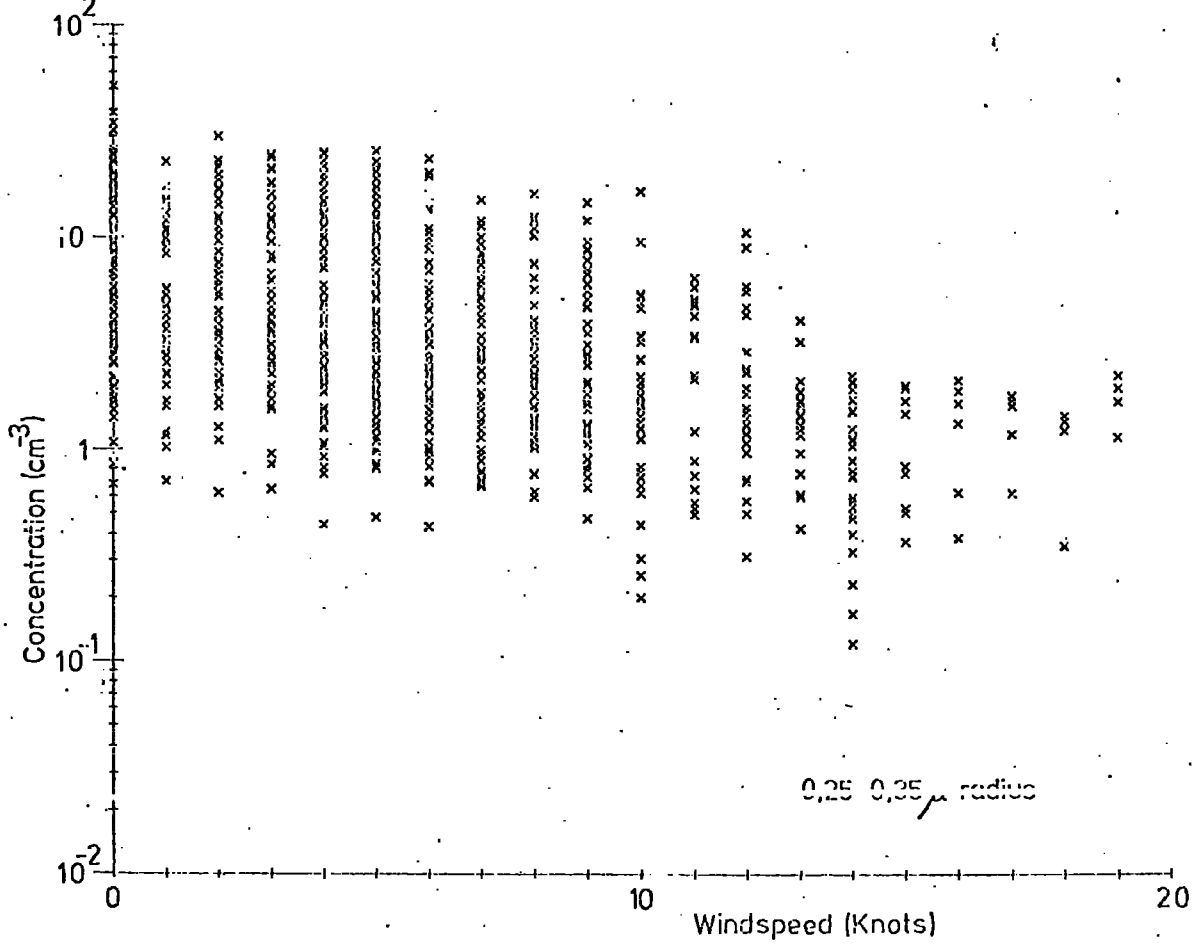

FIGURE 5.8

Particle Number Concentration versus Relative Humidity

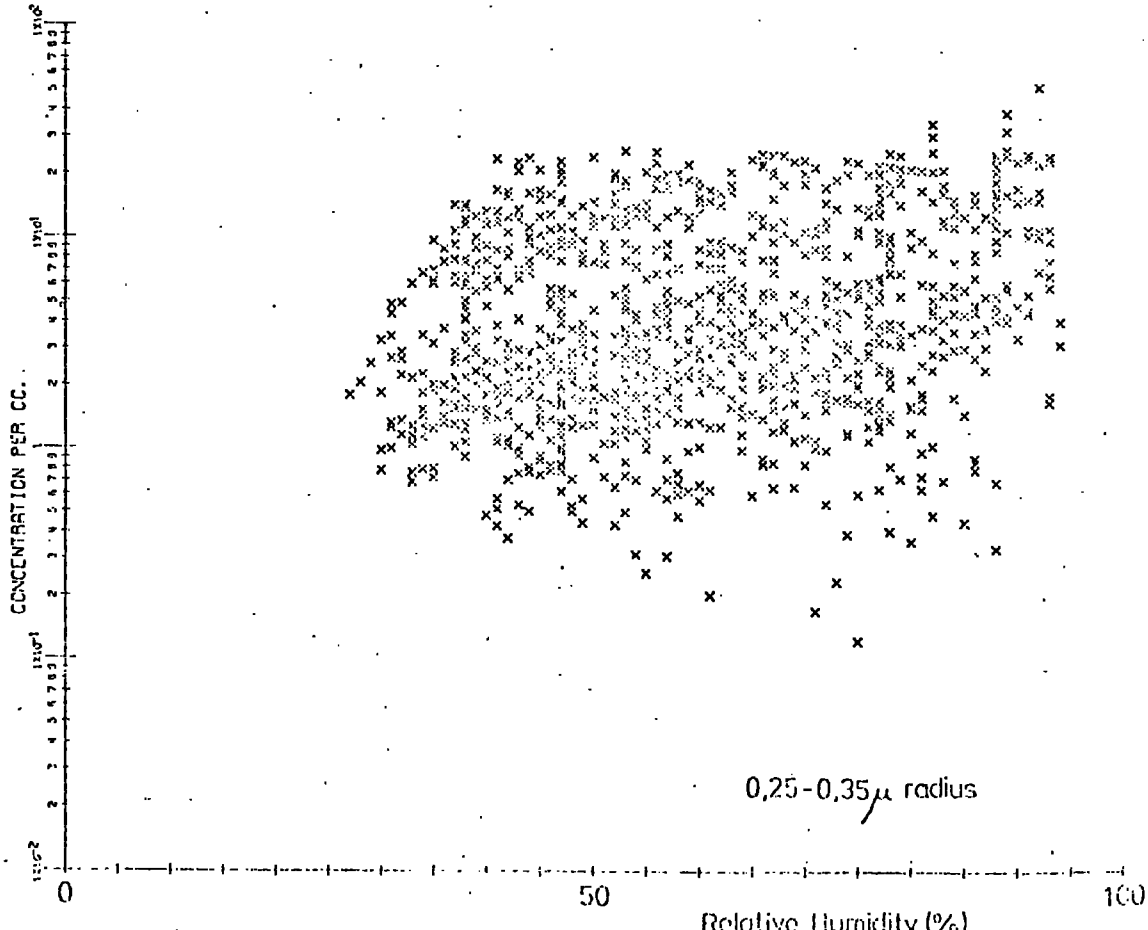

distribution in the size range from 0.25 to 1.4 micrometres in radius is distinctive in that it assumes a shape which is approximately an inverse relation to that normally measured for the sub-micrometre Aitken particle distribution.

The diurnal variation of the total particle concentration in the size range 0.7 to 5.0 micrometres averaged over 49 days at Durham Observatory compares favourably with measurements made by Harple, Sverdrup and Whitby (1976) along the Harbor Freeway in Los Angeles, California. Their measurements, made in the size range 0.5 to 5.0 micrometres, were taken during the dates 19, 20, 21, 27, 28 and 29 September using an average of 15 measurements per hour. The mean values in the radius range 0.5 - 5.0 micrometres are shown

Wind direction	Number of particle counts	%
NE	265	22.3
SE	88	7.4
SW	489	41.1
NW	349	29.3

Table 5.4 Wind direction during period of counting

in Figure 5.9a. The diurnal shape compares favourably with the diurnal variation of the total concentration of particle size in the radius range 0.7 - 5.0 micrometres averaged over 49 days at Durham Observatory, plotted in Figure 5.9b.

The general increase in particle concentration particularly in the lower size ranges in the period 0000 to 0600 hours can probably be partly attributed to the increase in humidity, as also reflected in the positive correlation between the parameters, seen in Table 5.2. The distinct minimum in the period from about 1400 to 2000 hours may be partly due to coagulation with Aitken particles which have been shown by several workers to have a high concentration in this period.

The results from Figures 5.5 and 5.6 indicate that particle size distributions can be made less frequent, by as much as twenty-fold, without significant loss of information. This is important since the operating time of the measurement system can be increased

Figure 5,9 Diurnal Variation of the natural aerosol

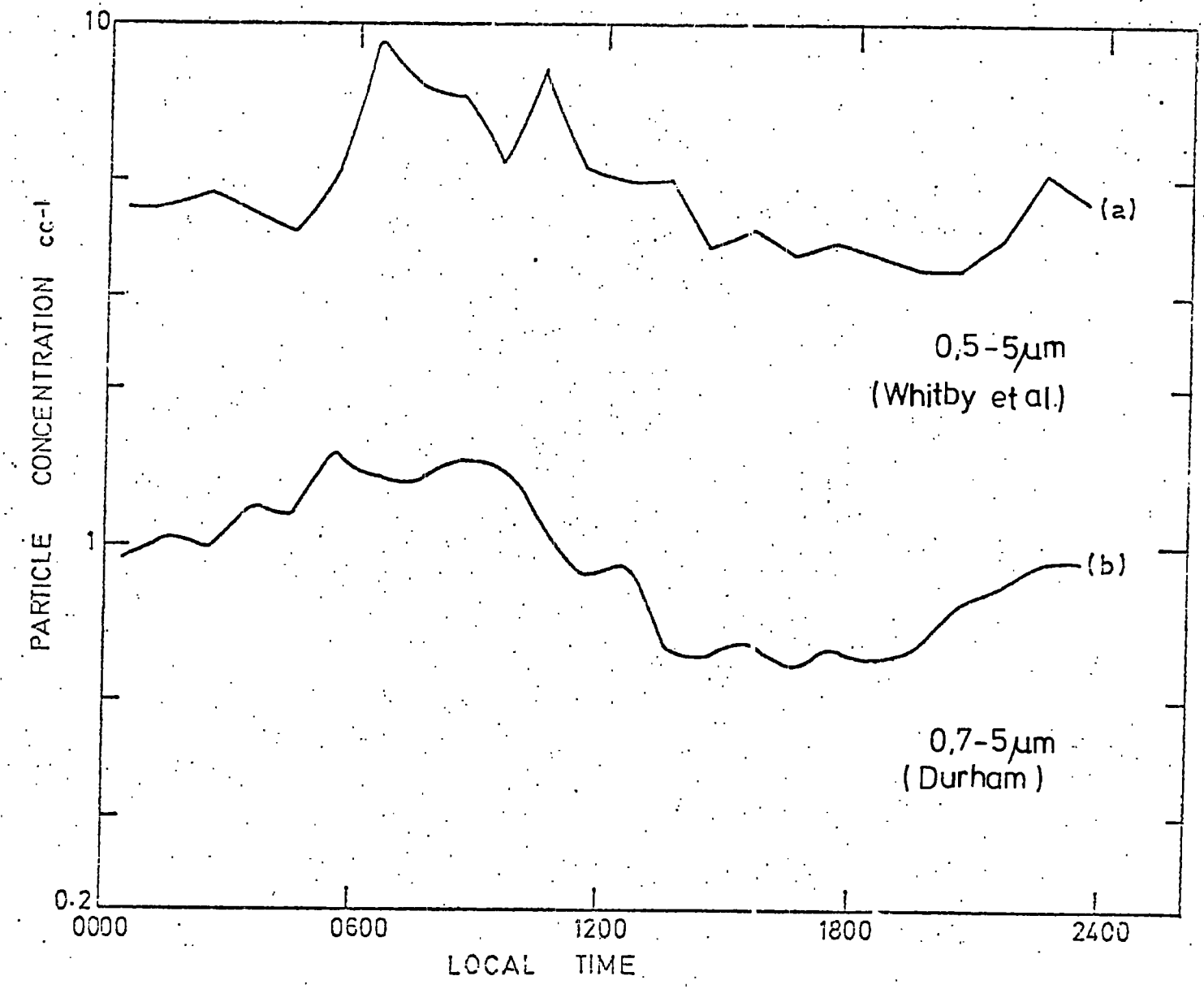

before servicing is required and in addition the volume of particle size data required for analysis can be substantially reduced.

REFERENCES

Blanchard,D.C. and Syzdek,L. (1972) Variations in Aitken and Giant Nuclei in Marine Air. J. Phys. Oceanog. 2, 255-262

Brock,J.R. (1972) Condensational Growth of Atmospheric Aerosols. J. Colloid and Interface Sci. 39 No.1,32-36

Cartwright,J., Nagelschmidt,G. and Skidmore,J.W. (1956) The Study of Air Pollution with the Electron Microscope. Q. J. R. Met. Soc. 82,82-86

Covert,D.S., Charlson,R.J. and Ahlquist,N.C. (1972) A Study of the Relationship of Chemical Composition and Humidity to Light Scattering by Aerosols. J. App. Met. 11, 968-976

Dessens,H. (1949) The Use of Spiders' Threads in the study of Condensation Nuclei. Q. J. R. Met. Soc. 75, 23-26

De Marcus,W.C. and Thomas,J.W. (1952) U.R.N.L. Report 1413 (available from Office of Technical Services, Dept. of Commerce, Washington D.C.)

Diermendjian,D. (1960) Atmospheric Extinction of Infrared Radiation. Q. J. R. Met. Soc. 86, 371-381

Eggleton,A.E.J. and Atkins,D.H.F. (1969) The Chemical Composition of Atmospheric Aerosols on Tees-side and its Relation to Visibility. Atmos. Environ. 3, 355-372

Fuchs,N.A., Stechkina,I.B. and Starosselskii,V.I. (1962) On the Determination of Particle Size Distribution in Polydisperse Aerosols by the Diffusion Method. Brit. J. Appl. Phys. 13, 280-281

Garland,J.A. (1969) Condensation on Ammonium Sulphate Particles and its Effect on Visibility. Atmos. Environ. 3, 347-354

Hänel,G. (1970) The Size of Atmospheric Aerosol Particles as a Function of the Relative Humidity. Beit. Phys. Atm. 43, 119-132

Hänel,G. (1971) New Results concerning the dependence of Visibility on Relative Humidity and their significance as a Model for Visibility Forecast. Beit. Phys. Atm. 44, 137-167

Hänel,G. (1972) Computation of the Extinction of Visible Radiation by Atmospheric Aerosol Particles as a function of the Relative Humidity, based on Measured Properties. Aerosol Science 3, 377-386

Heard,M.J. and Wiffen,R.D. (1969) Electron Microscopy of Natural Aerosols and the Identification of Particulate Ammonium Sulphate. Atmos. Environ. 3, 337-340

Jennings,S.G. and Elleson,R.K. (1976) Natural Aerosol Size Distributions in the 0.25 - 5.0 micrometre Radius Range. Submitted to Atmos. Environ.

Junge,C. (1952) The Constitution of Atmospheric Aerosols. Annln. Met. 5, supplement

Junge,C. (1953) Die Rolle der Aerosole und der gasförmigen Beimengungen der Luft im Spurenstoffhaushalt der Troposphäre. Tellus 5, 1-26

Junge,C. (1963) Air Chemistry and Radioactivity. Academic Press, New York

Junge,C. and Jaenicke,R. (1971) New Results in Background Aerosol Studies from the Atlantic Expedition of the R.V. Meteor, Spring 1969. Aerosol Science 2, 305-314

Katz,U. and Kocmond,W.C. (1973) An Investigation of the Size-Supersaturation Relationship of Soluble Condensation Nuclei. J. Atmos. Sci. 30, 160-165

Keefe,D., Nolan,P.J. and Rich,T.A. (1959) Charge Equilibrium in Aerosols according to the Boltzmann Law. Proc. R. Irish Acad. 60, 27-45

Kelvin,Lord (1870) On the Equilibrium of Vapour at a Curved Surface of Liquid. Proc. R. Soc. Edin. 7, 63

Köhler,H. (1921) Zur Kondensation des Wasserdampfes in der Atmosphäre. Geophys. Publ. 2

Köhler,H. (1936) The Nucleus in and the Growth of Hygroscopic Droplets. Trans. Farad. Soc. 32, 1152-1161

Kottler,F. (1950) The Distribution of Particle Sizes. J. Franklin Inst. 250, 419-441

Liu,B.Y.H., Whitby,K.T. and Yu,H.H.S. (1966) A Condensation Aerosol Generator for producing Monodispersed Aerosols in the size range 0.036 - 1.3μ. J. de Res. Atmosphériques 3, 397-406

Low,R.D.H. (1969a) A Comprehensive Report on Nineteen Condensation Nuclei. ECOM-5249, White Sands Missile Range, New Mexico

Low,R.D.H. (1969b) A Generalised Equation for the Solution Effect in Droplet Growth. J. Atmos. Sci. 26, 608-611

McDonald,J.E. (1953) Erroneous cloud-physics applications of Raoult's Law. J. Meteor. 10, 68-70

Marple,V.A., Sverdrup,G.M. and Whitby,K.T. (1976) Private communication

Mason,B.J. (1971) The Physics of Clouds (2nd. Ed.) Clarendon Press, Oxford

May,K.R. (1973) The Collison Nebulizer: Description, Performance and Application. Aerosol Science 4, 235-243

Metnieks,A.L. and Pollak,L.W. (1959) Instruction for the Use of Photoelectric Condensation Nucleus Counters. Geophysical Bulletin No. 16. Dublin Inst. for Advanced Studies

Metnieks,A.L. and Pollak,L.W. (1961) Tables and Graphs for Use in Aerosol Physics.
Part I Mobility v. Radius and Vice Versa
Part II Number of Uncharged Particles in per cent total number of particles v. Radius and Vice Versa.
Geophys. Bull. No. 19-20. Dub. Inst. Adv. Studies

Middleton,W.E.K. (1963) Vision through the Atmosphere University of Toronto Press

Mie,G. (1908) Beitrage zur Optik trüber Medien, speziell kolloidaler Metallösungen. Ann. d. Physik 25, 377

Newall,H.E. and Eaves,A. (1962) The Effect of Windspeed and Rainfall on the Concentration of Sulphur Dioxide in the Atmosphere. Int. J. Air Wat. Poll. 6, 173-177

Nolan,J.J., Nolan,P.J. and Gormley,R. (1938) Diffusion and Fall of Atmospheric Condensation Nuclei. Proc. R. Irish Acad. 45-A4, 47

Nolan,P.J. and Pollak,L.W. (1946) The Calibration of a Photoelectric Nucleus Counter. Proc. R. Irish Acad. 51, 9-31

Orr,C.Jr., Hurd,F.K., Hendrix,W.P. and Corbett,W.J. (1956) An Investigation into the Growth of Small Aerosol Particles with Humidity Change. Final Report Project No. A-162. Engineering Experiment Station of the Georgia Institute of Technology, Atlanta, Georgia

Orr,C.Jr., Hurd,F.K. and Corbett,W.J. (1958a) Aerosol Size and Relative Humidity. J. Colloid. Sci. 13, 472-482

Orr,C.Jr., Hurd,F.K., Hendrix,W.P., and Junge,C. (1958b) The Behaviour of Condensation Nuclei under Changing Humidities. J. Meteor. 15, 240-242

Pasceri,R.E. and Friedlander,S.K. (1965) Measurements of the Particle Size Distribution of the Atmospheric Aerosol. J. Atmos. Sci. 22, 577-584

Pedder,M.A. (1971) On the Analysis of Continuous Records of Total Concentration and Equivalent Radius in Rural Aerosol. Aerosol Sci. 2, 175-183

Penndorf,R.B. (1962) Scattering and Extinction Coefficients for Small Absorbing and Nonabsorbing Aerosols. J. Opt. Soc. Am. 52, 896-904

Sinclair,D. (1947) Light Scattering by Spherical Particles J. Opt. Soc. Am. 37, 475-480

Stratton,J.A. and Houghton,H.G. (1931) A Theoretical Investigation of the Transmission of Light through Fog. Phys. Rev. 38, 159-165

Thomas,J.W. (1955) The Diffusion Battery Method for Aerosol Particle Size Determination. J. Colloid Sci. 10, 246-255

Thomas,J.W. (1958) Gravity Settling of Particles in a Horizontal Tube. J. Air Poll. Control Ass. 8, 32

Twomey,S. (1971) The Composition of Cloud Nuclei. J. Atmos. Sci. 28, 377-381

Twomey,S. and Severynse,J. (1964) On the Relation between Sizes of Particles and their ability to nucleate Condensation of Natural Clouds. J. Resh. Atmos. 1, 81-85

Whitby,K.T., Clark,W.E., Marples,V.A., Sverdrup,G.M., Sem,G.J., Willeke,K., Liu,B.Y.H., and Pui,D.Y.H. (1975) Characterisation of California Aerosols - 1. Size Distribution of Freeway Aerosol. Atmos. Environ. 9, 463-482

Whitby,K.T. and Husar,R.B. (1971) Generation of Artificial Aerosols. The Second International Workshop on Condensation and Ice Nuclei, Dept. Atmos. Sci., Colorado State University, 29-32

Winkler,P. and Junge,C. (1972) The Growth of Atmospheric Aerosol Particles as a Function of the Relative Humidity. J. Resh. Atmos. 6, 617-638

Wright,H.L. (1936) The Size of Atmospheric Nuclei: some deductions from measurements of the numbers of charged and uncharged nuclei at Kew Observatory. Proc. Phys. Soc. 43, 675-689

Wright,W.D. (1939) Atmospheric Opacity: a study of visibility observations in the British Isles. Q. J. 65, 411-442

ACKNOWLEDGMENTS

The author wishes to express his sincere thanks to all those who helped during the course of this work. Thanks are particularly due to Dr. S.C. Jennings, his supervisor, for his constant advice and enthusiastic support at all stages.

The assistance given in the practical areas of this research by Mr. J. Moralee is also greatly appreciated.

Finally, the author is indebted to his wife for her extreme patience in the typing of this thesis.

This work was sponsored by the U.S. Army, European Research Office under research contract No. DAJ. A37 - 75 - C - 1913.